Thèse présentée pour obtenir le grade de docteur
Université de Lille

GEMTEX : *Laboratoire de Recherche Textile Roubaix*
École doctorale n° 72 : *Science Pour l'Ingénieur Université Lille Nord-de-France*

Discipline : Mécanique

Textile Reinforcement based on Advanced Textile Technology for Composites Manufacturing

Renforcement textile basé sur une technologie textile avancée pour la fabrication de composites

PAR : **CHAN HUI**

MEMBRES DU JURY:

Président : **Chung-Hae PARK**, Professeur des Universités, IMT-Lille-Douai
Rapporteuse : **Emmanuelle VIDAL-SALLÉ**, Professeur des Universités, INSA de Lyon
Rapporteur : **Joël BREARD**, Professeur des Universités, Université Le Havre Normandie
Examinateur : **Philippe DAL SANTO**, Professeur des Universités, ENSAM
Directeur : **Xavier LEGRAND**, Professeur des Universités, ENSAIT
Co-directeur : **Peng WANG**, Professeur des Universités, Université de HAUTE-ALSACE

Date de soutenance : Le 26/01/2021

To My Family

ACKNOWLEDGEMENTS

My grateful appreciation to the CSC, China who provide financial support throughout the thesis, and to the generous supports in terms of materials, equipment, software licenses of ENSAIT/GEMTEX, France. They are the basis to complete the present thesis research.

J'exprime tout ma gratitude, à mes superviseurs Prof. Xavier LEGRAND et Prof. Peng WANG pour m'avoir bien soutien tout au long da la thèse, de la sélection du titre, de la conception de la méthode expérimentale, de l'analyse des résultats à la rédaction de thesis. Leurs immenses connaissances, leur motivation et leur patience ont découvert plus de possibilités sur la recherche et m'ont donné plus de puissance et d'esprit dans la rédaction.

Je tien également à témoigner ma reconnaissance pour tout le personel de ENSAIT/GEMTEX. Tout particulièrment M. Mathieu TRICAUD qui est quitté et Dr. Imen GNABA pour avoir répondu à plusieurs de mes préoccupations au début de ma thèse. Et aux techniciens, en particulier Nicolas DUMONT et Laurant pour leur aide sur le découpe des échantillons.

Tout mes remerciments aux doctorant et ingénieurs de la MDS. Un grand merci à Dr. Chen CHEN avec qui j'ai eu le plaisir de travailler durant son stage et Mme. Nouné MAKHSIYAN qui ont termininé ses étude master IMS. Dont les résultats pendant leur stages ont apporté des contributions agréables à ma thèse. Et à touts les stagiaires qui m'ont aideée à réaliser ces travaux, j'exprime tout ma gratitude.

I will always remember my fellow colleagues who become my friends: Dr. Kaichen WANG, Dr. Xin ZHAO, Dr. Shengchang ZHANG, Dr. Kehui SONG and Dr. Cheng CHI. They mean a lot to me.

Je voudrais remercier les membres du jury de ma thèse: Prof. Emmanuelle VIDAL-SALLÉ et Prof. Joël BREARD pour la lecture de cette rédaction en être rapporteurs;

Je le remercie aussi, Prof. Philippe DAL SANTO et Prof. Chung-Hae PARK d'avoir accepté d'être les examinateurs.

PS: I would like here to thank myself, no matter what happened in the past few years, I have survived and always adhere to the thing most wanted: Only love cannot live up to (唯有爱不可辜负). For what I want to do, for whom I want to cherish.

Chan HUI

General Introduction

Thesis statement

The composite materials are being increasingly used in various areas, especially in the aeronautics field, attracted by their interesting mechanical performance and lightweight, multi-layer is used extensively in the last few years. The latest generations of aircraft from the two major manufacturers, Airbus and Boeing, use more than 50 % of composite materials. Fig. 0-1 gives the textile applications in Airbus 380. With the development of three-dimensional (3D) textile technologies, 3D reinforcement is gradually taking the place of the multi-layer reinforcement. It is also due to 3D composites with better through-the-thickness strength and stiffness, which is becoming an emerging research topic in the field of composites.

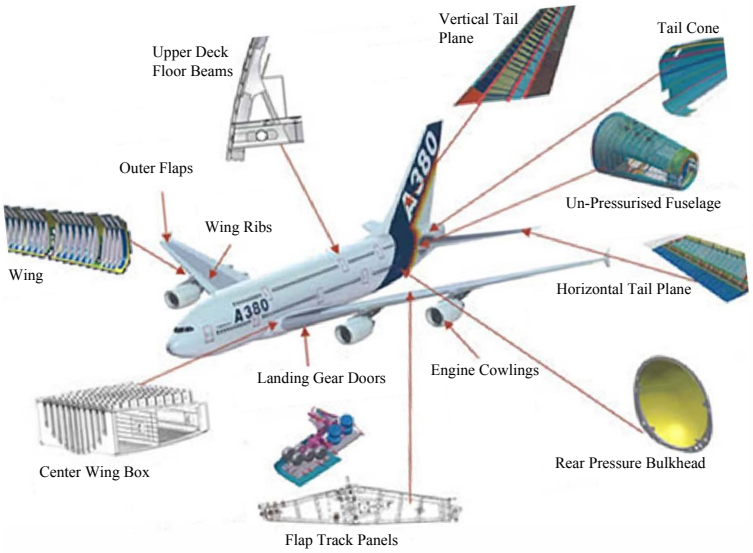

Fig. 0-1. Textile composite applications in Airbus 380 [www.airbus.com]

Through-thickness reinforcement (TTR) in 3D architectures is not only applied to address the delamination issue of multi-layer dry textile reinforcements, but also an attempt to manufacture the lighter and stronger composites part. The delamination is reduced due to the additional of a Z-direction reinforcement. TTR can be achieved by 3D weaving, z-pinning, and stitching/tufting technologies [1–4]. 3D weaving limitation is the low productivity which is due to many fibre bundles which are interlaced with several layers, and the ability rate limit of the textile machine [5]. Z-pinning is a relatively slow and expensive process [6], and it is suitable only for the aerospace market [7]. Tufting is a promising TTR technique for composites fabrication, which involves high-tension strength tufting thread, e.g. carbon threads, through the thickness reinforcements [8]. Tufting technology is an advanced technology, which originates from the traditional carpet manufacture, and its earliest application in the composites field can be found in the literature dates back to 1973 [9, 10].

In recent years, the GEMTEX Laboratory focused on the research of the tufting technology to achieve the TTR composites by adding the Z-direction thread, especially since an academic tufting device was designed by Lui et al. [11]. As the 3D laminated TTR technology, it does not only improve the mechanical performance, but also, on the one hand, it adapts to various materials, and it is easy to achieve various patterns just by changing the tufting density and tufting direction, and therefore, the realization is easier than 3D orthogonal TTR technologies (3D weaving, braiding and knitting technologies). On the other hand, this technology can not only reinforce the preform, the flat appearance, but also to assembly multiple preforms to develop the complex structure. Meanwhile, the mechanism to realize the tufting technology is relatively simple and the production equipment is low cost, the stitching damage is reduced, and thick structures up to 30 mm can be reinforced. However, as a promising technology, there are still problems to be studied. For instance, to understand its mechanical performance, to develop new tufting structures, to fully understand the the working mechanism of tufitng threads, etc.

In the present study, the tufting technology is used as an entry point and investigated in multi-scales: tufting thread and its degradation, tufted laminate composites and its interlaminar shear properties, and tufted panel assembly composites and its manufacture as well as the mechanical properties, respectively. The present

thesis is classified as follows:

1. At tufting thread scale, to well understanding the degradation behaviours of tufting threads, then to propose a novel tufting process.
2. At tufted laminate scale, to explore an interlaminar shear test under mode II sliding loading condition on tufted preform and composites, respectively.
3. At tufted plate assembly scale, to develop this novel plate assembly composite by tufting, and then to study the basic mechanical properties under tensile loading.
4. Based on the tufting thread properties, the tufting path in the composite and the cross-section of tufting thread to propose a geometrical model of tufting thread.

Outline of the thesis

In addition to this chapter, the manuscript is divided into six ones as follows:

The present chapter gives an overview of this thesis, including the problem statement, the aim of the thesis, and the outline of the thesis.

The chapter 1 provides the literature review on the textile composite, including an overall overview of textile reinforcements and technologies. This is followed by a broad overview of the tufting technology and tufted composites.

The chapter 2 presents a novel tufting mechanism based on the exploration of the reasons of tufting thread degradation during the tufting process. The quasi-static tensile and image-observation of tufted threads and non-tufted to understand the degradation of tufting thread. Followed by a novel tufting mechanism is proposed, meanwhile, the two abovementioned methods are used to verify the feasibility of this novel tufting process. Furthermore, the effect of tufting density on the tufting thread degradation is also presented in detail.

The chapter 3 focuses on the interlaminar shear properties under mode II sliding loading condition of the tufted products. Including the dry tufted preform (DTP) and cured tufted composite with tufting thread (CTC) or without (CT'C), respectively. The respective intragroup and intergroup comparison results of ultimate shear strength and shear angle based on the various tufting densities are discussed in detail.

The chapter 4 demonstrates the manufacturing of plate assembly composite based on tufting technology. Its basic mechanical properties under tensile loading are fully discussed, including the influence of tufting density, free tuft loop (FTL), and tufting pattern on these mechanical properties. The results are shown in terms of the failure positions and the tensile properties histograms are compared and discussed in detail. Besides, A novel geometrical model of the tufting thread is proposed based on the shape and path of the tufting thread and the cross-section of the tuft point. Subsequently, A macro (M)-level model of tufted plate assembly

composite is established on the basis of the tufting thread model.

The last chapter contributes to the overall conclusion of the thesis and gives perspectives for future work.

The schematic outline of this thesis is shown as Fig. 0-2 in below:

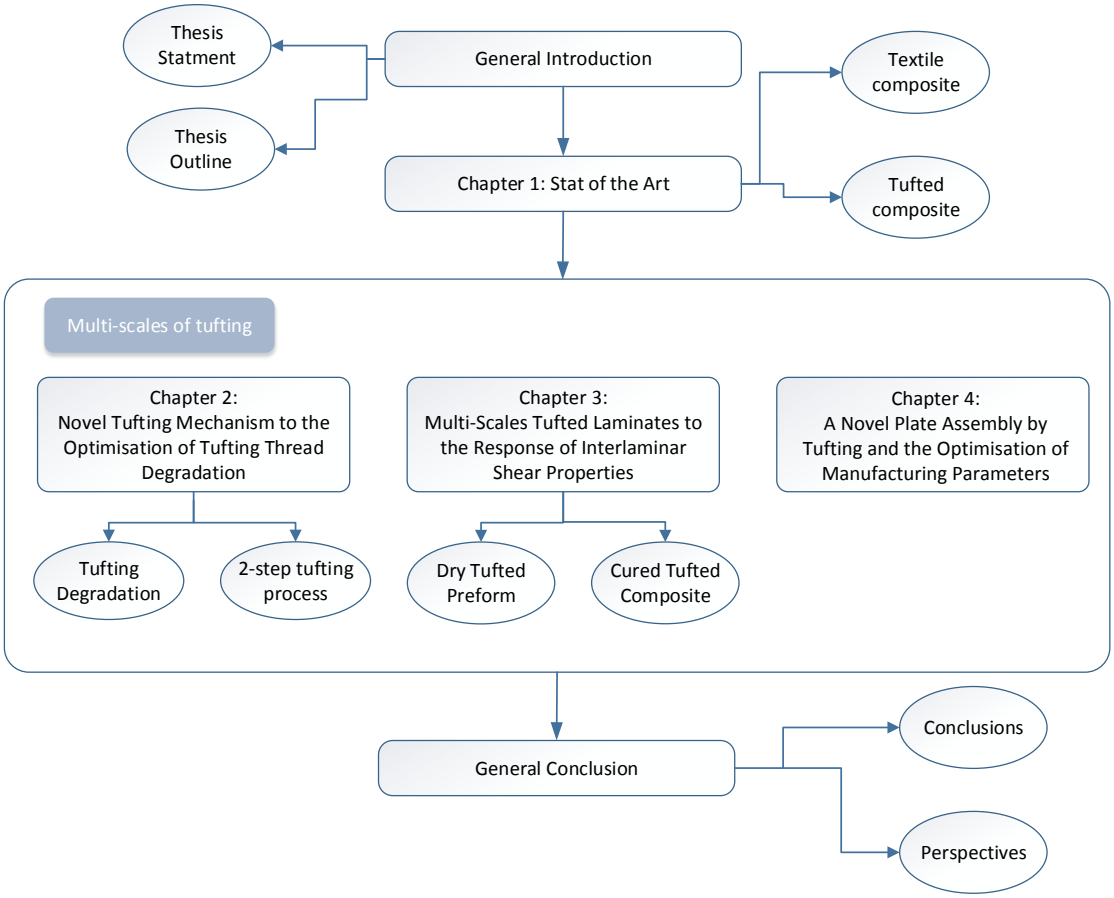

Fig. 0-2. Outline of thesis

Bibliography

[1] A. P. Mouritz. Design dilemma for Z-pinned composite structures. *27th Congress of the International Council of the Aeronautical Sciences 2010, ICAS 2010*, 3:1895–1905, 2010.

[2] AP Mouritz. Review of z-pinned composite laminates. *Composites Part A: Applied Science and Manufacturing*, 38(12):2383–2397, 2007. ISSN 1359835X.

[3] K Dransfield, C Baillie, and YW Mai. Improving the delamination resistance of CFRP by stitching—a review. *Composites Science and Technology*, 50(3):305–317, 1994. ISSN 02663538.

[4] G Dell'Anno, JWG Treiber, and IK Partridge. Manufacturing of composite parts reinforced through-thickness by tufting. *Robotics and Computer-Integrated Manufacturing*, 37:262–272, 2016. ISSN 07365845.

[5] BG Falzon, SC Hawkins, CP Huynh, R Radjef, and C Brown. An investigation of Mode I and Mode II fracture toughness enhancement using aligned carbon nanotubes forests at the crack interface. *Composite Structures*, 106:65–73, 12 2013. ISSN 02638223.

[6] P Potluri, E Kusak, and A Cumellas. Structural performance of orthogonal and bias stitched sandwich structures with rigid close-cellular foams. In *procedding 44th AIAA/ASME/ASCE/AHS/ASC Structures, Structural Dynamics, and Materials Conference*, page 1949, 2003.

[7] P Potluri, E Kusak, and TY Reddy. Novel stitch-bonded sandwich composite structures. *Composite structures*, 59(2):251–259, 2003.

[8] A Henao, M Carrera, A Miravete, and L Castejón. Mechanical performance of through-thickness tufted sandwich structures. *Composite Structures*, 92(9): 2052–2059, 2010. ISSN 02638223.

[9] DW Bauer and WV Kotlensky. Relationship between structure and strength for CVD carbon infiltrated substrates. Part II- Three dimensional woven, tufted and needled substrates. *SAMPE Quarterly*, 4(2):10–20, 1973.

[10] S.D. Green and G. Dell'Anno. Impact resistance of carbon/epoxy L-sections reinforced through-the-thickness by tufting. In *Proceeding of the 21th International Conferences on Composite Materials(ICCM)*, 2017.

[11] LS Liu. *Development and optimization of the tufting process for textile composite reinforcement*. PhD thesis, Université de Lille 1, 2017.

CONTENTS

General Introduction **i**

Thesis statement i

Outline of the thesis iv

Bibliography v

1 Stat of the Art **1**

1.1 Introduction of chapter one 1

1.2 General knowledge of composite materials 2

1.2.1 Moulding process of composite materials 2

1.2.2 Textile reinforcement architectures and technologies 4

1.3 The advanced tufting technology 15

1.3.1 Applications and devices of tufting technology 16

1.3.2 Manufacturing of tufted composites 22

Preparatory work: the definition of tufting density 25

1.3.3 Micro - and meso-structure of tufted composites 28

1.3.4 Advantage of tufting 31

1.3.5 Disadvantage of tufting 39

1.4 Conclusion of chapter one 40

Bibliography 41

2 Novel Tufting Method to the Optimisation of Tufting Threads Degradation **55**

2.1 Introduction of chapter two 55

2.2 Materials and methods 57

2.3 Problems of degradation in classical tufting 58

2.3.1 Description of classical tufting 58

2.3.2 Image-observation of inserted tufting threads 59

2.3.3 Tensile tests of the tufting threads 64

2.4 New tufting process 66

2.4.1 Description of the two-step tufting process 66

2.4.2 Image-observation of inserted tufting threads 68
2.4.3 Tensile tests of the tufting threads 70
2.5 Discussion 71
2.6 Conclusion of chapter two 74
Bibliography 74

3 Multi-Scales Tufted Laminates to the Response of Interlaminar Shear Properties 79
3.1 Introduction of chapter three 79
3.2 Materials and methods 81
3.2.1 Raw materials 81
3.2.2 The preparation of test samples 82
3.2.3 Preparing and setting tufting configurations 84
3.2.4 Interlaminar shear characterisation 85
3.3 Results 89
3.3.1 Interlaminar shear test of dry tufted preform samples 89
3.3.2 Interlaminar shear test of cured tufted composite samples . . 91
3.4 Discussions 96
3.5 Conclusion of chapter three 99
Bibliography 100

4 A Novel Plate Assembly by Tufting and the Optimisation of Manufacturing Parameters 105
4.1 Introduction of chapter four 105
4.2 Materials and methods 107
4.2.1 Materials and samples 107
4.2.2 Testing procedure 113
4.3 Results 115
4.3.1 Failure position observations 115
4.3.2 Tensile testing results 116
4.4 Discussion 125
4.5 Conclusion of chapter four 127
4.6 Perspective of chapter four 128
4.6.1 Modelling of the tufting thread 128
4.6.2 Modelling of the tufted plate assembly composite 132
Bibliography 137

General Conclusions **i**
Conclusions i
Perspectives ii

LIST OF TABLES

1-1 Development of preform architecture classification 6
1-2 Main parameters of tufting device [29]. 22
1-3 Delamination area [118]. 35
1-4 Ultimate compressice strength on CBI and CAI tests, and the residual ratio (CAI/CBI) [83]. 37
1-5 Experimental results in terms of CAI strength [109]. 37

2-1 Main properties of tufting threads. 58
2-2 Influence of tufting spacing on the degradation of inserted tufting threads. 62
2-3 Influence of tufting spacing on the degradation of inserted tufting threads. 68

3-1 Description of test tufted samples. 85
3-2 Conclusive interlaminar shearing resistance results of all samples. . . 97

4-1 Samples that meet various influencing factors and their designated nomination. 112
4-2 Failure position of tufted assembly. 116
4-3 Tensile properties of group A samples. 118
4-4 Tensile properties of group B samples (Without FTL). 118
4-5 Tensile properties of group C samples ($\pm$ 45° tufting patterns). 120
4-6 The comparison results of specific breaking force between tufted plate assembly composites with and without FTL. 126

LIST OF FIGURES

0-1 Textile composite applications in Airbus 380 [www.airbus.com] . . . i
0-2 Outline of thesis v

1-1 Overview of the chapter. 1
1-2 The classification of varying closed-moulding techniques. 4
1-3 Classification of textile preform by Wang, Legrand and Soulat [11]. . 5
1-4 Standard weave structures (a) plain weave, (b) twill weave and (c) satin weave [18]. 7
1-5 Standard knit structures (a) warp knit and (b) weft knit [19, 20]. . . . 7
1-6 Basic braid structures (a) regular braid, (b) diamond braid and (c) hercules braid [24]. 8
1-7 (a) Braiding machine in GEMTEX and (b) Principe of braiding [24]. . 9
1-8 Example of (a) flat braid and (b) tubular braid [20]. 9
1-9 Examples of 3D interlock weaves structures [20]. 11
1-10 Examples of 3D knit structure (a) chain stitch and (b) tricot stitch [35]. 11
1-11 Examples of 3D (a) square braid [34] and (b) braid structure [20]. . . 12
1-12 Examples of laminate configurations [36]. 12
1-13 Schematic of z-pinning technology [27, 37]. 13
1-14 Schematic of (a) lock stitches, (b) modified lock stitches and (c) chain stitches [38, 43–45]. 14
1-15 Schematic of OSS technologies (a) Double-needle Double-thread stitching (ITA), (b) Double-needles Single-thread stitching (Altin) and (c) Blind stitching (KSL) [46–50]. 14
1-16 Schematic of tufting technology (a) conventional process, (b) partial or fully penetration and (c) angled tufting process [50, 51]. 15
1-17 Aerotiss® 03 tufting principle [59]. 16
1-18 Schematic of aviation applications in (a) flat panel, (b) convex panel, (c) bi-bonvex pane, (d) nozzle of rocket engine and (e) spacecraft nose [70]. 17

1-19 A "Tufting Head" developed by KSL GmbH, Lorrsch and DLR, Institute of Structural Mechanics, Brunswick for operation on conventional CNC machine [25]. 18
1-20 (a) Stitching robot and (b) tufting head used in QinetiQ Company [73]. 19
1-21 (a) Kavasaki FN20 stitching robot and (b) KSL KL150 tufting head [64]. 20
1-22 (a) Stitching robot system and (b) tufting head developed by Alitin Näthechnik GmbH [75]. 21
1-23 Tufting device (a) using in GEMTEX Lab. and (b) CAD version [29]. . 22
1-24 Schematic of tufting parameters [29]. 23
1-25 Cylindrical support [70]. 24
1-26 Tuft loops emended in the closed, foam filled preform [77]. 24
1-27 Schematic of liquid resin infusion process [9]. 25
1-28 Definition of tufting density, schematic of tufting direction of (a) 0 angle (b) with a direction angle. 26
1-29 Degradation of tufting thread [57]. 29
1-30 Resin-rich zones of tufted composites [74]. 30
1-31 Inclined tuft [57]. 31
1-32 Tufted and untufted composites delamination characteristic in static: (a) force versus crack displacement and (b) G_{IC} versus crack length [94]. 33
1-33 Standard and tufted NCF composites response to delamination: (a) force versus crack displacement, (b) strain energy release rate [96]. . 33
1-34 Energy absorption after failure in all composites [86]. 35
1-35 Size of lightning strike damaged area [119]. 36
1-36 Results of Mills (a) Spar tufting and (b) Energy absorption [120]. . . . 38
1-37 Results of kratz (a) Testing specimens in four-point bending and (b) First failure load-displacement plot for skin-stringer tests [125]. . . . 39

2-1 Bobbin of tufting thread. 58
2-2 The tufted sample using the tufting square pattern of 9×9 mm^2. . . 58
2-3 Classical tufting process (a-b) schematics view and (C) with GEMTEX tufting device. 59
2-4 (a) hollow needle and (b) schematic view of cross section. 60
2-5 (a) the tufted preform,(b) the inserted threads picked in one tufting cycle and (c) the scanned image of inserted threads in one tufting cycle. 61

2-6 Image-observation of the non-inserted tufting thread and the inserted tufting threads with different tufting spacing. 63
2-7 Tensile test of the single tufting thread. 64
2-8 Tensile load *vs.* strain curves of the non-inserted and inserted tufting threads. 65
2-9 Schematics of two-step tufting process. 67
2-10 Two-step tufted carbon thread with tufting spacing of (a) 9 mm, (b) 6 mm, (c) 3 mm. 69
2-11 Comparison of the degradation in pixel between the classical and two-step tufting. 70
2-12 Tensile load *vs.* strain curves of the inserted tufting threads in two-step tufting. 71
2-13 Comparison of the tensile properties between the classical and two-step tufting. 73

3-1 The layout of the chapter 81
3-2 (a) E-glass fabric and (b) schematic of the laminated preform. 82
3-3 Dry tufted preform (a) top view and (b) bottom view. 83
3-4 The tufted preform sample under the LRI process. 83
3-5 Cured tufted composite (a) top view and (b) bottom view. 84
3-6 Interlaminar shear (a) mode II shear delamination, (b) test set-up and (c) schematic view. 88
3-7 Representative shear load-shear angle curves of DTP specimens . . . 90
3-8 Representative shear properties of DTP specimens. 91
3-9 Representative shear load-shear angle curves of CT'C samples. . . . 92
3-10 Representative shear load-shear angle curves of CTC samples. 93
3-11 Comparison of the shear properties between CT'C and CTC samples. 95
3-12 Three principal states of specimens under the Mode II loading test . 98
3-13 Comparison of rupture position for CTC specimens 99

4-1 Schematic view of (a) tufted tubular assembly, (b) tufted plate assembly. 107
4-2 Tufted plate assembly (a) schematic view, (b) dry preform samples with a tufting spacing of 9 mm. 109

4-3 (a) Dimensional schematic of tensile test for tufted plate assembly sample (*Top:* Top view; *Bottom:* Front view). (b) *Left:* INSTRON® Universal Testing Machine; *Right:* Tensile test set-up. 114
4-4 Tensile load *vs.* strain curves of group A samples. 117
4-5 Tensile load *vs.* strain curves of group B samples (without FTL). . . . 119
4-6 Tensile load *vs.* strain curves of group C samples ($\pm$ 45° tufting patterns). 120
4-7 Comparison of the tensile properties (a) maximum tensile load and (b) breaking strain of tufted plate assembly composite between with and without FTL. 122
4-8 Comparison of the tensile properties of tufted plate assembly composite with different pattern. 124
4-9 Comparison of specific breaking force between tufted assembly composite part with FTL and without FTL. 126
4-10 Basic morphology assumption of tufting thread 129
4-11 The sectional view of tufting thread through the thickness by ***QMicroCapture***. 130
4-12 Polygonal section-cross by ***Solidwork***. 131
4-13 Geometrical model of tufting thread by ***TexGen***. 132
4-14 Parts of tufted plate assembly model. 133
4-15 Element meshing (a) glass/epoxy element and (b) cohesive element . 134
4-16 Tufting thread meshing 135
4-17 Tufting thread (a) optimized geometrical model and (b) meshing resolution 136
4-18 Overall view of tufted plate assembly meshing 136
4-19 The unit cell of tufted architecture. 137

CHAPTER 1

STAT OF THE ART

1.1 Introduction of chapter one

To manufacture the overall preform is commonly recognized to improve the mechanical performance of the final composite part. Firstly, general knowledge about the composite material is introduced in Section 1.2, including the cured moulding methods to complete the final composite, and the manufacture methods of reinforcement to achieve the composite preform. Then, a typical tufting technology is reviewed in Section 1.3, focusing on its applications and its devices to date, as well as on the characteristics and properties of resin-based tufted reinforced composites. Finally, a brief conclusion is made in the last Section 1.4. The present chapter overview is shown in Fig.1-1.

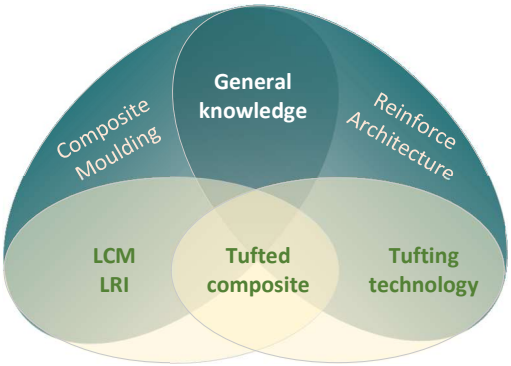

Fig. 1-1. Overview of the chapter.

1.2 General knowledge of composite materials

The increasing importance has been placed on composites and their promising future according to recent market shares and predictions. Definition in general [1, 2], composite materials (composite for short) are formed by combining materials together to form an integrated structure with properties that differ from those of the individual components. There are two categories of constituent materials: matrix and reinforcement. The matrix material surrounds and supports the reinforcement materials by maintaining their relative positions. Reinforcement imparts their special mechanical and physical properties to enhance the matrix properties. A synergy produces material properties unavailable from the individual constituent materials [3, 4].

As an important subclass of composites, textile reinforced composites, also known as Fiber-Reinforced Polymer (FRP) composites [5], are made from polymer matrix where the reinforcement is a textile material comprised of natural or artificial fibres. Of which, the matrix protects the fibres from environmental and external damage, while transferring loads among the fibres. The textile, in turn, provides strength and stiffness to reinforce the matrix whilst helping it to resist cracks and fractures.

Composites are used in a wide variety of markets due to their high stiffness and strength to weight ratio, including aerospace, architecture, automotive,civil engineering, energy, infrastructure, marine, military as industrial composites, and sports, recreation as consumer composites. They are typically designed with a particular application in mind, such as better strength, efficiency, or durability. They have played an important role throughout human history, from housing early civilizations to enabling future innovations [6].

1.2.1 Moulding process of composite materials

Composites moulding process is the basis and condition for the development of composite industry. With the broadening of the application area of composite materials, a number of moulding processes have been perfected, while new moulding

methods have emerged. The present chapter describes two groups of moulding techniques, respective open-moulding and closed-moulding. Each moulding technique corresponds to a variety of methods and has its own characteristics.

- **The open-moulding**

The open-moulding technique [7] is typically used for a large size range of composites parts that cannot be manufactured in more automated processes. Or for composite parts which are manufactured in low volumes that cannot accomplish the higher mould costs of automated processes. The dry reinforcement and resin are placed in an open mould, where the cure or harden process is realised while exposed to the air. The benefits of this moulding technique are its flexibility and relatively low tooling cost. The open-moulding technique can therefore be used in prototype manufacturing and short production. It is known that **Hand lay-up, spray up** and **filament winding** are three significant methods of this moulding technique.

- **The closed-moulding**

The closed-moulding technique [8, 9] is used to manufacture large quantities of precision composite parts or to respond to the two-sided finish of the final product. In the course of the closed-moulding process, the dry reinforcement is placed onto the mould, then to close the mould. Meanwhile, the resin is introduced into the closed cavity using a pressure pump or vacuum. When the preform is cured, open the mould and remove the composite part. The advantages of this moulding technique are its low-cost tooling, product consistency, high productivity, repeatable process, and environment friendly. Thanks to its closed mould system, which allows resin emissions to be reduced. The following chart, shown as Fig.1-2, summarises the various methods of performing closed-moulding techniques in accordance with the literature review.

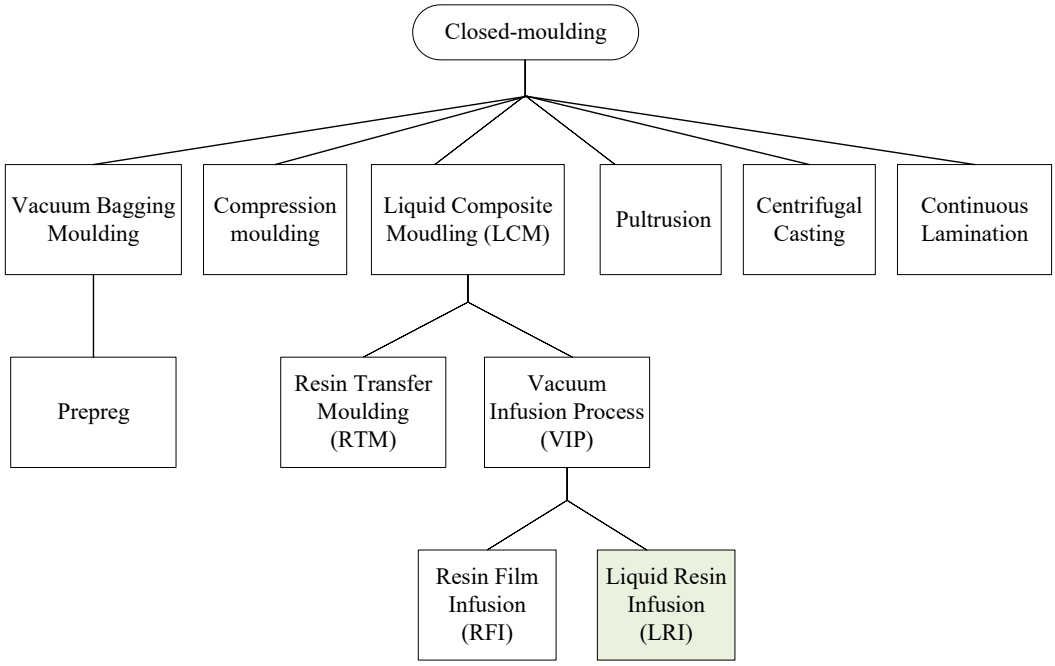

Fig. 1-2. The classification of varying closed-moulding techniques.

Wherein, LRI technique [10] is used as the moulding method to complete the final composite parts throughout the present thesis. Because it is a simple, low-cost 3D preform moulding technology.

1.2.2 Textile reinforcement architectures and technologies

Many textile technologies have been developed for the manufacture of reinforcement, also known as "composite preform", prior to the moulding stage. In this section, the classification methods of textile reinforcement are presented, followed by an introduction of some textile reinforcement techniques, together with a demonstration of the corresponding composite preforms.

- **Classification of textile reinforcement structures**

There are various ways to classify reinforcement architectures recapped as follows:

According to the dimension: 1D, 2D, 2.5D (2D+), 3D,...

According to the number of orientation: Non-axial, mono-axial, biaxial, triaxial,...

According to the textile technology: Weaving, knitting, braiding, non-weaving, novel advanced technologies,...

Fig. 1-3 shows one of the classifications proposed by Wang, Legrand, and Soulat [11]. Meanwhile, there are other classifications of composite preform architecture that have been developed in the past decades. Its development is shown in Table 1-1, four kinds of ***Definition Method*** could be figured out as 1) based on two complementary criteria, the dimension of the final preform and the number of fibre orientation; 2) focus on the number of different orientations are also posed as a criterion for the dissociation of reinforcement; 3) based on the reinforcement architectures and the associated technology for the production of the preform and 4) focus on the 3D architectures.

<table>
<tr><th>Orientation / Dimensions</th><th>randomly</th><th>mono axial</th><th>bi axial</th><th>tri axial</th><th>multi axial</th></tr>
<tr><td>1D</td><td>fibre</td><td>tow, yarn</td><td></td><td></td><td></td></tr>
<tr><td>2D</td><td>non woven</td><td>uni directional</td><td>Fabric: woven, knitting, bi axial braiding</td><td>tri axial braiding: flat, over braid</td><td>NCF stitch bonded, NCF woven</td></tr>
<tr><td>2D+</td><td>thick non woven</td><td></td><td>woven interlock</td><td colspan="2">multi axial multi-layer interlock</td></tr>
<tr><td rowspan="2">3D</td><td>surface</td><td>shaped non woven</td><td></td><td>tetrahedron ply
stamping</td><td colspan="2">over-braiding, preforming, stamping of braid or/and multi axial</td></tr>
<tr><td>volume</td><td></td><td></td><td>assemblies by tufting, stitching, nailing/pinning</td><td>cross of shaped</td><td>BWS, cross of stiffeners (integral 3D)</td></tr>
</table>

Fig. 1-3. Classification of textile preform by Wang, Legrand and Soulat [11].

Table 1-1
Development of preform architecture classification .

Year	Authors	Definition Method
2016	Wang, Legrand, Soulat [12]	1 (Fig.1-3)
2003	Nemoz [13]	1
2000	Kamiya et al. [14]	4
1998	Ko and Du [15]	3
1992	Lee [16]	2
1986	Fukuta and Aoki [17]	1

- **Textile reinforcement architectures and their technologies**

Various forms of reinforcement can be used to meet the requirements of different processes and final products, regardless of the selection of raw material. Materials supplied as reinforcement include roving, milled fibre, chopped strands, continuous, chopped, or thermoformable mats. Reinforcement materials can be designed with unique fibre architectures and performed according to product requirements and manufacturing processes. In the following, the reinforcement architectures presented are based on 2D and 3D textile technologies.

a) Bidimensional (2D) architectures

The 2D weaving

Weaving is a traditional textile technology that makes it possible to obtain a biaxial surface textile structure by the intersection at right angles of warp yarn and weft yarn. Three standard weave structures shown in Fig.1-4 are distinguished: plain, twill, and satin weave.

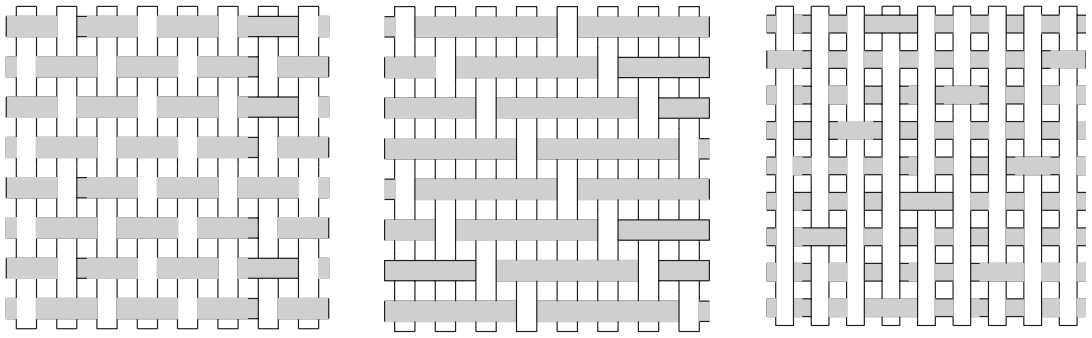

Fig. 1-4. Standard weave structures (a) plain weave, (b) twill weave and (c) satin weave [18].

The 2D knitting

Knitting is another traditional textile technology for shaping textile structures from one or more strands. Knits are obtained by interlacing a thread with itself to form a chain of stitches connection. Depending on the direction in which the loops are formed, weft or warp knits can be obtained, as shown in Fig.1-5. Knitted reinforcements are feasible for making complex composite pieces. However, the strong shrinkage (crimp of the twisted yarn) generated during the knitting process makes their own in-plane mechanical properties are restricted.

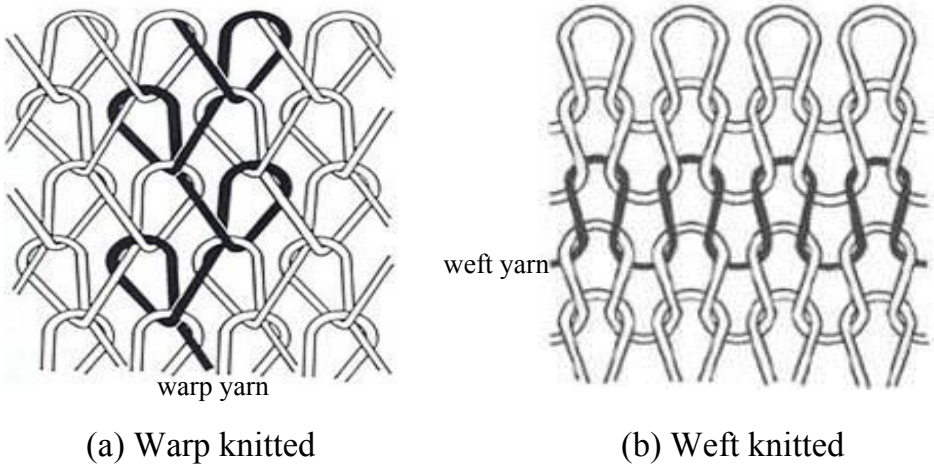

Fig. 1-5. Standard knit structures (a) warp knit and (b) weft knit [19, 20].

The 2D braiding

Braiding is a typical textile technology for producing high-volume, yet low-cost composite preforms [21]. Shown as Fig. 1-6 that the regular, the diamond and Hercules structures are three common types of braided structures. One braiding machine, one braid product, braiding machine is therefore a key factor in braiding technology. A conventional braiding machine (shown in Fig. 1-7 (a)) has fibre carriers moving in a circular pattern [22]. Fig. 1-7 (b) explodes that half of the carriers move clockwise, and the others counterclockwise, in an intertwining serpentine motion producing the desired braided structure, such as the examples shown in Fig. 1-8: 2D flat and tubular braids [23].

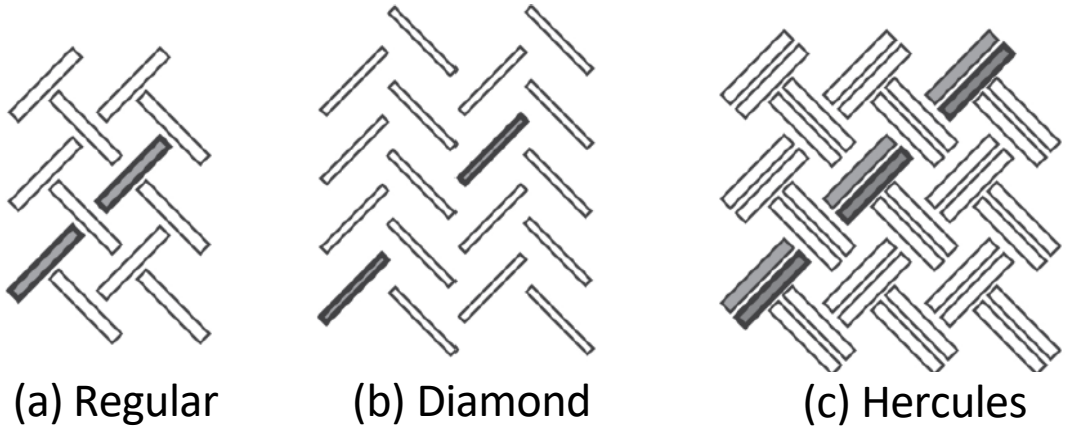

Fig. 1-6. Basic braid structures (a) regular braid, (b) diamond braid and (c) hercules braid [24].

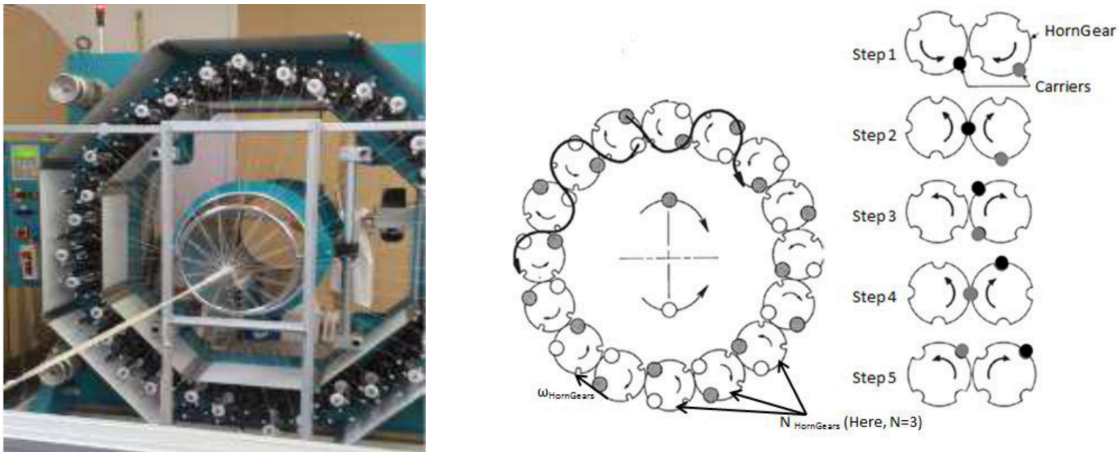

(a) Braiding machine in GEMTEX (b) Principe of braiding

Fig. 1-7. (a) Braiding machine in GEMTEX and (b) Principe of braiding [24].

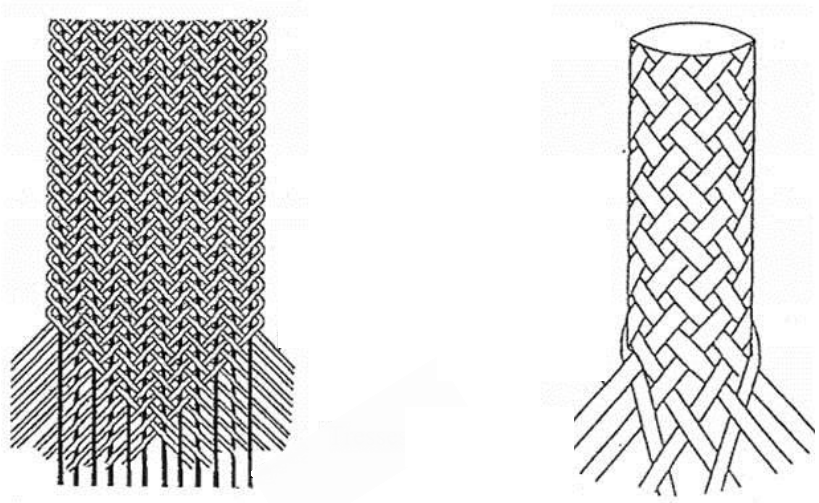

(a) Flat braid & triaxial (b) Tubular braid & biaxial

Fig. 1-8. Example of (a) flat braid and (b) tubular braid [20].

b) Tridimensional (3D) and Pseudo-Tridimensional (2D+) structures

Various approaches to manufacturing 3D preform architectures have been brought out. For instance, 3D weaving, knitting, braiding [5, 25, 26], z-pinning [27], stitching [28] and tufting [29, 30]. By means of the insertion of a through-thickness fibrous to obtain a 3D preform architecture, which is referred to as the Through-Thickness Reinforcement (TTR for short). 3D reinforced architectures have been applied for the thick and complex composite area, while filling the inherent shortcomings of the 2D laminate architectures, such as delamination, low impact tolerance, joint strength, and other out-of-plane properties.

The 3D/2D+ weaving, knitting and braiding

3D/2D+ weaving, knitting, and braiding are integral 3D textile technologies to achieve integral 3D composite preforms that make up for the lack of mechanical properties of the 2D preform structures.

3D/2D+ weaving: It is possible to obtain surface or volume structures (namely "Interlock structure") depending on the weaving process. They are achieved by superimposing several layers of weft yarns, then linked together among the warp yarns. Two main types of 3D woven preform architecture are demonstrated as follows: 3D and 2D+ interlock structures [31]: 1) 3D orthogonal interlock, 3D orthogonal layer-to-layer (LtL) interlock and 3D through-the-thickness (TtT) angle interlock [32]); 2) 2D+ layer-to-layer (LtL) angle interlock and 2D+ layer-layer (LL) angle interlock [33]. Even more, it has been proved that the preforms obtained by 3D weaving are characterized by good compressive and delamination resistance properties [34], some examples are shown in Fig.1-9.

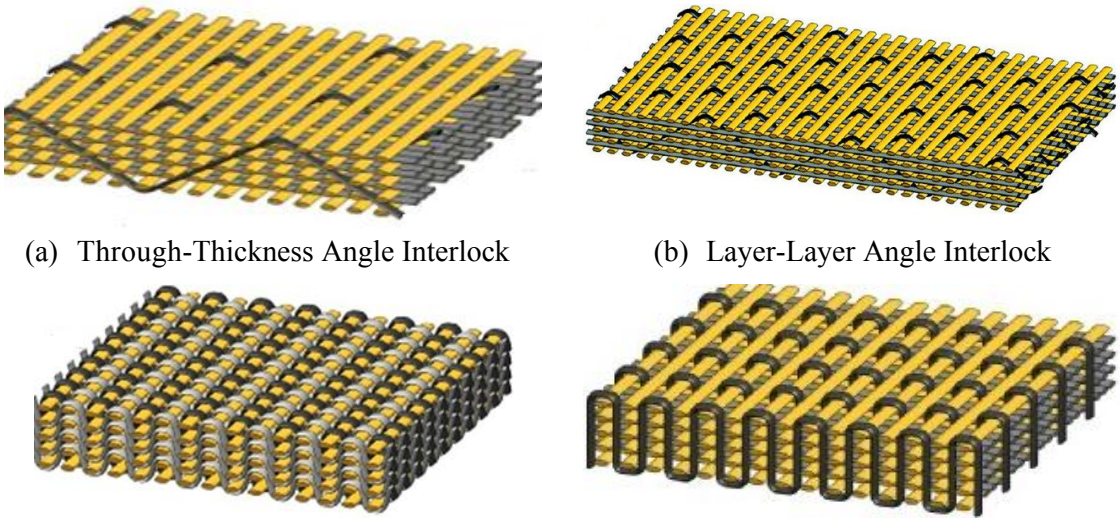

(a) Through-Thickness Angle Interlock (b) Layer-Layer Angle Interlock

(c) Layer to Layer Angle Interlock (d) 3D orthogonal

Fig. 1-9. Examples of 3D interlock weaves structures [20].

3D knitting: 3D knitted preforms are similar to 2D ones in that facilitates to reproduce of complex structure pieces. 3D knitting consists of several knits joined together by a Z-direction yarn(shown in Fig. 1-10). Therefore, they are particularly appreciated for their lightness and deformability. However, there is little literature on knitted structures in composites compared to other textile structures.

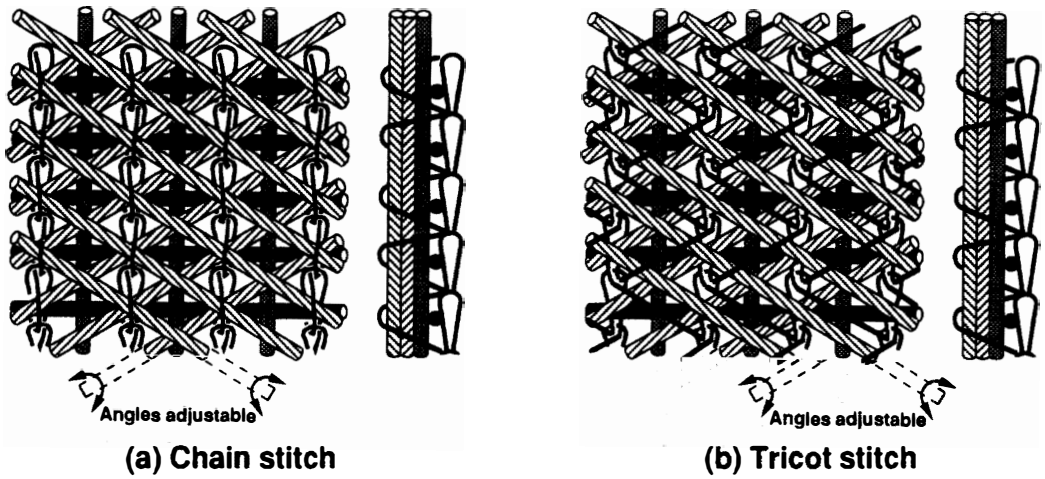

Fig. 1-10. Examples of 3D knit structure (a) chain stitch and (b) tricot stitch [35].

3D braiding: 3D braiding technology is an extension of 2D braiding. 3D braiding involves creating superimposed braided layers that are linked together by interlac-

ing layer-to-layer (LtL). It improves the resistance to delamination. Fig.1-11 shows an example of a square braid product and a 3D braid structure.

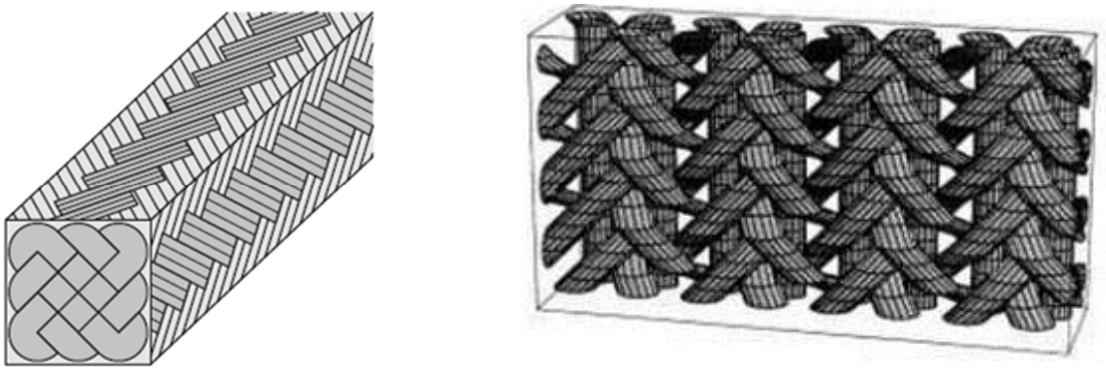

Fig. 1-11. Examples of 3D (a) square braid [34] and (b) braid structure [20].

The Laminates

Laminates (multi-layered structures) are composite preforms with the superposition of plies, oriented at different angles, and then directly cured and moulded by resin infusion, or inserted Z-reinforcement prior to the resin infusion. Fig.1-12 gives examples of the superposition of the UD layer, which can gain the desired mechanical properties for the final product. However, the limitations of the applications are due to the lack of reinforcement along the thickness direction. Some technologies which reinforce in Z-direction to ameliorate the out-of-plane mechanical properties of composite structures are literately reviewed as follows. These following technologies can be used in the manufacture of large, thick, and complex parts, and the final product can effectively improve its joint strength to reduce delamiantion.

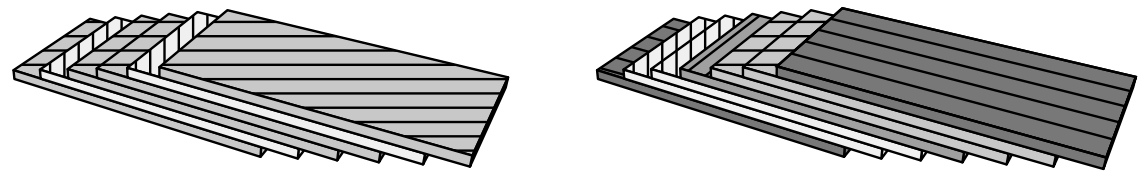

Fig. 1-12. Examples of laminate configurations [36].

The Z-pinning

Z-pinning is one of the very first technologies developed for thickness reinforcement of conventional 2D laminates. The principle consists of pins through the thickness of the laminates, and the process of which is illustrated step by step in Fig. 1-13. Z-pinning is considered as the only technology for reinforcing prepreg laminates along the thickness direction in large mass production [27].

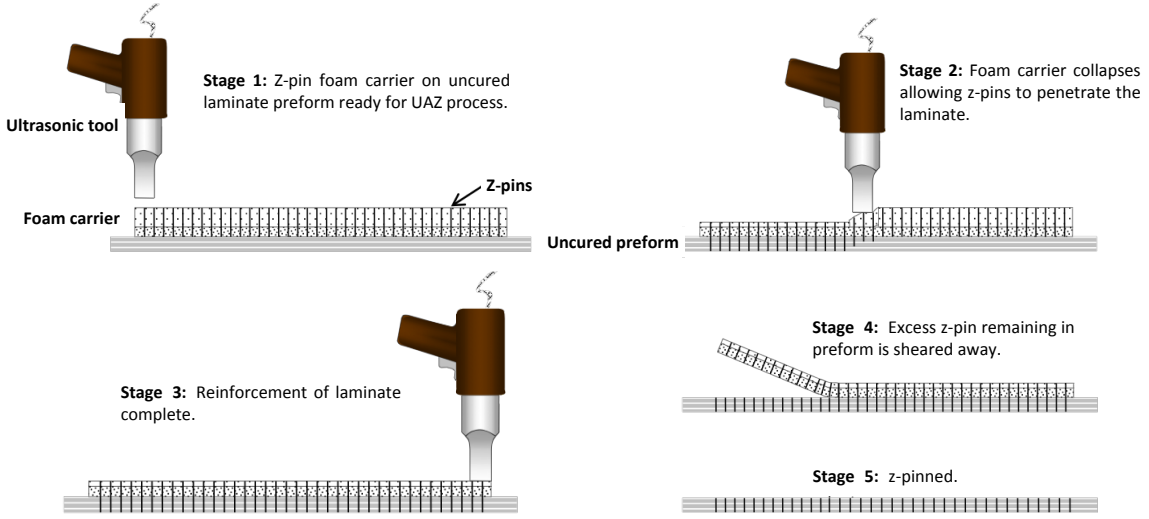

Fig. 1-13. Schematic of z-pinning technology [27, 37].

The stitching

Stitching is initially a sewing technique, using two interlocking threads [38–41], which has been applied to the TTR laminate composite since mid-1980s. Three most common types of stitches (**lock stitch, modified lock stitch** and **chain stitch**), used to reinforce the 2D laminates have been shown in Fig. 1-14. Meanwhile, in the late 1980s, its better damage resistance has been revealed and fully proven through the wing application by NASA. However, due to the need for accessing both sides of the preform to be reinforced (laminates in general) to interlock the threads, a high investment in the stitching device is required [42]. In this case, one-sided stitching technologies which only require access from a single side of the preform have been exploited, referred to as OSS for further introduction in the following:

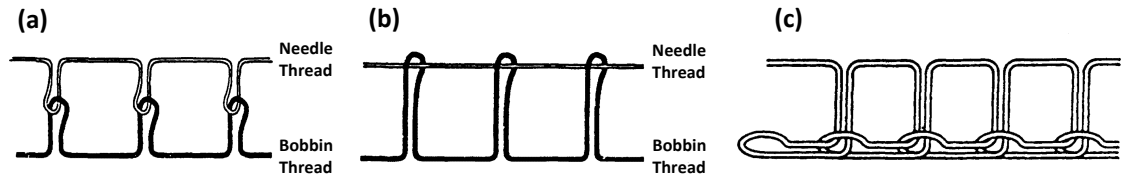

Fig. 1-14. Schematic of (a) lock stitches, (b) modified lock stitches and (c) chain stitches [38, 43–45].

The OSS:

OSS is named after Single-Sided Stitching, and various technologies are continuously explored. Herein reveals three common ones: two straight needles are used both for **ITA stitching** and **Altin stitching** technologies, the difference is whether to reinforce with two-thread or a single-thread. Unlike the previous two OSS technologies, a curved needle is required for the **Blinding stitching** technology. The principles are shown in Fig.1-15.

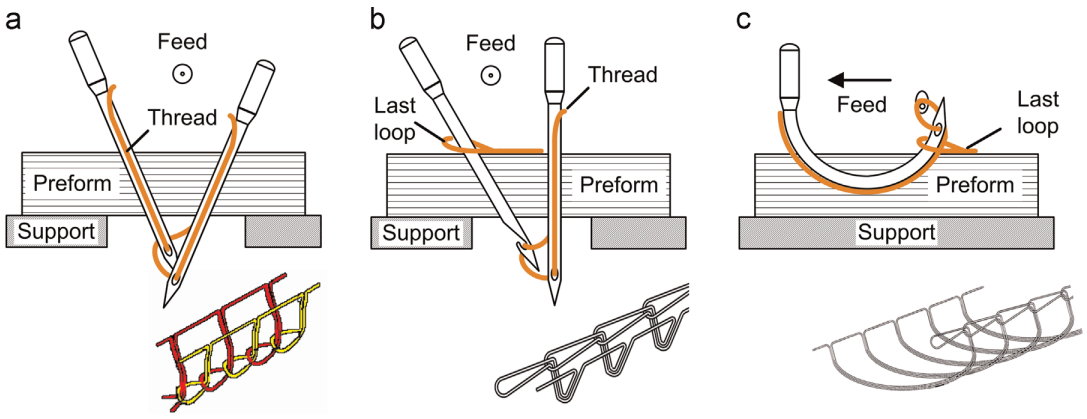

Fig. 1-15. Schematic of OSS technologies (a) Double-needle Double-thread stitching (ITA), (b) Double-needles Single-thread stitching (Altin) and (c) Blind stitching (KSL) [46–50].

The tufting

Tufting is a kind of OSS technology to assemble dry textile reinforcements by inserting the thread in Z-direction; it is found in Fig. 1-16 that the tufting thread (z-reinforcement) penetrates into the preform with very low tension, and the needle

retreats leaving a free loop, which is external to the laminates protrudes a few millimetres. However, with the deepening of research, the depth of penetration is adjustable, and the loop can also be generated inside of the laminates. Meanwhile, it can also be performed from different angles. The present thesis focused on the tufting technology for composite manufacturing. The following reviews the literature on the tufting process, the application, and manufacturing of tufted composites, as well as its pros and cons in terms of mechanical properties.

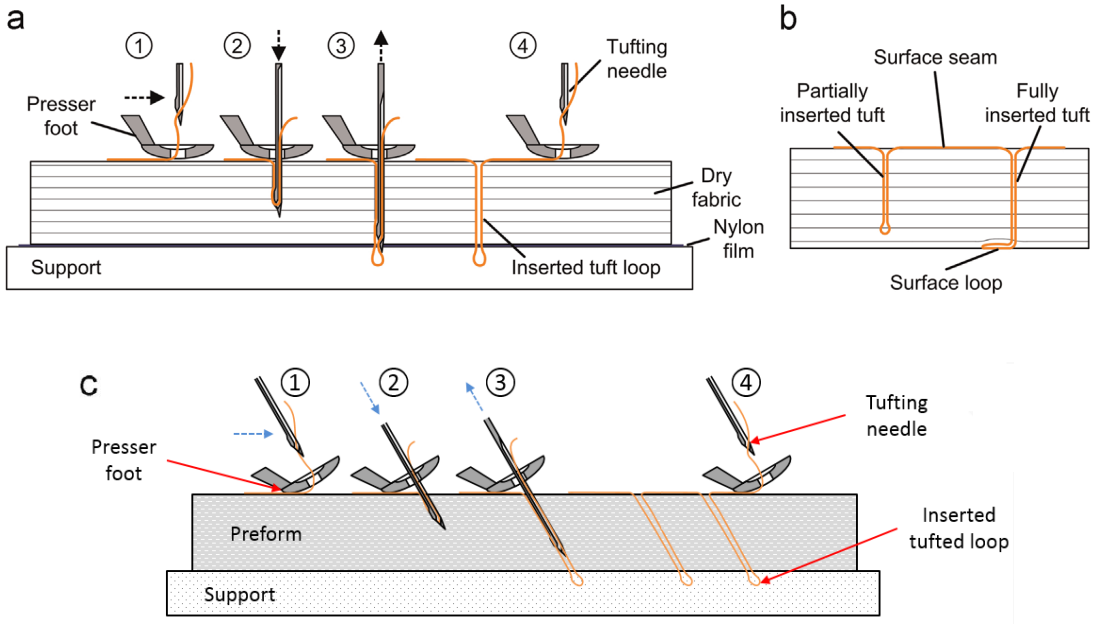

Fig. 1-16. Schematic of tufting technology (a) conventional process, (b) partial or fully penetration and (c) angled tufting process [50, 51].

1.3 The advanced tufting technology

Aerotiss® 03S [52–56], which is a typical OSS technology mentioned above. It is better known as tufting technology due to its development from the initial application of a traditional tufted carpet manufacturing area. As shown in Fig. 1-17, tufting is considered an advanced textile technology for the manufacture of composite products, which uses a single-threaded needle to assemble dry textile reinforcements by inserting threads through the thickness of the preform without tension.

Moreover, only one thread, instead of two, is required during the tufting process [25, 29, 57]. Because of the reasonable lack of the second thread and the locked thread, the Aerotiss® 03 stitching (tufting) is simpler than the conventional stitching [11, 58]. Recently, research on tufting technology has also expanded its application possibilities due to its economic-saving and lightweight characteristics.

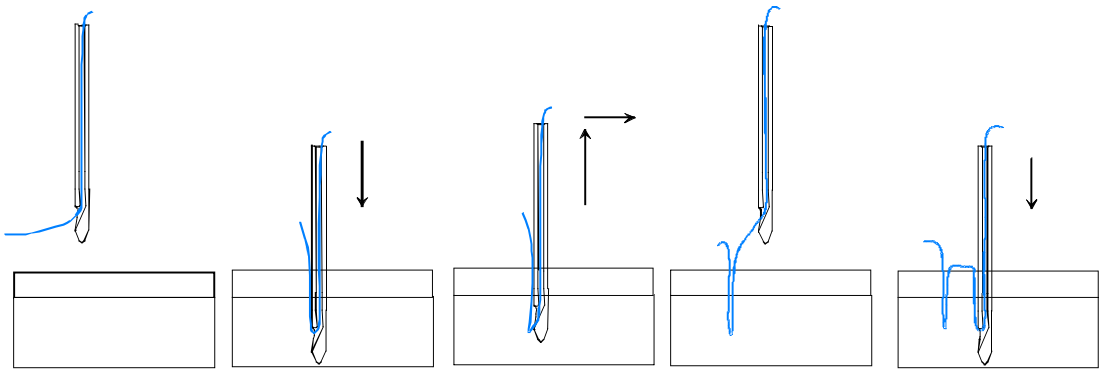

Fig. 1-17. Aerotiss® 03 tufting principle [59].

1.3.1 Applications and devices of tufting technology

- **Applications**

Tufting technology is gradually being applied to various composites manufacturing fields in response to the growing demands of the composites market for lightweight, environmentally friendly. Tufting technology has evolved from its initial application in carpet manufacturing to industrial applications in composites, realising a 3D TTR technology from the light industry to the aerospace, transport, energy, and civil engineering industries... It has been successfully applied in the aircraft door [60]. Bauer and Kotlensy[61] reveal that the first time tufting technology was applied to the composites field can be traced back to 1973. With the improvement of the tufting technology, the final tufted composites have been applied to varies fields, whether in high performance (HP) or grand diffusion (GD) markets. Such as in Mercedes SLR, tufting is used in the production of the frame rail to join

I-stiffeners to a braided oval crash tube to enhance its energy absorption during impact [62]. Laourine [63] applied tufting on a complex three-dimensional composite structure of an undercarriage demonstrator where other technologies could not be used due to the spatial restrictions [64]. Stickler et al. used partial tufting insertion to connect the T-shaped composite butt joint [65–69]. Fig. 1-18 shows several conceptional applications of tufting technology on aviation composite parts realised on the prototype of tufting head by Cahuzac Georges from Airbus Group SAS [54]. To extend the potential application of tufting, a novel assembly structure by tufting is figured out in the Chapter 4 of the present thesis.

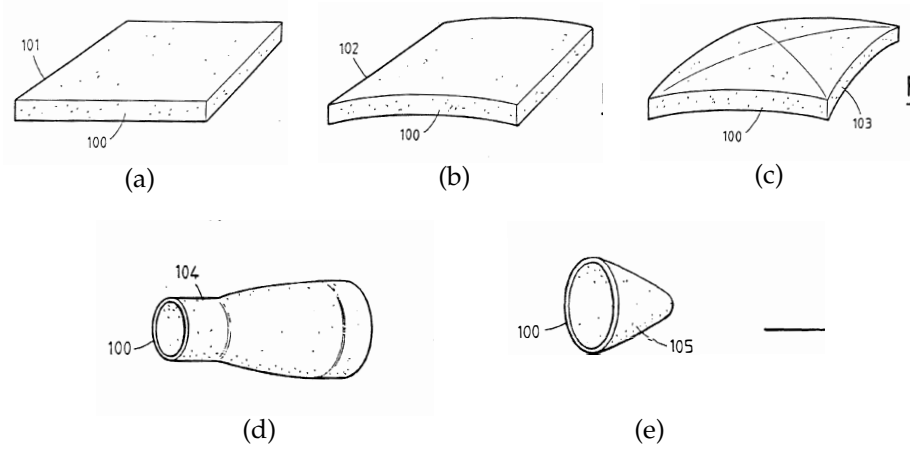

Fig. 1-18. Schematic of aviation applications in (a) flat panel, (b) convex panel, (c) bi-bonvex pane, (d) nozzle of rocket engine and (e) spacecraft nose [70].

- **Tufting device**

On account of the requirement of cost-effective manufacturing in the composites industry, the tufting process is therefore anxious to automate. This section will introduce the tufting device founded in the open literature. The commercial tufting head (see Fig. 1-19) developed by the German Aerospace Centre (DLR) Institute of Structural Mechanics in Brunswickin cooperation with Keilmann Sondermaschinenbau (KSL) GmbH (Lorsch) is operated on a conventional CNC sewing unit at the DLR. Tufting thread is carried by a specially designed needle with an inclined needle eye to penetrate the dry perform and is held by the friction between the

thread and the surrounding fabric. A presser foot helps to avoid the pulling-out of the inserted loops during subsequent penetration. The tufting head can be used which allows for inserting the stitching thread under various angles and at the lowest possible thread tensions [71]. CNC sewing unit provides a 60 mm lift of the crankshaft, which allows for the stitching of, particularly thick materials. A large application area can be covered by controlling the needle position in a bandwidth of 0 to 40 mm. A particularly small "hold-down" device also allows for inaccessible areas such as the notches of mounted stringers on the wing shell to be stitched. The simple tufting mechanism and compact tufting head design allow maximum variability in stitch spacing of 2-10 mm, seam radius, insertion angle (45° - 135°) and up to 1000 tufts per minute are possible [72].

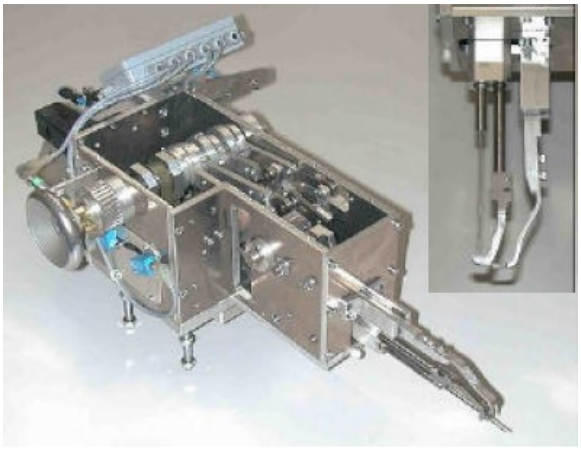

Fig. 1-19. A "Tufting Head" developed by KSL GmbH, Lorrsch and DLR, Institute of Structural Mechanics, Brunswick for operation on conventional CNC machine [25].

Fig. 1-20 reveals that QinetiQ Company uses an automated tufting equipment supplied by KSL for the production of TTR dry fibre preforms with robotic tufting techniques. Structural health monitoring systems have also been incorporated into thick section composites using these techniques. The robot is mounted on a 5 m rail to enable the production of large components typical of those required by the aircraft industry, and it is teamed with a tufting head, allowing both preform production and addition of through-thickness reinforcement. This equipment can handle large 3D shaped preforms of up to 3 x 2 mm^2. The maximum thickness of the tufted preform can be up to 40 mm. Stitch distance is variable between 2 to 10 mm. The maximum sewing speed is 600 rpm. It is possible to tuft in a variable angle with a

wide range of sewing threads [Fiche technique QinetiQ].

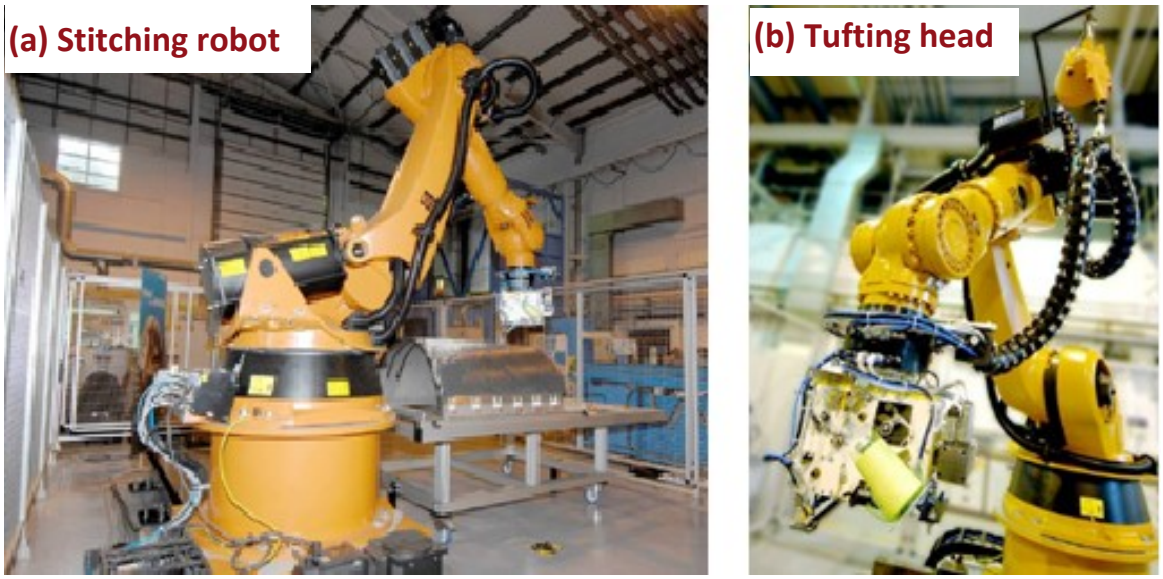

Fig. 1-20. (a) Stitching robot and (b) tufting head used in QinetiQ Company [73].

Dell'Anno G et al. [74], used a KSL KL150 tufting head, interfaced to a Kawasaki 6-axis robot arm FS 20N. The control of the tufting process is achieved using AS a machine programming language designed specifically for use with Kawasaki robot controllers, and the dedicated KCWIN software from Kawasaki. Fig. 1-21 shows the complete tufting needle arrangement. The machine set up has an adjustable tufting speed which can insert up to 500 tufts per minute.

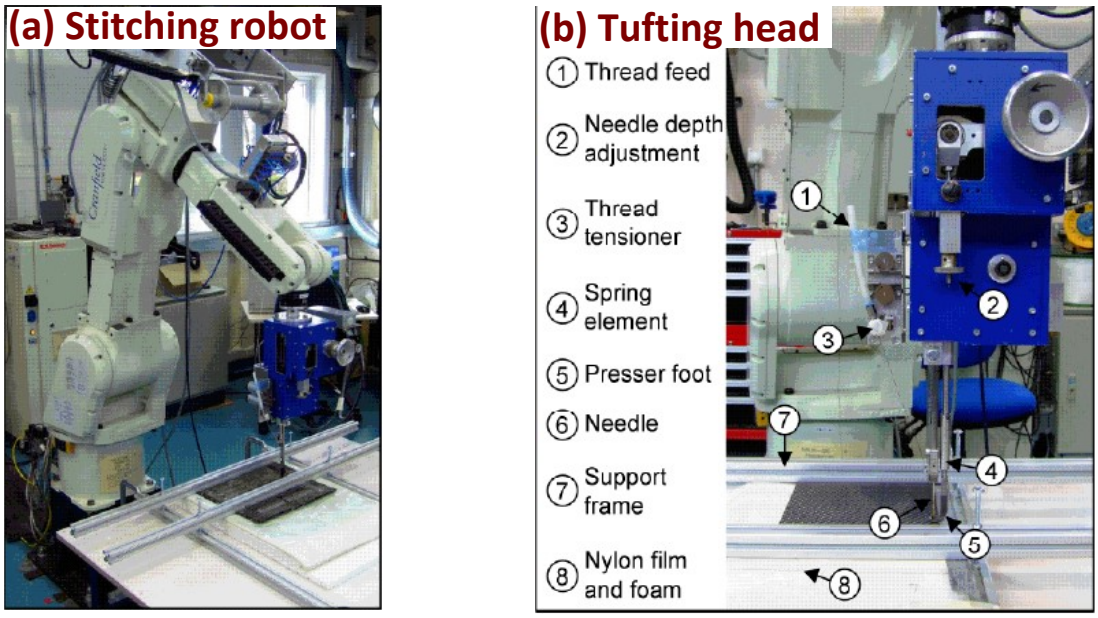

Fig. 1-21. (a) Kavasaki FN20 stitching robot and (b) KSL KL150 tufting head [64].

To overcome the stitching technique limitations, which are not efficient and cannot be applied in the majority of cases, mostly due to the large dimensions and the 3D structure of the FRP components. Altin Näthechnik GmbH produced a new type of unilateral tufting suture device: a robot-supported 3D stitching system (Fig. 1-22(a)) which is adapted to the tufting process. It integrates the stitching process into the stitching head, and connects the stitching head with a high-precision robot with multiple degrees of freedom so that the shape and size of the stitching preform are no longer limited by the equipment [71]. A major advantage is that the stitching machine does not need workpiece feed items known from conventional stitching machines. Therefore, careful handling of the workpiece is ensured and the structural damage caused by the transport system can be prevented. The process is applicable for performing the preform up to 40mm of thickness. The tufting head as shown in Fig. 1-22(b) is variable regarding its stitch length, insertion angle, and the length of the loops. Moreover, negative values for the loop length can be achieved, resulting in a partial reinforcement of the preform. Since for such a reinforcement it is not required to penetrate the workpiece completely, it is possible to reinforce the preform directly with the RTM tool. The wide range of parameters for stitch distance, needle insertion, and loop length is adjusted by electro-mechanical

means and can therefore be modified via the robot control system while performing stitching (tufting included) jobs.

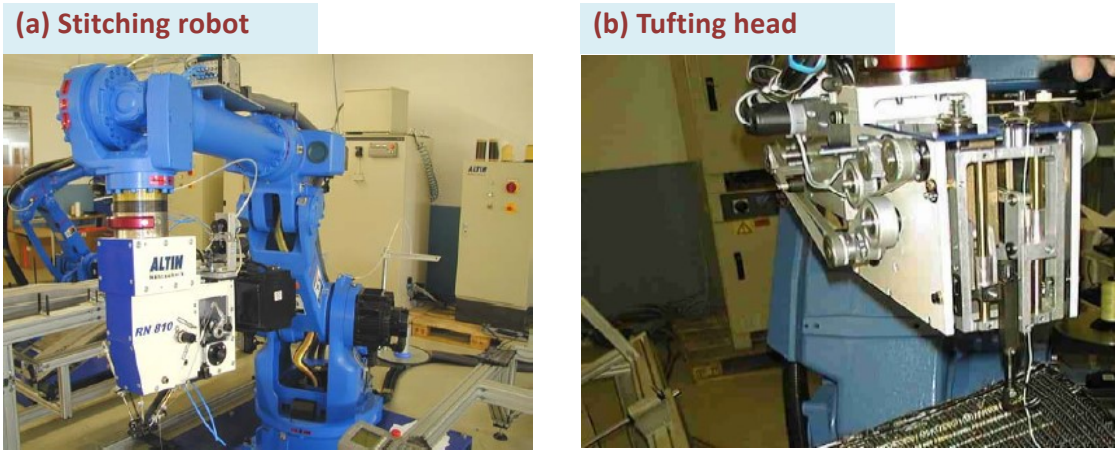

Fig. 1-22. (a) Stitching robot system and (b) tufting head developed by Alitin Näthechnik GmbH [75].

Additionally, on account of the study in-depth of the tufting process, a small-size tufting device is developed to meet the laboratory research environment. For example, since 2014, our laboratory (GEMTEX) began to use a home-design tufting device to perform the tufted preforms. This is an automated tufting equipment designed by Liu et al. [57], as shown in Fig. 1-23. The present tufting device is 700 $\times$ 400 mm^2, and it is made up of two pneumatic systems and four main systems: tufting system, presser foot system, and feeding system. The tufting process begins with the tufting thread (twisted or untwisted,various raw materials), which is unwound from the bobbin carried by the feeding system, firstly passing through a tension controller into a tufting needle (for example a hollow needle with a diameter of 2 mm in the present thesis), then the tufting needle and the presser foot cooperate with each other to penetrate into the preform, and the free loop is performed in the foam thanks to the tufting system, presser foot system and the frame, whose responsibility is to support the foam and the tufting head. Meanwhile, some essential tufting parameters such as tufting spacing, tufting length, tufting direction, and presser foot pressure can be predetermined with this automated tufting device. For instance, the maximum tufting length is determined by the range of the pneumatic cylinder which links with the tufting needle [29, 76]. Simultaneously, another pneumatic is in charge to preset the pressure of the tufting needle

and presser foot. Table 1-2 shows the main parameters of the present tufting device.

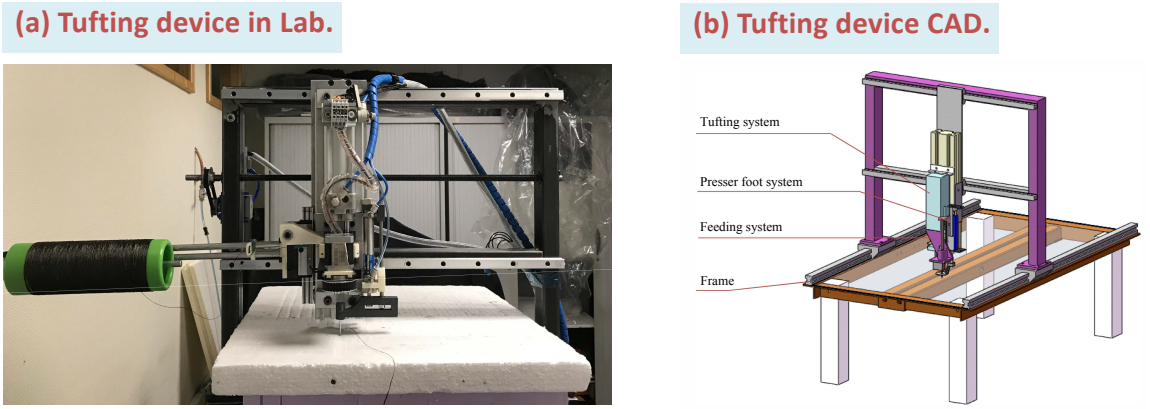

Fig. 1-23. Tufting device (a) using in GEMTEX Lab. and (b) CAD version [29].

Table 1-2
Main parameters of tufting device [29].

Parameter	Values
Size of tuft machine	$700 \times 400\ mm^2$
Needle inserting speed (after optimisation)	$60\ mm/s$
Needle retreating speed (after optimisation)	$60\ mm/s$
Needle diameter	$2\ mm$
Maximum needle stroke	$50\ mm/s$

1.3.2 Manufacturing of tufted composites

Tufting is a type of local 3D textile technology, which differs from the integral 3D weaving, knitting, braiding technologies, where the former is a localized Z-reinforcement penetrated into the 2D preform (laminate preform in general). The principle consists of the insertion of a reinforcement thread in the Z-direction; which can also be executed with different angles. The thread is introduced with very low tension and the needle retreats, leaving a loop. The penetration depth is adjustable. The loop could be internal or external to the laminate and overflow by a few millimetres.

Fig. 1-24 shows that only one thread access to one side of the preform, instead of two, is required during the tufting process. Developed from conventional stitching technology, tufting technology is a method used to link together dry reinforcements or strengthen the composite by inserting thread through the thickness of the preform. It involves the novel aspect that it uses a single needle to introduce a thread into the structure without tension. In traditional stitching technology or other technologies such as braiding and knitting technology, threads are bound by forming a knot or interlock in the preform. Because of the shear force between the threads, the performance of the reinforcement is weakened. Comparing with other 3D forming technologies, tufting applies a tension-free tuft which can reduce the sewing effect on interlaminar performance and avoid the weakened zone around the tuft.

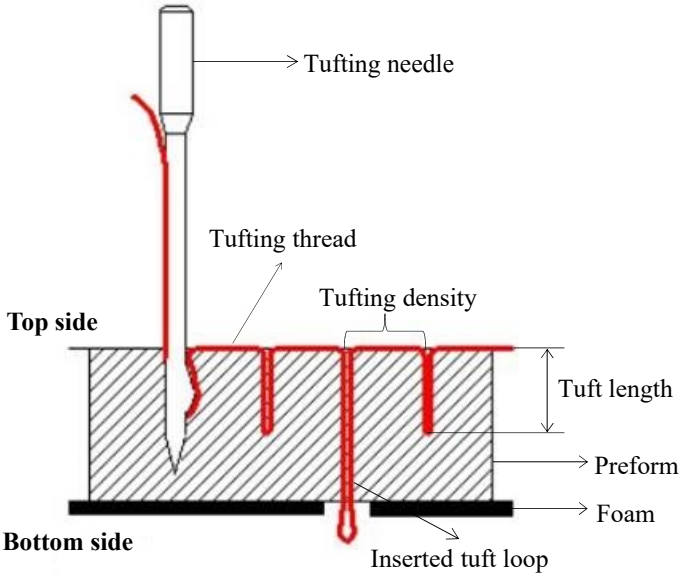

Fig. 1-24. Schematic of tufting parameters [29].

Tufting can achieve various complex shapes, such as a cylindrical hollow shape with a cylindrical foam mentioned in the patent applied in 1995 of Aerotiss® [70], and its concept schematic is shown in Fig. 1-25. Apart from the abovementioned tufting parameters, the foam is also a very influential one, which plays an important role to influence the tufting quality. The researchers [76, 77] are also agreed that foam with a proper density and softness can help the tuft loop stay well in the preform and foam to complete the tufted preform. Moreover, Dell'Anno [77] proposes two kinds of partially inserted tufts, a nice idea for tufting a tubular preform

is demonstrated in Fig. 1-26.

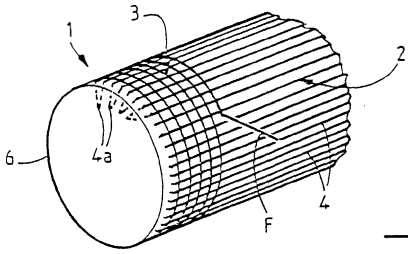

Fig. 1-25. Cylindrical support [70].

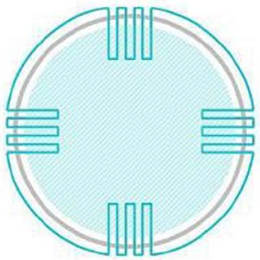

Fig. 1-26. Tuft loops emended in the closed, foam filled preform [77].

Tufting is fairly suitable for load-bearing structures intended to be manufactured via dry fabric/liquid resin infusion processes. The latter is the closed moulding method used to cure tufted preforms, with the most common Liquid Composite Molding (LCM) process after the tufting process. In the open literature, numerous researchers [78–86] prefer the Vacuum-Assisted Resin Transfer Moulding (VARTM) process to accomplish high-quality tufted composite parts. This process injects the resin into the fibre preform placed between rigid moulds to control the dimensional tolerances. On the contrary, there are some other researchers [57, 87] who would like to select the Liquid Resin Infusion (LRI) process to manufacture the final tufted composite pieces. The process is utilized in flexible conditions, such as in low-cost open moulds with vacuum bags in nylon or silicone [9]. This is the reason that LRI process is chosen in the present thesis. The LRI set-up is presented in Fig. 1-27, which demonstrates the LRI principle: the preform is firstly placed on the caul plate with the release film. And then is enclosed in a vacuum bag, then the peel ply and infusion flow media are superposed on the preform sequentially to complete the LRI set-up. While the resin injecting differential pressure is created by a vacuum at the vent of the resin system, it leads to the impregnation of the compressible perform in the transverse direction.

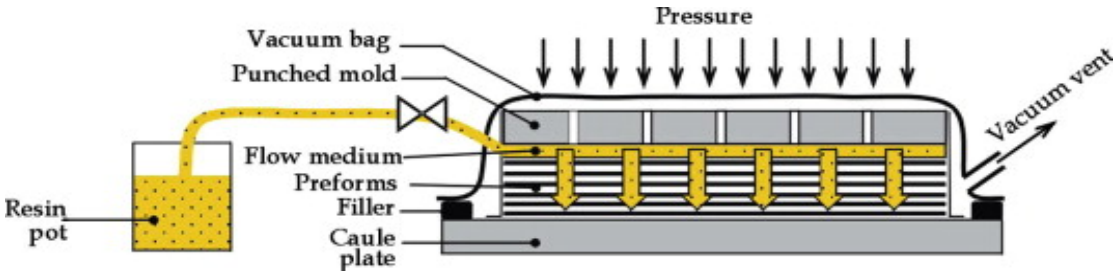

Fig. 1-27. Schematic of liquid resin infusion process [9].

Preparatory work: the definition of tufting density

Lack of criteria and uniform definition in the literature, the definition system of tufting density proposed by us is shown in Fig. 1-28. It includes lengthwise density, widthwise density, and total tufting density in the present system. Moreover, it is obviously found that this tufting density system can even be suitable to the angular tufting path (namely, ***path angle*** θ) shown in Fig. 1-28 (b). The column spacing is perpendicular to the machine direction and, conversely, the row spacing is parallel to the machine direction. Tufting spacing therefore depends on the row spacing and tufting path angle, and vice versa. Initially, it needs to define the ***Tuft Point*** (***tuft*** for short), which refers to the insertion point of the tufting threads left on the top side (the unit is pts).

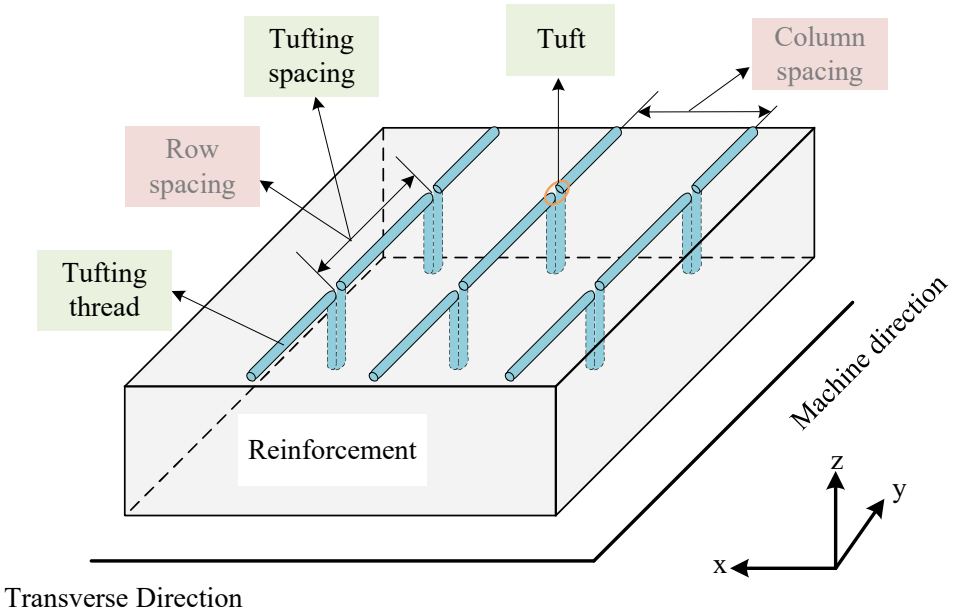

(a)

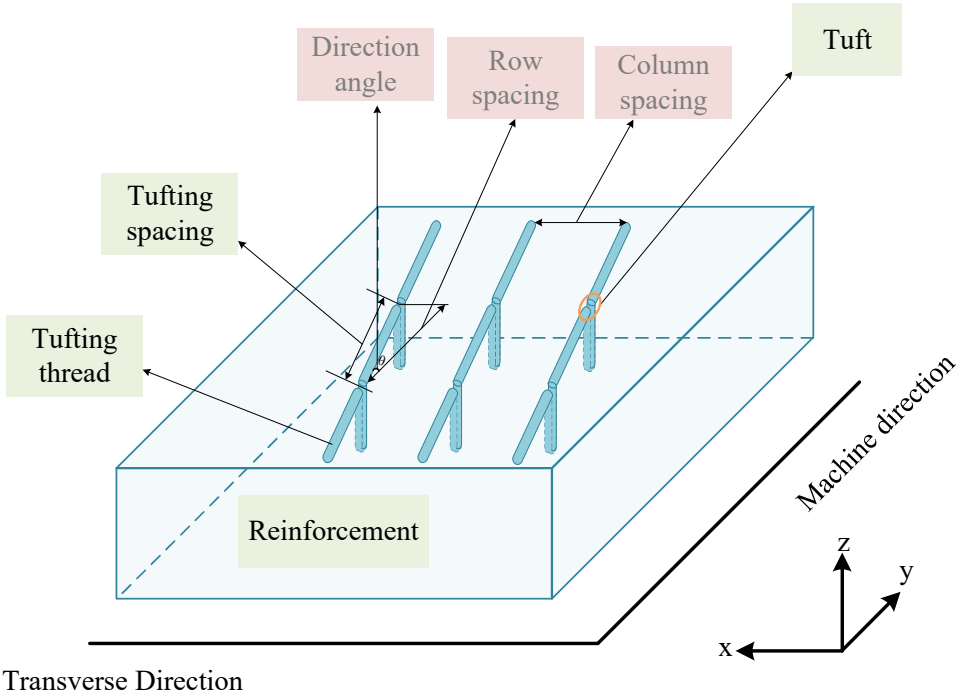

(b)

Fig. 1-28. Definition of tufting density, schematic of tufting direction of (a) 0 angle (b) with a direction angle.

The definitions of the items are given in the following:

Tufting path angle(θ) refers to the angle between the machine direction and the tufting path direction (in °).

Column spacing (S_x) is the distance between two adjacent tufting columns (in mm).

Tufting spacing (S_t) is the distance between two adjacent tufts (in mm); Therefore, the **row spacing(S_y)** (in mm) can be calculated as Eq.(1.1):

$$S_y = S_t \times \cos\theta \tag{1.1}$$

Lengthwise density (D_l): The total tufts within the unit length in each column of the preform (in pts/cm), here take the number of tufts within 1 cm to count along the machine direction and multiply by ten, shown in Eq.(1.2):

$$D_l = \left\lceil \frac{10}{S_y} \right\rceil = \left\lceil \frac{10}{S_t \times \cos\theta} \right\rceil \tag{1.2}$$

Widthwise density (D_w): The total tufts within the unit length in each row of the preform (in pts/cm), here take the number of tufts within 1 cm to count along the transverse direction and multiply by ten, shown in Eq.(1.3):

$$D_w = \left\lceil \frac{10}{S_x} \right\rceil \tag{1.3}$$

Tufting density (D_t): The total tufts per square unit of the preform (in pts/cm^2), calculated as Eq.(1.4):

$$D_t = \left\lceil \frac{100}{S_x \times S_y} \right\rceil = \left\lceil \frac{100}{S_x \times S_t \times \cos\theta} \right\rceil \tag{1.4}$$

According to several validation calculations, the value of tufting density is logically rounded up as shown in the above formulas. On the basis of the definition procedure, the tufting density can be characterized by different parameters depending on the situation, which leads the research more accurate and simplified. Such as tufting spacing, total tuft points (total tufts) of the whole preform, namely as total tufts in sample.

1.3.3 Micro - and meso-structure of tufted composites

- **Fiber undulation, crimp and degradation**

As shown in Fig. 1-29, a slight degradation of the tufting thread can be observed and the tufting thread has become slightly untwisted during the tufting process. Meanwhile, there is the knowledge that using the twisted tufting thread could facilitate insertion and avoid degradation during tufting [57]. Only one-sided thread is required in the tufting process, the stability of the thread is less than two threads stitching. The degradation and winding occur during both the tufting and curing process. Additionally, it is assumed to date that these defaults may arise due to the tooling, preform structures, and laminates configurations. However, less research has been carried on this topic, particularly the tufting degradation. It is of interest to understand the degradation mechanism of tufting thread, it will be investigated in detail in Chapter 2 of the present thesis.

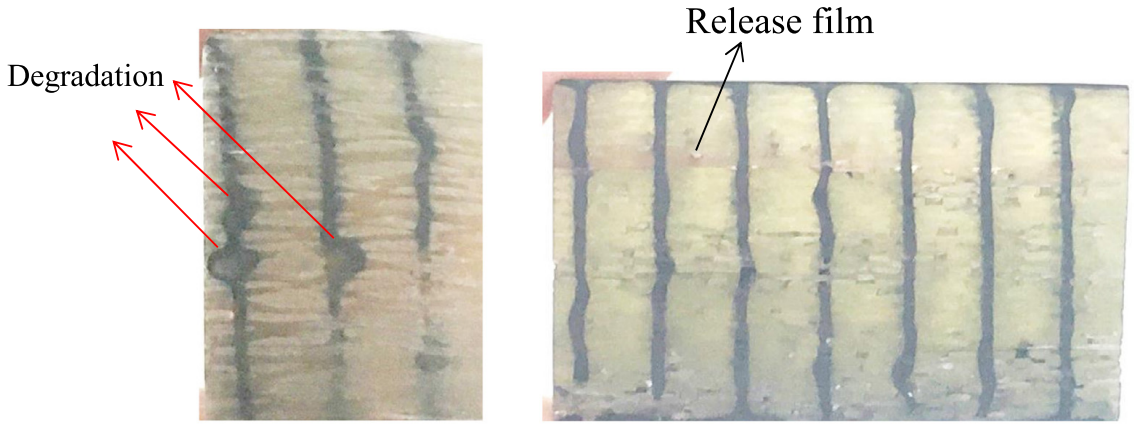

(a) Degraded threads (b) Winding threads

Fig. 1-29. Degradation of tufting thread [57].

- **Resin-rich zones**

As shown in Fig. 1-30, an eye-like resin-rich area around each tuft (two resin pockets and a tuft) can be found by means of micro-observation, and it is generated after the needle penetration and subsequent mould curing stages. The resin-rich zone is a defect phenomenon, with the penetration of the thread, the laminated fibres pushing apart around the tuft, bringing a void which will be filled with resin during the resin infusion process, and the resin pocket product. The area is resin-rich zone. If the tufting spacing is too closed that the resin-rich zone (resin pockets) may overlap, where may easily occur crack initiation and propagation because of the stress concentration [57, 64, 74, 84]. On account of resin-rich zone can occur at different scales of composites. It makes sense to optimise the tufting process, including the optimisation of tufting parameters (tufting density, tuft length, free tuft loop, etc), the improvement of tufting machine, and the selection of raw materials for tufting thread, tufting needle, and foam. The influence and optimisation of tufting density is fully investigated at different tufting scales (tufting thread in Chapter 2, tufted laminates in Chapter 3 and tufted assembly in Chapter 4) in the present thesis.

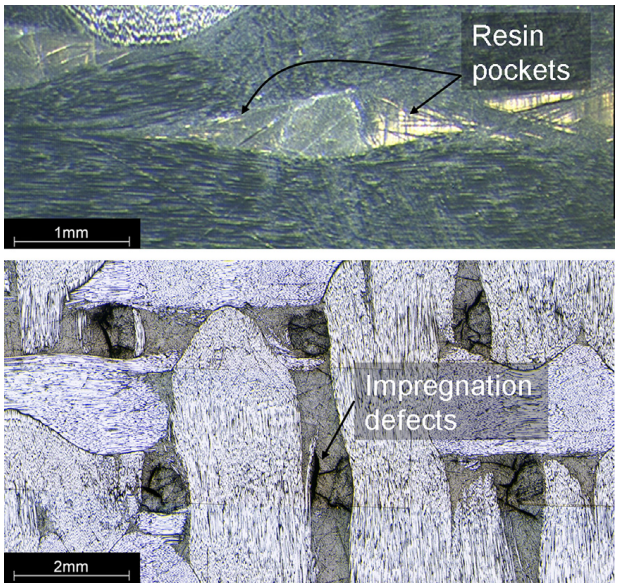

Fig. 1-30. Resin-rich zones of tufted composites [74].

- **Tuft inclined**

Fig. 1-31 shows the micro-observation of the cross-section of a tufted composite sample. The tufting thread with a free loop and glass yarns can be observed. There is no concentrated porosity but some resin-rich zones are around the tufting thread. Meanwhile, it is noticed that the tufting threads are slightly inclined, and the inclination is inferior of 4 °. Liu et al. [57] have proposed that it is probably caused by the flow of resin during the infusion stage. It is considered that the tuft inclination may occur unintentionally during manufacturing affecting the delamination. In general, such inclined tufts, especially unintentional inclination, may bring detrimental effects on the delamination toughness. Of course, except for special circumstances, like Lombetti [88] has pointed out that the inclined tuft could improve the delamination toughness under mode II sliding loading. It makes therefore interesting to investigate the interlaminar shearing behaviours of tufted products at different scales under the mode II sliding loading. And it will be given in-depth account on the topic in Chapter 3 of the present thesis.

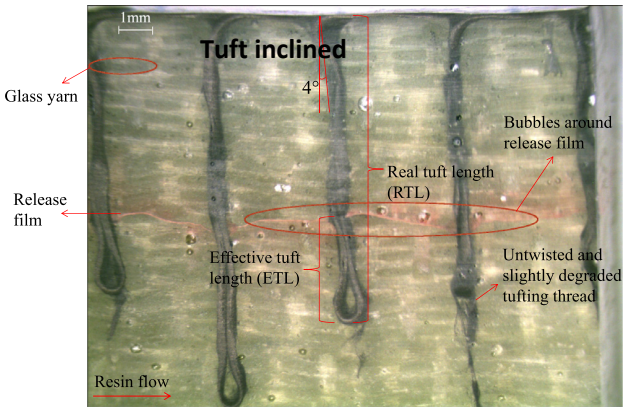

Fig. 1-31. Inclined tuft [57].

1.3.4 Advantage of tufting

As an ongoing TTR technology in composite , research on tufting has not sufficient than other TTR technologies. However, its good out-of-plane performance while the weakened in-plane performances have been still studied according to the open literature. The story about "mechanical properties of tufted composites" will therefore be taken up in terms of both pros and cons in the present and the next sections, respectively. Firstly, some open studies have confirmed the enhancement of tufted composite in the fracture toughness. Meanwhile, the good impact damage resistance and joint strength of the tufted composite have been determined, as introduced below.

- **Interlaminar fracture toughness properties**

The improvement of interlaminar fracture toughness gained by the tuft. To date, some studies have revealed that tufting reinforcement provides a significant improvement on the fracture toughness and delamination resistance by reducing the crack opening displacement and by resisting the crack sliding displacement under **Mode I** and **Mode II** loading, respectively [83, 89, 90]. Meanwhile, interlaminar tufting increases its properties under **mixed modes I/II** loading condition. How-

ever, with the lack of significant demand at the engineering application level, little research may focus on the delamination resistance under the Mode III loading condition.

The delamination crack initiation toughness of the tufted composite has not improved but has been relatively reduced [88]. It is believed that due to the resin layer of the delamination, the plane of tufted composites is thinner, compared to that of the untufted one (also called non-tufted). Moreover, the interlaminar fracture toughness properties under mode I loading of tufted laminates have been characterised by experimental and Finite Element(FE) analysis [91, 92]. The toughness has been measured using the mode I double cantilever beam (DCB) test for laminated composites [92]. The mode II properties have been measured using the end-notch flexure (ENF) [81], end-loaded-split (ELS) [51] fracture toughness test. A large number of experimental studies using the ENF test method have measured the mode II delamination resistance and identified the toughening mechanisms of tufted carbon epoxy laminates. However, there is a lack of work in the literature reporting the fracture behaviour of tufted laminates under mode II loading. It could be related to the difficult to apply pure mode II loading due to the opening mechanism acting in the delamination crack. However, a 5-fold increase of the total fracture toughness under shear loading for the tufted specimens mentioned by Bigaud [93]. Delamination toughness is, without doubt, the most studied property of tufted composites [81, 84, 91, 92, 94]. Interlaminar fracture comprises energy losses in terms of matrix cracking, fibre breakage, fibre pull-out, fibre slipping, and fibre debonding, which differ from metals where fracture toughness depends on the energy dissipated at the crack tip [95]. Mode I fracture toughness values more than 16 times greater compared with non-tufted composites by Colin de Vediere et al. [94] (see Fig. 1-32). Colin de Verdiere et al. [96] have also studied the tufting effect on mode II fracture toughness of carbon non-crimp fabric composites. It showed about 2 times higher than the non-tufted samples, as Fig. 1-33 revealed. Furthermore, tufting increases the interlaminar toughness of long cracks under mode I, II, and mixed modes I/II loadings.

It is important to understand this subject to better control the tufting technology, and contributes along with other textile technologies [95, 97–107] to improve the delamination behaviour of composite structures.

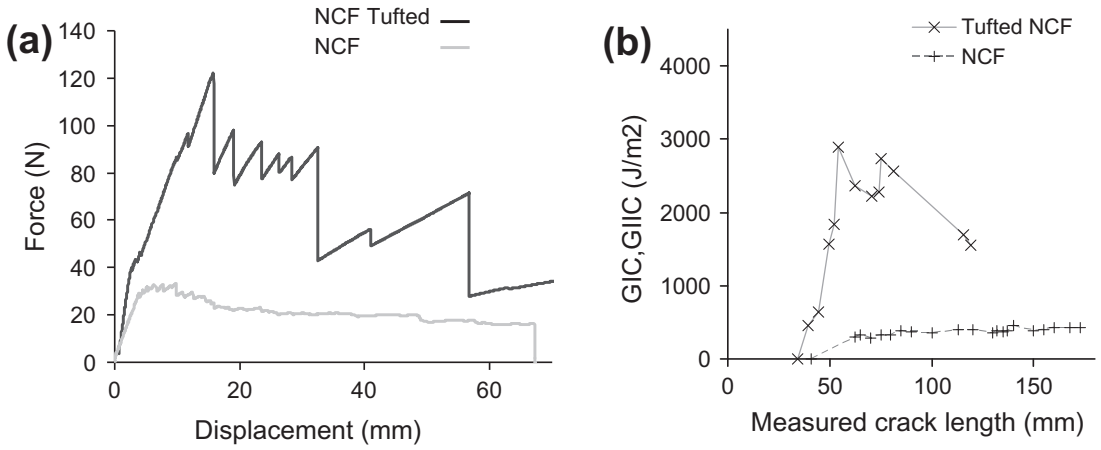

Fig. 1-32. Tufted and untufted composites delamination characteristic in static: (a) force versus crack displacement and (b) G_{IC} versus crack length [94].

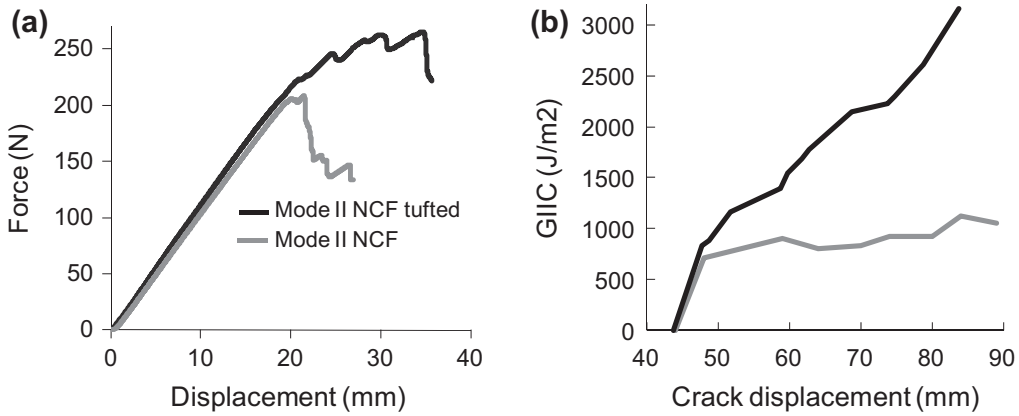

Fig. 1-33. Standard and tufted NCF composites response to delamination: (a) force versus crack displacement, (b) strain energy release rate [96].

- **Impact damage tolerance properties**

Studies on damage tolerance and CAI behaviour demonstrate that even though all TTR methods have a positive effect, tufting is expected to have the best performance compared to either stitching (regardless low pretension or high pretension) or z-pinning, with minimal in-plane strength decay [27, 108]. Other studies [109] have also shown some effect of tufting parameters, such as tufting density, raw materials, layup of reinforcement laminate, and thickness of the tufted composite, on the strength of the final composite part [86, 110, 111]. The impact is a dynamic event that refers to the momentary load on a small area, and it can also be seen as a transient process in which energy is transferred from the outside to a structural system [112, 113]. It can be determined by 1) **Impact damage tolerance:** which associate with the reduced stability and strength of the structure due to the damage [114, 115]; and 2) **Impact damage resistance:** which is related to the response and damage caused by the impact [116, 117]. The introduction of Z-direction reinforced thread has well improved the impact damage caused by the encountered in conventional laminated composites [58, 78–80, 83, 85, 86, 94, 118–121]. For instance, a low-velocity Izod impact is presented in the study of Najafloo et al. [86], and as shown in Fig.1-34. Deconinck et al. [118] have studied the effect of tufting density of Z-direction carbon thread reinforced composites on high-velocity impact-induced behaviour. The results (see Table 1-3) have revealed that the delamination area can be maximum decreased till 24 % while the tufting density increases compared to untufted composite laminates.

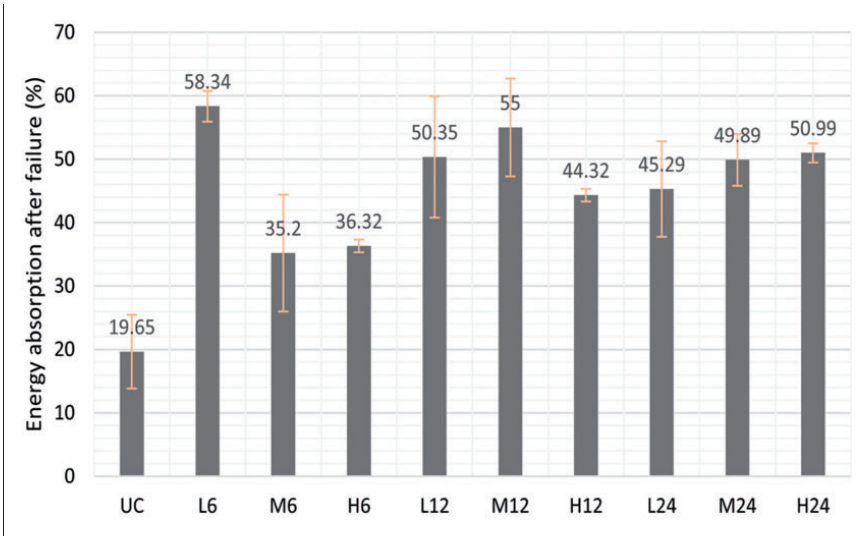

Fig. 1-34. Energy absorption after failure in all composites [86].

Table 1-3
Delamination area [118].

Reference	Tufting areal density (%)	Normalized delaminated area
None	–	1.00
2K-p_1	d_1	0.76
2K-p_1	d_1	0.76

Furthermore, a large improvement is that the damaged area is decreased and the ultimate compressive strength is increased. Tufting reinforcements are found to decrease the damaged area up to 4 times when compared to the non-tufted laminates. Recently, Lombetti et al. [119] have studied the lightning strike impact behaviour of metal tufted carbon composites. The results have shown that the metal tufted brings lightning strike impact damage suppressed significantly with internal damage decreasing around 90 % and 75 % compared to untufted laminates for copper and stainless steel as shown in Fig.1-35.

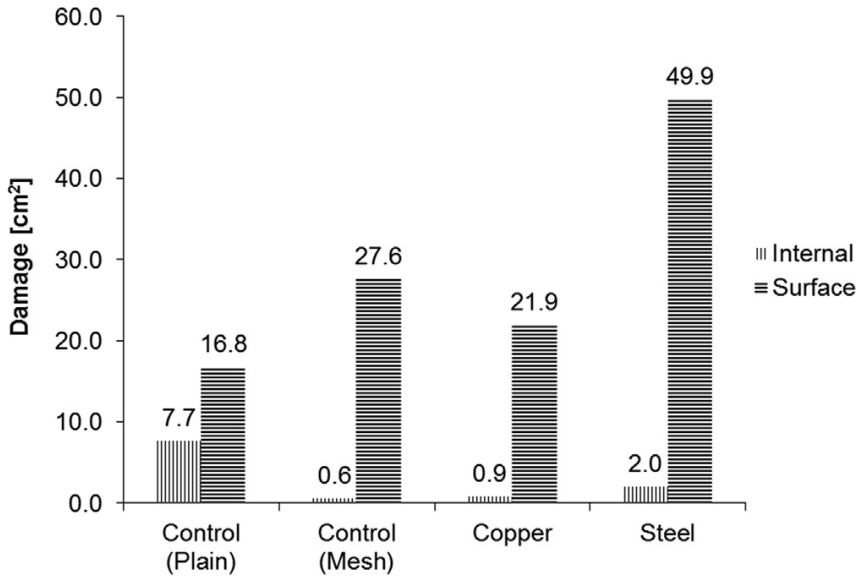

Fig. 1-35. Size of lightning strike damaged area [119].

The improved impact resistance achieved by tufting often results in higher CAI properties [74, 81, 83, 109, 122]. Compression testing after impact (CAI) is a testing method to determine the strength of the impacted specimens still contained after initial testing. It is a destructive test, which can be used to determine the ultimate stress and strain of a specimen after impact. The results can be used to distinguish whether the impacted sample meets the design requirements, meanwhile to optimize the parameters of the composite and its manufacturing process[123]. In accordance with the research on the impact and CAI behaviours of carbon thread composite laminates with various tufting densities, under the tufting configurations of square pattern and angular pattern, respectively, by Matin et al. [83]. The study has pointed out the residual ratio of CAI to CBI (Compression Before Impact). The specimens which achieved the best results on CAI were compared with those on

CBI as a manner of evaluating in-plane properties of the tufted composite. Table. 1-4 has shown that the carbon thread reinforcement with different tufting configurations finally contributes the increase up to 30 % and 28 % of the residual ratio, respectively. The residual ratio of glass and carbon tufted thread composite laminates increased the residual ratio to 25 % and 27 %, respectively, according to the study of Dell'Anno et al. [74]. The loss of in-plane ultimate compressive strength arrived until 29 % to T5 configuration and 40 % to A5. This reduction has been reported by many authors whose research on TTR [81, 95, 106, 121]. Moreover, Scarponi et al. [109] have studied the CAI strength of various TTR composites, e.g., tufting, z-pinning, and lock stitch under low and high tension techniques with carbon Z-direction yarn. It is calculated that the CAI strength of tufted composite laminates is superior to the others, which can be specified in the second row of the Table 1-5.

Table 1-4
Ultimate compressice strength on CBI and CAI tests, and the residual ratio (CAI/CBI) [83].

	Ultimate strength (Mpa $\pm$ SD)			Residual ratio(%)	Residual ratio(%)
	CBI	CAI 25J	CAI 60J	25J	60J
REF	453.1 ± 40.9	176.1 ± 1.3	137.4 ± 1.1	38.9	30.3
T5	323.9 ± 28.9	223.5 ± 2.5	171.5 ± 2.9	69.0	52.9
A5	271.9 ± 19.7	178.9 ± 4.9	157.8 ± 4.9	58.8	58.0

Table 1-5
Experimental results in terms of CAI strength [109].

	No stitched	Low tensioned lock stitch	High tensioned lock stitch	Tufting	No z-pins (hybrid panel)	z-pins (hybrid panel)
CAI (MPa)	282	323	303	328	295	276
Dev. st.	25.3	20	11.5	28	19.1	17.3
CV %	9	6.2	3.8	8.5	6.3	6

- **Joints strength**

As the role of the tufting thread is to link two or more layers of the basic 2D preform, the joint strength is becoming an interesting problem to study. The strength of composites reinforced by tufting technology has been verified by experimental testing [65–69, 78, 120, 124–126]. Tufting technology has been used to reinforce the stiffeners to enhance their performance and damage tolerance. In 2006, Cartié et al. [78] have investigated the joint behaviours by tufting and stitching. Milles et al. [120] have investigated the influence of tufting density and thread material on carbon fibre T-stiffeners (see Fig. 1.36(a)). The manufacture of the structures utilized a pre-infused and cured web plate, positioned between the two flanges of the dry preform. The flanges were tufted on the skin, and subsequently, the infusion process moulded of the whole moulded T-stiffener plate with two different regions reinforced by glass and carbon threads. The pull-off test carried out on the specimens has shown a considerable enhancement of the absorbed energy, especially for the densest tufting specimens, 309 % and 215 % for carbon and glass fibre threads, respectively. The maximum load has also improved up to 54 % and 62 %, for carbon and glass fibre threads, respectively, when compared to the control structures. Fig.1.36(b) has shown the comparison results of energy absorption under pull-off loading on carbon and glass tufted thread with the non-tufted specimen.

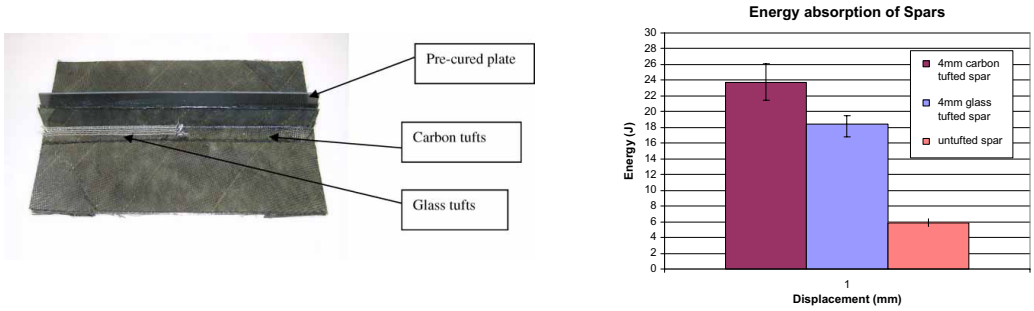

(a) (b)

Fig. 1-36. Results of Mills (a) Spar tufting and (b) Energy absorption [120].

Kratz et al. [125] have studied the damage of four bending tests on the T-stiffener, the results are shown in Fig.1-37. Back in the year 2011, Préau et al. [124] have demonstrated their research results of Ω-stiffener by tufting on "comptes-rendus des JNC 17". Whilst, other assembly parts can be taken into account. [52] outline

tests performed on T-joints with different stitching or tufting patterns and combined tensile shear loading conditions.

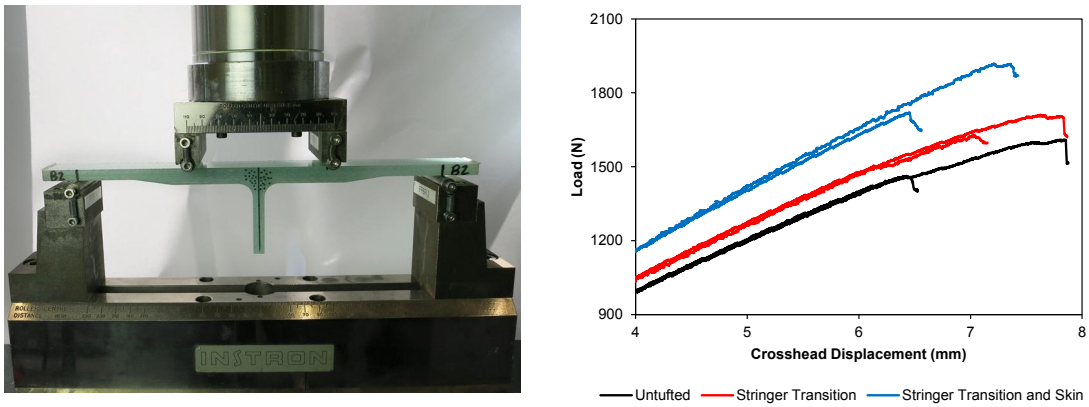

(a) (b)

Fig. 1-37. Results of kratz (a) Testing specimens in four-point bending and (b) First failure load-displacement plot for skin-stringer tests [125].

1.3.5 Disadvantage of tufting

The advantages of improvement in interlaminar fracture toughness and impact damage tolerance are detailed above, which are typically accompanied by a reduction of in-plane properties. Reduced to the elastic properties, the strength and fatigue performance due to tufting are examined and compacted to change the in-plane properties of composite materials with other types of TTR [27, 38, 91, 92, 109, 127]. The low tension under the tufting thread inserted results in a reduction of the stitching effect on the in-plane properties of polymer matrix composites [95]. Although relative to the research on the advantages of this product, the research on the disadvantages is relatively litter, there are still some researches on this aspect. However, the reduction of in-plane mechanical performance is concerned during manufacturing. The related references have revealed that the in-plane tension strength and compression properties of the 3D tufted composite are 10-15 % lower than that of 2D non-tufted composites with the same lay-up consequence. Treiber [64] and Dell'Anno [74] have studied the effects of tufting and the tufting process in detail, and they have observed that tufting can significantly

improve the delamination resistance (by threefold) within a laminate with only a small reduction (approximately 10 %) in the in-plane mechanical properties due to the disruption of the tuft on the fibre alignment. JWG [64] has pointed out that fibre misalignment and local stress concentration are essential factors for the observed reduction in axial tensile strength of up to -19% in unidirectional composites. Suppression of delamination and natural fibre waviness (in woven laminates) have reduced the detrimental effect to only -11 % and -1.5 % for biaxial non-crimped fabric (NCF) and woven fabric respectively. Fibre breakage from needle penetration has no effect on the tensile strength. The reduction in strength properties of the tufting laminate has been reported by some researchers [95, 121]. The longitudinal modulus of the 3D specimen was 6 % lower than that of the 2-D specimen in tensile as well as compression. The failure strength of the 3D specimens was 6 and 13 % lower than that of the 2D specimens in tension and compression, respectively [122]. Karuppannan et al. [95] compared unidirectional and quasi-isotropic tufted carbon fabric composites and showed that in-plane properties of quasi-isotropic and notched composites are not well affected by transversal tufting reinforcement.

1.4 Conclusion of chapter one

The present chapter first briefly accounts for the composite materials. Then moulding technologies, textile reinforcement architecture (from 2D to 3D), and corresponding technologies for particular textile composites (from traditional methods to the specialties ones) have been introduced in sequence. Followed by a full overview of published research and development work on tufting technologies and tufted composites. Over the past decades, there has been some significant progress, with advantages such as better interlamination resistance, damage tolerance, and joint strength. However, the poor in-plane mechanical properties of tufting products, due to the presence of in-plane threads which destroy the 2D structure. The present thesis investigates the tufting at multi-scales in order to fully understanding the tufting. The first topic is on the tufting thread scale. This topic focuses on understanding the degradation mechanism of tufted yarns and proposes a solution in terms of the tufting process. The following topic is about the tufted laminate scale. The topic concentrates on the investigation of the inter-

laminar shear properties of tufted laminates at multi-scales architecture, in order to fully understand the role of each parameter in the development of mechanical properties for the final composite product. The final topic is the most interesting one. This topic contributes to the conception and the manufacturing of tubular assembly composites by tufting, in which a prototype of tufted tubular assembly is proposed, and a tufted plate assembly composite is manufactured. By means of the investigation on basic mechanical properties under tensile loading, various parameters are investigate and optimised. Throughout the whole thesis, it is found that the tufting thread is a crucial influence. Therefore, a preliminary work on the modelling and simulation of tufted tubular/plate assembly composite based the tufting thread will be presented as in perspective section.

Bibliography

[1] CompositeLab. What Are Compsite, . URL `http://compositeslab.com/composites-101/what-are-composites/`.

[2] Wikipedia. Composite meterial. URL `https://en.wikipedia.org/wiki/Composite_material`.

[3] M Fazeli, JP Florez, and RA Simão. Improvement in adhesion of cellulose fibers to the thermoplastic starch matrix by plasma treatment modification. *Composites Part B: Engineering*, 163:207–216, 2019.

[4] R Elhajjar, V La Saponara, and A Muliana. *Smart Composites: Mechanics and Design (Composite Materials)*. CRC Press, 2017. ISBN ISBN 978-1-138-07551-1.

[5] L Tong, AP Mouritz, and MK Bannister. *3D fibre reinforced polymer composite*. Elsevier, 2002.

[6] J Bai. *Advanced Fibre-Reinforced Polymer (FRP) Composites for Structural Applications*. Elsevier, 2013. ISBN 978-0-85709-418-6.

[7] CompositeLab. Open Molding, . URL `http://compositeslab.com/composites-manufacturing-processes/open-molding/`.

[8] CompositeLab. Closed Molding, . URL `http://compositeslab.com/composites-manufacturing-processes/closed-molding/`.

[9] P Wang. *Étude numérique et expérimentale de procédé d ' élaboration des matériaux composites par infusion de résine*. PhD thesis, Ecole Nationale Supérieure des Mines de Saint-Etienne, 2010.

[10] P Wang, S Drapier, J Molimard, A Vautrin, and JC Minni. Characterization of Liquid Resin Infusion (LRI) filling by fringe pattern projection and in situ thermocouples. *Composites Part A: Applied Science and Manufacturing*, 41(1): 36–44, 1 2010. ISSN 1359835X.

[11] P Wang, X Legrand, and D Soulat. Three-Dimentional Textile Preform Using Advanced Textile Technologies for Composite Manufacturing. In *Textiles for Advanced Applications*, pages 161–189. BoD–Books on Demand, 2017.

[12] RQ Wang, L Zhang, DY Hu, X Liu, CH Cho, and B Li. Progressive damage simulation in 3D four-directional braided composites considering the jamming-action-induced yarn deformation. *Composite Structures*, 178:330–340, 2017. ISSN 02638223.

[13] G Nemoz. Textures textiles tridimensionnelles. *Techniques de l'ingénieur*, 2003.

[14] R Kamiya, BA Cheeseman, P Popper, and TW Chou. Some recent advances in the fabrication and design of three-dimensional textile preforms: a review. *Composites Science and Technology*, 60(1):33–47, 2000. ISSN 0266-3538.

[15] FK Ko and GW Du. Textile preforming. In S.T Peters, editor, *Handbook of Composites*, pages 397–424. Springer, Boston, MA, 1998.

[16] SM Lee. *Handbook of composite reinforcements*. John Wiley \& Sons, 1992.

[17] K Fukuta and E Aoki. 3D fabrics for structure composites. In *Proceeding of the 15th Textile Research Symposium*, Philadephia, PA, 1986.

[18] G Hivet and P Boisse. Consistent 3D geometrical model of fabric elementary cell. Application to a meshing preprocessor for 3D finite element analysis. *Finite Elements in Analysis and Design*, 42(1):25–49, 2005. ISSN 0168874X.

[19] P Tan, L Tong, and G P Steven. Modelling for predicting the mechanical properties of textile composites—A review. *Composites Part A: Applied Science and Manufacturing*, 28(11):903–922, 1997. ISSN 1359-835X. doi: https://doi.org/10.1016/S1359-835X(97)00069-9.

[20] Y Song. *Évaluation De L' Apport Simultané Des Coutures Sur La Perméabilité Des Préformes Cousues Et Sur Les Performances Mécaniues Des Structures Composites Cousues*. PhD thesis, 2015.

[21] David Branscomb, David Beale, and Royall Broughton. New directions in braiding. *Journal of Engineered Fibers and Fabrics*, 8(2):11–24, 2013. ISSN 15589250.

[22] LR Sanders. Braiding-A mechanical means of composite fabrication. *SAMPE Quarterly*, 8(2):38–44, 1977.

[23] C Ayranci and J Carey. 2D braided composites: A review for stiffness critical applications. *Composite Structures*, 85(1):43–58, 2008. ISSN 0263-8223. doi: 004.

[24] B Duchamp. *Contribution à l'élaboration de préformes textiles pour le renforcement de réservoirs souples*. PhD thesis, 2016.

[25] AP Mouritz, MK Bannister, PJ Falzon, and KH Leong. Review of applications for advanced three-dimensional fibre textile composites. *Composites Part A: Applied Science and Manufacturing*, 30(12):1445–1461, 1999. ISSN 1359835X.

[26] FK Ko. Three-dimensional fabrics for composites. *Elsevier Science Publishers, Textile Structural Composites*, pages 129–171, 1989.

[27] AP Mouritz. Review of z-pinned composite laminates. *Composites Part A: Applied Science and Manufacturing*, 38(12):2383–2397, 2007. ISSN 1359835X.

[28] K Dransfield, C Baillie, and YW Mai. Improving the delamination resistance of CFRP by stitching—a review. *Composites Science and Technology*, 50(3):305–317, 1994. ISSN 02663538.

[29] LS Liu, T Zhang, P Wang, X Legrand, and D Soulat. Influence of the tufting yarns on formability of tufted 3-Dimensional composite reinforcement.

Composites Part A: Applied Science and Manufacturing, 78:403–411, 2015. ISSN 1359835X.

[30] J Witting. In-mold-reinforcment of performs by 3 dimensional tufting. In *Proceecing of the 47th international SAMPE symposium and exhibition*, pages 1043–51, Long Beach, CA.

[31] Y Rahali, M Assidi, I Goda, A Zghal, and JF Ganghoffer. Computation of the effective mechanical properties including nonclassical moduli of 2.5D and 3D interlocks by micromechanical approaches. *Composites Part B: Engineering*, 98:194–212, 2016. ISSN 13598368.

[32] S Adanur and T Liao. 3D modeling of textile composite preforms. *Composites Part B: Engineering*, 29(6):787–793, 1998. ISSN 13598368.

[33] C El-Hage. *Modélisation du comportement élastique endommageable de matériaux composites à renfort tridimensionnel*. PhD thesis, Université de Technologie de Compiègne, 2006.

[34] A Leca. *Contribution à l' étude de la santé-matière de préformes carbone*. PhD thesis, Le Havre, 2015.

[35] GW Du and F Ko. Analysis of Multiaxial Warp-Knit Preforms for Composite Reinforcement. *Composites Science and Technology*, 56(3):253–260, 1996. ISSN 02663538.

[36] L Gornet. Généralités sur les matériaux composites. Technical report, Ecole centrale de Nantes, 2008.

[37] A P Mouritz. Review of z-pinned laminates and sandwich composites. *Composites Part A*, 2020. ISSN 1359-835X. doi: doi:10.1016/j.compositesa.2020.106128.

[38] AP Mouritz, KH Leong, and I. Herszberg. A review of the effect of stitching on the in-plane mechanical properties of fibre-reinforced polymer composites. *Composites Part A: Applied Science and Manufacturing*, 28(12):979–991, 1997. ISSN 1359835X.

[39] U Beier, JKW Sandler, V Altstädt, H Spanner, and C Weimer. Mechanical performance of carbon fibre-reinforced composites based on stitched and

bindered preforms. *Composites Part A: Applied Science and Manufacturing*, 40 (11):1756–1763, 2009. ISSN 1359835X.

[40] S Dutton, D Kelly, and A Baker. *Composite Materials for Aircraft Structures (Second Edition)*. American Institute of Aeronautics and Astronautics, 2004. ISBN 1563475405.

[41] MB Dow and HB Dexter. Development of Stitched, Braided and Woven Composite Structures in the ACT Program and at Langley Research Center. 1997.

[42] AV Hawley. Preliminary Design of an Advanced Technology Composite Wing for a Transport Aircraft. In *53rd Annual Conference, Long Beach, California, May 23-25*, page 17, Long Beach, California, 1994. Society of Allied Weight Engineers, Inc.

[43] NE Vandermey, DH Morris, and JE Masters. Damage development under compression-compression fatigue loading in a stitched uniwoven graphite/epoxy composite material. Technical report, NASA, 1991.

[44] A Morales. Structural stitching of textile preforms. *Advanced Materials: Looking Ahead to the 21st Century*, pages 1217–1230, 1990.

[45] AP Mouritz and BN Cox. Mechanistic approach to the properties of stitched laminates. *Composites Part A: Applied Science and Manufacturing*, 31(1):1–27, 2000. ISSN 1359835X.

[46] K Klopp, KU Moll, and B Wuifhorst. Stitching technology for technical textiles and composites. *Technische Textilien*, 43(4):E–67, 2000.

[47] T Thurm. Applications of one-sided stitching techniques for resin infusion preforms and structures. *SAMPE journal*, 41(1):64–67, 2005.

[48] T Grundmann, T Gries, M Kordi, and B Corves. *Robot-supported joining of reinforcement textiles with one-sided sewing heads*, volume 49. 2006.

[49] Thomas Gries and Kai Klopp. *Füge-und oberflächentechnologien für textilien: Verfahren und anwendungen*. Springer, 2007.

[50] G Dell'Anno, JWG Treiber, and IK Partridge. Manufacturing of composite parts reinforced through-thickness by tufting. *Robotics and Computer-Integrated Manufacturing*, 37:262–272, 2016. ISSN 07365845.

[51] M Scott, G Dell' Anno, and H Clegg. Effect of Process Parameters on the Geometry of Composite Parts Reinforced by Through-the-Thickness Tufting. *Applied Composite Materials*, 25(4):785–796, 2018. ISSN 15734897.

[52] P Pérès, B Desmars, and JP Léard. Composite behavior of assemblies with AEROTISS® 03S technology. In *16th International conference on composite materials*, pages 1–5, 2007.

[53] G Cahuzac. A revolutionary way for assembling Aerotiss® O3S technology. In *Composie 2003-matériaux et structure composites*, Paris, 2003.

[54] Georges Cahuzac. Stitching head and machine for producing a plate-shaped frame for a piece of composite materialm: France, FR2718759[P], 1994.

[55] Jean-Louis Darrieux. Procede pour la realisation d'une armature de fibres pour piece de matiere composite, et piece composite comportant une telle armature: France, FR2687173[P], 1992.

[56] Georges Cahuzac. Process for producing a fiber reinforcement for a composite material part with non-coplanar walls, and a composite part comprising such an armature: France, FR2687174[P], 1992.

[57] LS Liu. *Development and optimization of the tufting process for textile composite reinforcement*. PhD thesis, Université de Lille 1, 2017.

[58] A Henao, M Carrera, A Miravete, and L Castejón. Mechanical performance of through-thickness tufted sandwich structures. *Composite Structures*, 92(9): 2052–2059, 2010. ISSN 02638223.

[59] J Bertrand and B Desmars. Aerotiss® O3S stitching for heavy loaded structures. *JEC Magazine #18*, pages 34–36, 2005.

[60] J Sloan. Integrated, optimized aircraft door. *High-performance composites*, pages 61–68, 2012.

[61] DW Bauer and WV Kotlensky. Relationship between structure and strength for CVD carbon infiltrated substrates. Part II- Three dimensional woven, tufted and needled substrates. *SAMPE Quarterly*, 4(2):10–20, 1973.

[62] P Schiebel and AS Herrmann. Textile preform technologies in the aviation sector –chances and challenges for the automotive sector. In *Industrial Fabrics Association International-Advanced Textiles Europe Conference*, 2008.

[63] E Laourine. *Einseitige Nähtechnik für die Herstellung von dreidimensionalen Faserverbundbauteilen*. PhD thesis, Lehrstuhl für Textilmaschinenbau und Institut für Textiltechnik, 2005.

[64] JWG Treiber. *Performance of tufted carbon fibre/epoxy composites*. PhD thesis, Cranfield University, 2011.

[65] PB Stickler, M Ramulu, and PS Johnson. Experimental and numerical analysis of transverse stitched T-joints in bending. *Composite Structures*, 50(1): 17–27, 2000. ISSN 0263-8223.

[66] PB Stickler and M Ramulu. Investigation of mechanical behavior of transverse stitched T-joints with PR520 resin in flexure and tension. *Composite Structures*, 52(3):307–314, 2001. ISSN 0263-8223.

[67] PB Stickler and M Ramulu. Parametric analyses of stitched composite T-joints by the finite element method. *Materials & Design*, 23(8):751–758, 2002. ISSN 0261-3069.

[68] PB Stickler and M Ramulu. Damage progression analyses of transverse stitched T-joints under flexure and tensile loading. *Advanced Composite Materials*, 15(2):243–261, 1 2006. ISSN 0924-3046.

[69] PB Stickler and M Ramulu. Experimental study of composite T-joints under tensile and shear loading. *Advanced Composite Materials*, 15(2):193–210, 2006. ISSN 09243046.

[70] Cahuzac Georges and François Monget. Process and machine for the production of armature for a piece of composite material: France, FR0678609 B1[P], 1994.

[71] J Wittig. Recent development in robotic stitching technology for textile structural composites. In *International Sampe Technical Conference*, pages 540–550, 2001.

[72] C Sickinger and A Herrmann. Structural stitching as a method to design high-performance composites in future. In *Proceedings TechTextil Symposium*, 2001.

[73] DJ Bishop. QinetiQ invests in stitching robot for composite dry fibre preforms. pages 9–10, 2007.

[74] G Dell'Anno, DD Cartié, IK Partridge, and A Rezai. Exploring mechanical property balance in tufted carbon fabric/epoxy composites. *Composites Part A: Applied Science and Manufacturing*, 38(11):2366–2373, 2007. ISSN 1359835X.

[75] TW Chou. Microstructural design of fibre composites. *Cambridge University Press*, pages 382–390, 1992.

[76] LS Liu, P Wang, X Legrand, and D Soulat. Investigation of mechanical properties of tufted composites: Influence of tuft length through the thickness reinforcement. *Composite Structures*, 172:221–228, 2017. ISSN 02638223.

[77] G Dell'Anno. *Effect of tufting on the mechanical behaviour of carbon fabric/epoxy composites*. PhD thesis, 2007.

[78] DDR Cartié, G Dell'Anno, E Poulin, and IK Partridge. 3D reinforcement of stiffener-to-skin T-joints by Z-pinning and tufting. *Engineering Fracture Mechanics*, 73(16):2532–2540, 2006. ISSN 00137944.

[79] JW Hartley, J Kratz, C Ward, and IK Partridge. Effect of tufting density and loop length on the crushing behaviour of tufted sandwich specimens. *Composites Part B: Engineering*, 112:49–56, 2017. ISSN 13598368.

[80] J Hartley and C Ward. Improving the understanding of tufted energy absorbing sandwich structures. In *32nd Technical Conference of the American Society for Composites*, volume 3, pages 2260–2273, 2017. ISBN 9781510853065.

[81] M Colin de Verdiere, AK Pickett, AA Skordos, and V Witzel. Evaluation of the mechanical and damage behaviour of tufted non crimped fabric composites using full field measurements. *Composites Science and Technology*, 69(2): 131–138, 2009. ISSN 02663538.

[82] DB Bortoluzzi, GF Gomes, D Hirayama, and AC Ancelotti. Development of a 3D reinforcement by tufting in carbon fiber/epoxy composites. *The International Journal of Advanced Manufacturing Technology*, 100(5-8):1593–1605, 2019. ISSN 14333015.

[83] AT Martins, Z Aboura, W Harizi, A Laksimi, and K Khellil. Analysis of the impact and compression after impact behavior of tufted laminated composites. *Composite Structures*, 184:352–361, 2018. ISSN 02638223.

[84] C Osmiani, G Mohamed, JWG Treiber, G Allegri, and IK Partridge. Exploring the influence of micro-structure on the mechanical properties and crack bridging mechanisms of fibrous tufts. *Composites Part A: Applied Science and Manufacturing*, 91:409–419, 2016. ISSN 1359835X.

[85] A Henao, R Guzman Villoria, J Cuartero, M Carrera, J Picón, and A Miravete. Enhanced Impact Energy Absorption Characteristics of Sandwich Composites through Tufting. *Mechanics of Advanced Materials and Structures*, 22(12): 1016–1023, 2015.

[86] B Najafloo, AM Rezadoust, and M Latifi. Effect of through-the-thickness areal density and yarn fineness on the mechanical performance of three-dimensional carbon-phenolic composites. *Journal of Reinforced Plastics and Composites*, 35(20):1447–1459, 2016. ISSN 15307964.

[87] C Williams, J Summerscales, and S Grove. Resin Infusion under Flexible Tooling (RIFT): a review. *Composites Part A: Applied Science and Manufacturing*, 27(7):517–524, 1996. ISSN 1359-835X.

[88] DM Lombetti. *Tufting of complex composite structures*. PhD thesis, Cranfield University, 2015.

[89] PH Tan, WP Han, WJ Zhao, ZH Wu, K Chang, H Wang, YF Wang, N Bonini, N Marzari, N Pugno, G Savini, A Lombardo, and A. C Ferrari. The shear mode of multilayer graphene. *Nature Materials*, 11(4):294–300, 2012. ISSN 14764660.

[90] A Martins. *Analysis of damage mechanisms in composite structures reinforced by tufting*. PhD thesis, Université de technologie compiègne, 2018.

[91] G Pappas, S Joncas, V Michaud, and J Botsis. The influence of through-thickness reinforcement geometry and pattern on delamination of fiber-reinforced composites: Part II –Modeling. *Composite Structures*, 184:379–390, 2017. ISSN 02638223.

[92] G Pappas, S Joncas, V Michaud, and J Botsis. The influence of through-thickness reinforcement geometry and pattern on delamination of fiber-reinforced composites: Part I –Experimental results. *Composite Structures*, 184: 924–934, 2018. ISSN 02638223.

[93] J Bigaud. *Analyse du comportement mécanique de structures composites renforcées par coutures*. PhD thesis, Universié de Technologie de Compègne, 2016.

[94] M Colin de Verdiere, AA Skordos, M May, and AC Walton. Influence of loading rate on the delamination response of untufted and tufted carbon epoxy non crimp fabric composites: Mode I. *Engineering Fracture Mechanics*, 96:11–25, 2012. ISSN 00137944.

[95] V Karuppannan, D Sivaraman and Ramesh Ramesh Ajith Gaddikeri, Kotresh M Sundaram. Effect of tufting on mechanical properties of laminated composites. In *ISAMPE National Conference on composite Materials*, page 54, 2012.

[96] M Colin de Verdiere, AA Skordos, AC Walton, and M May. Influence of loading rate on the delamination response of untufted and tufted carbon epoxy non-crimp fabric composites/Mode II. *Engineering Fracture Mechanics*, 96: 1–10, 2012. ISSN 00137944.

[97] HA Maples, O Smith, C Burgstaller, P Robinson, and A Bismarck. Improving the ply/interleaf interface in carbon fibre reinforced composites with variable stiffness. *Composites Science and Technology*, 128:185–192, 2016. ISSN 0266-3538.

[98] B M'membe, S Gannon, M Yasaee, SR Hallett, and IK Partridge. Mode II delamination resistance of composites reinforced with inclined Z-pins. *Materials and Design*, 94:565–572, 2016. ISSN 18734197.

[99] MS Sohn and XZ Hu. Mode II delamination toughness of carbon-fibre/epoxy composites with chopped Kevlar fibre reinforcement. *Composites Science and Technology*, 52(3):439–448, 1994. ISSN 0266-3538.

[100] JE Masters. Improved Impact and Delamination Resistance through Interleafing. *Key Engineering Materials*, 37:310–317, 1989. ISSN 1662-9795.

[101] AJ Kinloch, K Masania, AC Taylor, S Sprenger, and D Egan. The fracture of glass-fibre-reinforced epoxy composites using nanoparticle-modified matrices. *Journal of Materials Science*, 43(3):1151–1154, 2008. ISSN 00222461.

[102] N Sela and O Ishai. Interlaminar fracture toughness and toughening of laminated composite materials: a review. *Composites*, 20(5):423–435, 1989. ISSN 0010-4361.

[103] A Peijs, RW Venderbosch, and PJ Lemstra. Hybrid composites based on polyethylene and carbon fibres Part 3: Impact resistant structural composites through damage management. *Composites*, 21(6):522–530, 1990. ISSN 00104361. doi: 10.1016/0010-4361(90)90425-V.

[104] DWY Wong, H Zhang, E Bilotti, and T Peijs. Interlaminar toughening of woven fabric carbon/epoxy composite laminates using hybrid aramid/phenoxy interleaves. *Composites Part A: Applied Science and Manufacturing*, 101:151–159, 2017. ISSN 1359-835X.

[105] K Shivakumar, S Lingaiah, H Chen, P Akangah, G Swaminathan, and L Russell. Polymer nanofabric interleaved composite laminates. *AIAA Journal*, 47 (7):1723–1729, 2009. ISSN 00011452.

[106] H Ning, Y Li, J Li, N Hu, Y Liu, L Wu, and F Liu. Toughening effect of CB-epoxy interleaf on the interlaminar mechanical properties of CFRP laminates. *Composites Part A: Applied Science and Manufacturing*, 68:226–234, 2015. ISSN 1359-835X.

[107] S Rechak and CT Sun. Optimal Use of Adhesive Layers in Reducing Impact Damage in Composite Laminates. *Journal of Reinforced Plastics and Composites*, 9(6):569–582, 1990.

[108] F Larsson. Damage tolerance of a stitched carbon/epoxy laminate. *Composites Part A: Applied Science and Manufacturing*, 28(11):923–934, 1997. ISSN 1359-835X.

[109] C Scarponi, AM Perillo, L Cutillo, and C Foglio. Advanced TTT composite materials for aeronautical purposes: Compression after impact (CAI) behaviour. *Composites Part B: Engineering*, 38(2):258–264, 2007. ISSN 13598368.

[110] AP Mouritz and BN Cox. A mechanistic interpretation of the comparative in-plane mechanical properties of 3D woven, stitched and pinned composites. *Composites Part A: Applied Science and Manufacturing*, 41(6):709–728, 2010. ISSN 1359835X.

[111] V Koissin, J Kustermans, SV Lomov, I. Verpoest, B Van Den Broucke, and V Witzel. Structurally stitched NCF preforms: Quasi-static response. *Composites Science and Technology*, 69(15-16):2701–2710, 2009. ISSN 02663538.

[112] D Kreculj and B Rasuo. Impact damage modeling in laminated composite aircraft structures. In Mohammad Jawaid and Mohamed B T Sustainable Composites for Aerospace Applications Thariq, editors, *Woodhead Publishing Series in Composites Science and Engineering*, pages 125–153. Woodhead Publishing, 2018. ISBN 978-0-08-102131-6.

[113] S Gholizadeh. a Review of Impact Behaviour in Composite Materials. *International Journal of Mechanical and Production Engineering*, 7:2321–2071, 2019.

[114] F Sarasini, J Tirillò, S D'Altilia, T Valente, C Santulli, F Touchard, L Chocinski-Arnault, D Mellier, L Lampani, and Paolo Gaudenzi. Damage tolerance of carbon/flax hybrid composites subjected to low velocity impact. *Composites Part B: Engineering*, 91:144–153, 2016. ISSN 1359-8368.

[115] A Katunin, K Dragan, and M Dziendzikowski. Damage identification in aircraft composite structures: A case study using various non-destructive testing techniques. *Composite Structures*, 127:1–9, 2015. ISSN 0263-8223.

[116] JM Koo, JH Choi, and CS Seok. Prediction of residual strength after impact of CFRP composite structures. *International Journal of Precision Engineering and Manufacturing*, 15(7):1323–1329, 2014. ISSN 2005-4602.

[117] B Li and M S Hoo Fatt. Impact damage and residual strength predictions of 2D woven SiC/SiC composites. *Finite Elements in Analysis and Design*, 113: 30–42, 2016. ISSN 0168-874X.

[118] P Deconinck, J Capelle, V Bouchart, P Chevrier, and F Ravailler. Delamination propagation analysis in tufted carbon fibre-reinforced plastic composites subjected to high-velocity impact. *Journal of Reinforced Plastics and Composites*, 33(14):1353–1363, 2014.

[119] DM Lombetti and AA Skordos. Lightning strike and delamination performance of metal tufted carbon composites. *Composite Structures*, 209 (November 2018):694–699, 2019. ISSN 02638223.

[120] AR Mills and J Jones. Investigation, manufacture, and testing of damage-resistant airframe structures using low-cost carbon fibre composite materials and manufacturing technology. In *Proceedings of the Institution of Mechanical Engineers, Part G: Journal of Aerospace Engineering*, volume 224, pages 489–497. SAGE Publications Sage UK: London, England, 2010.

[121] M Colin De Verdiere, AK Pickett, AA Skordos, and V Witzel. Effect of Tufting on the Response of Non Crimp Fabric Composites. In *Thematic conference on mechanical response of composites*, pages 12–14, Porto, Portugal, 2007.

[122] T Takatoya and I Susuki. In-plane and out-of-plane characteristics of three-dimensional textile composites. *Journal of composite materials*, 39(6):543–556, 2005.

[123] JM Duell. Impact testing of advanced composites. In *Advanced topics in characterization of composites*, pages 97–112. Trafford Publishing, 2004.

[124] IK Pattridge, JWG Treiber, and M Préau. Deformation and failure in a tufted carbon fabric / epoxy Ω –stiffener. In *Proceeding of the 11th international conference on deformation and fracture of composites.*, pages 1–5, 2011.

[125] J Kratz, H Clegg, G Dell'Anno, and IK Partridge. Improving the damage tolerance of composite joints with tufting. In *Proceeding of the 20th International Conferences on Composite Materials (ICCM20)*, pages 19–24, Copenhagen, 2015.

[126] HM Clegg, J Kratz, IK Partridge, and G Dell'Anno. Evaluation of the effects of tufting on performance of composite T-joints. In *Proceeding of the 17th European Conference on Composite Materials (ECCM2016)*, pages 1–7, 2016. ISBN 9783000533877.

[127] C. Leduc, S. Joncas, and J. S. Leclerc. Effect of process parameters on damage tolerance of carbon epoxy laminate preformed using one-sided stitching. In *16th European Conference on Composite Materials, ECCM 2014*, number June, pages 22–26, 2014. ISBN 9780000000002.

CHAPTER 2

NOVEL TUFTING METHOD TO THE OPTIMISATION OF TUFTING THREADS DEGRADATION

2.1 Introduction of chapter two

The increasing interest in 3-dimensional (3D) composite manufacturing has heightened the need for the through-the-thickness reinforcement (TTR) technology. TTR 3D structure is characterized by the insertion of the thread in Z-direction. Its main interest is the ability of such reinforcement to improve the mechanical properties of the final composite, such as the resistance to delamination, impact resistance, and damage tolerance by the insertion of the thread in z-direction [1–4]. TTR 3D structure can be achieved through various approaches, including 3D weaving, braiding, knitting, and other specific technologies such as z-pinning, stitching, and tufting [5–9].

Amongst of the 3D TTR technologies, tufting emerges as a well-known technology, which is used in the carpet manufacturing area, based on stitching technology. Tufting process is an advanced technology to assemble dry textile reinforcements by inserting thread through the thickness of the preform [10]. Currently, tufting has developed in the thicker and complex composite manufacturing field, much due to its simple and efficient process compared to the other TTR processes, 3D weav-

ing process for example. As shown in Fig. 1-24 (call back to Chapter 1). Only one thread access to one side of the preform, instead of two, is required during the tufting process. Besides, the thread remains in the preform by a simple friction while the needle is retracted [11–13].

The research on TTR tufting technology of 3D composite manufacturing has never stopped in recent years. Based on the literature study, tufted reinforcements provide out-of-plane improvements in mechanical properties. For instance, it increases fracture toughness, impact resistance, compression-after-impact (CAI) strength, interlaminar strength, and the stiffener's pull-off strength [14–23]. However, the reduction of in-plane mechanical performance is concerned during the manufacturing. The related references reveal that the in-plane tension strength and compression properties of 3D tufted composites are 10-15 % lower than that of 2D non-tufted composites with the same lamination configuration, and also point out that the reduced mechanical performance is attributed to the insertion of thread/needle during the tufting process and the flow of resin during the infusion process [14, 23, 24]. To improve the in-plane mechanical properties is essential to the 3D composite manufacturing.

These mechanical properties have generally been studied on dry preform and composite parts and focus on the optimization of tufting configuration [25, 26]. While Rudov-Clark et al. [27] have conducted on understanding the alteration in macro-mechanical performance by studies of the characterisation of variations on the meso-structure with the presence of thread. They have put forward that the reduction in the strength properties of the 3D woven composite can be controlled by z-binder yarns' damage during the weaving process. It is therefore interesting to notice that the damage to the tufting inserted thread during the tufting process can also reduce the strength properties of the 3D tufted composite. In addition, an investigation of particular interest by Liu et al. [12] recently demonstrated the contribution of the tuft length of threads to optimise the tufting process and to improve the mechanical performance of tufted reinforcements and composites, whilst "degradation" was first explored to examine the damage of tufting threads, it was deemed that the tufting thread might be degraded by the friction effect on the interface. However, it was just being put forward without depth research. A study by Leca [28] provided two analysed methods of thread degradation in terms of exper-

imental viewpoints (image-observation) and mechanical behaviour of degraded threads, in particular, tensile properties. Regrettably, a complete study of thread degradation is not available in the open literature and none of the effective methods to improve this phenomenon is proposed. In addition, some researches [29–31] mentioned that there are still some limitations of using tufting technology, due to its lack of understanding about the influence of the manufacturing process on performance, as well as the tufting mechanism still has a huge potential to further stage and large development to innovate.

The aim of the present chapter is to improve the tufting mechanism in terms of the reduction of threads degradation. To meet this aim, it firstly to evaluate the classical tufting mechanism efficiency and particularly its effect on the threads degradation. The chapter detailed firstly the preparation of the inserted thread (through tufting process) and non-inserted threads (without the tufting process) to provide the possibility and necessity of the present chapter. And then by means of the image-observation, the degradation of the tufting thread is visually analysed and quantified defined at the same time. Finally, through the quasi-static tensile test, the degradation of the tufting thread was studied from the view of mechanical behaviour (in particular tensile properties). Besides, the effect of tufting spacing was studied through preparing various tufting square patterns during the above-mentioned two experimentations. The present chapter will propose a novel tufting process, namely "two-step" tufting process, based on the primary results, used to carry out this improvement, and then to quantitatively evaluate its contribution to the mechanical performance of the tufting thread.

2.2 Materials and methods

In order to study the tufting threads degradation during the tufting process, the chosen preform is composed of twenty E-glass cross-plies [0/90°]. The preform with 20 plies provides the sufficient thickness to analyse the thread degradation. The influence of the number of plies is not considered in the present chapter. The areal density of a single ply is 454.5 ± 5.0 g/m^2. The tufting thread is the twisted carbon yarn (see Fig. 2-1) and its main properties are noted in Table 2-1. Moreover,

three types of tufted samples have been prepared with different tufting spacing, 9 mm, 6 mm, and 3 mm, respectively. Fig. 2-2 describes the definition of tufting spacing and demonstrates the tufting pattern used in the present chapter.

Fig. 2-1. Bobbin of tufting thread.

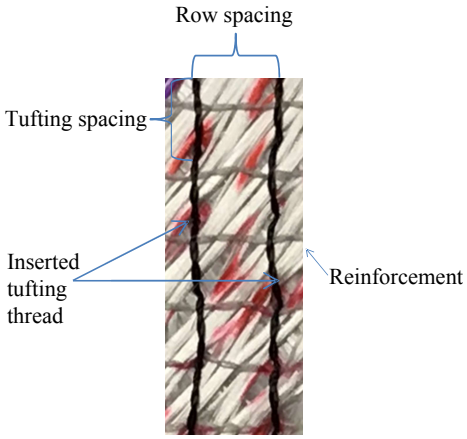

Fig. 2-2. The tufted sample using the tufting square pattern of 9×9 mm^2.

Table 2-1
Main properties of tufting threads.

Reference	Linear density (tex)	Number of filament	Twist(T/m)
Tenax®-J HTA-40	2×67	2×1000	240 ± 16

2.3 Problems of degradation in classical tufting

2.3.1 Description of classical tufting

The preform is tufted with a home-designed tufting device in GEMTEX, which is shown in Fig. 1-23, and its parameters shown in Table 1-2 in section 1.3.1. This device is made up by four main systems: tufting system, presser foot system, feeding system and frame. The presser foot system adjusts the pressure on the preform. The feeding system carries the bobbin of tufting threads and controls the tufting threads with a set-length and pretension. During the tufting process, the pressure

of the tufting needle and of the presser foot is 2.5 bar, while being initialised to a starting position based on the predetermined length of the tuft loop, which must be controlled constantly. The corresponding process is described as shown in Fig. 2-3. It contains one tufting needle carrying the tufting thread (threaded tufting needle), penetrates into the preform, and remains in the perform with a simple friction as described detailed in section 1.3.2.

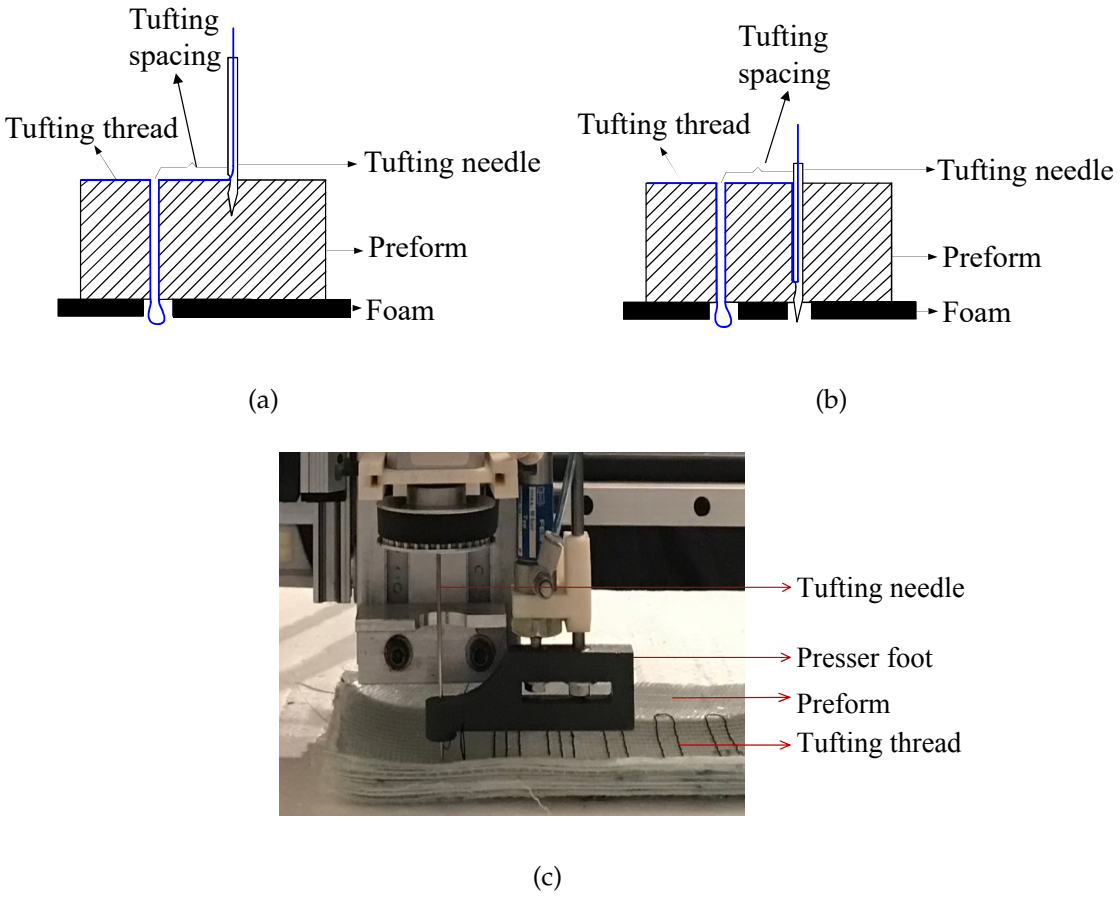

Fig. 2-3. Classical tufting process (a-b) schematics view and (C) with GEMTEX tufting device.

2.3.2 Image-observation of inserted tufting threads

In order to evaluate and analyse the degradation behaviours of tufting threads, the inserted threads should be brought out carefully. To bring out the inserted threads

without tension and friction, the inserted threads are picked after the tufted preform is unpicked. Even if a hollow needle (as shown in Fig. 2.4(a)) has been used during the tufting to reduce the friction effects on the tufting thread/preform interface, the significant degradation can be observed. The cross-section of the needle (see Fig. 2.4(b)) demonstrates that the "hollow" defines an axial needle passage which opens laterally and obliquely onto a non-throughway needle eye whose edge is remote from the needlepoint, and the thread travels through the interior of the needle.

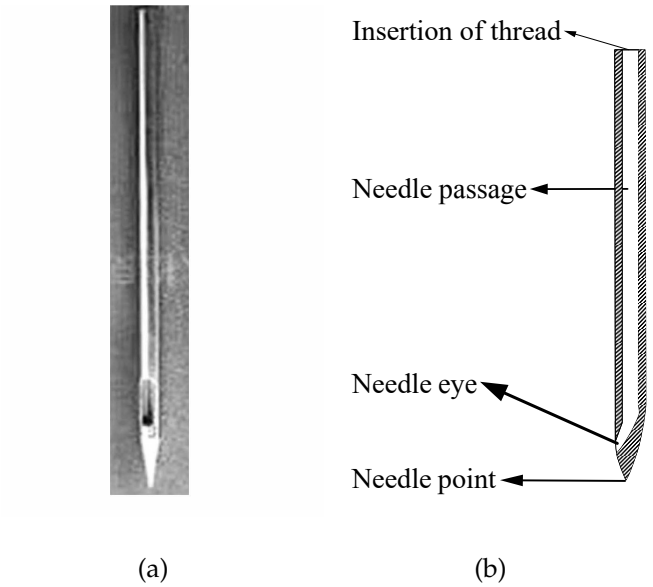

Fig. 2-4. (a) hollow needle and (b) schematic view of cross section.

The image-observation has been proposed firstly to analyse the tufting threads degradation. Fig. 2-5 presents the scanned image of an inserted thread picked from the tufted sample. The study can be performed in one tufting cycle defined in Fig. 2-5. Three parts (L1, L2 and L3) of inserted tufting threads in one tufting cycle are defined. L1 presents the length of the part where stays on the top side of the preform surface. It equals the tufting spacing. L2 is the length of the part inserted 100 % into the preform and depends on the preform thickness. Regarding the movement path of the tufting needle, L2 can be divided into two parts: L2-in and L2-out. L2-in part is formed during the tufting needle insertion through the preform, beginning at the insertion point (also called tufting point) on the top side to the bottom side of the preform and held into the preform. Compared to the L2-in part, L2-out part is formed in the tufting needle drawing back path. L2-in and L2-out have the same

length that equals to the preform thickness. L3 presents the total length of the tuft loop inserted into the foam.

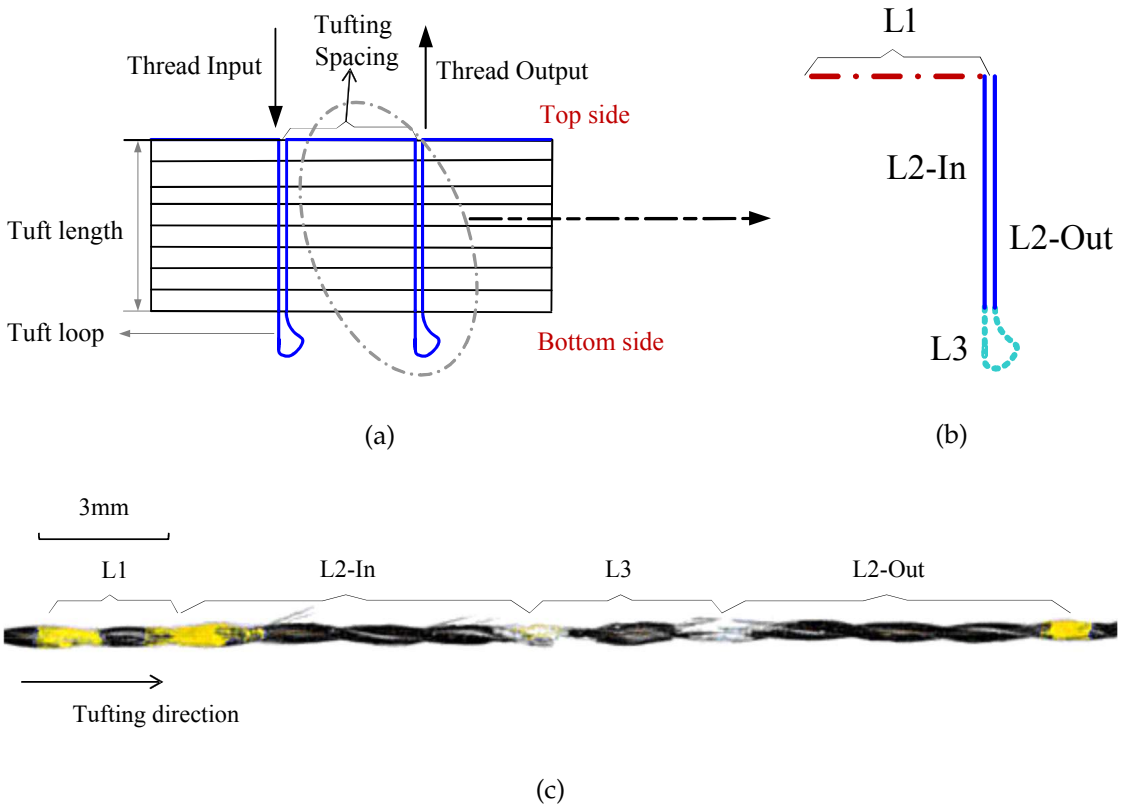

Fig. 2-5. (a) the tufted preform,(b) the inserted threads picked in one tufting cycle and (c) the scanned image of inserted threads in one tufting cycle.

Fig. 2-6 shows the first image-observation of the non-inserted and inserted tufting threads. Compared to the non-inserted threads, the degradation can be noted in the inserted threads. Furthermore, the degradation is only observed in L2-in part, and this phenomenon is repeated in each tufting cycle.

The threads hairiness (threads degradation) can be quantified using the image processing software "Image J". In the present image processing, it should first convert the size in pixel of each image into physical length in mm and then transform the image into the grayscale to finish the image scale setting. Then the pixels of an image are replaced by the fixed threshold values in the second step, called the thresholding process, in which a binary image is created to perform easily the following image analyses. The hairiness in pixel of the pre-treated image is analyzed and

measured to quantify the thread degradation per mm^2. Table 2-2 shows the mean degradation in pixel of the non-inserted (as reference) and inserted tufting threads with different tufting spacing (as 9, 6 and 3 mm). It is obvious that the degradation occurs on the inserted threads, but no expressively difference of degradation among three different spacings, typically about 550 pixels.

Table 2-2
Influence of tufting spacing on the degradation of inserted tufting threads.

Ref.of samples	Non-inserted threads	Tufting spacing 9 mm	Tufting spacing 6 mm	Tufting spacing 3 mm
Degradation (pixels)	0	571 ± 35	545 ± 27	555 ± 47

(a) Non-inserted tufting thread

(b) Tufting spacing of 9 mm

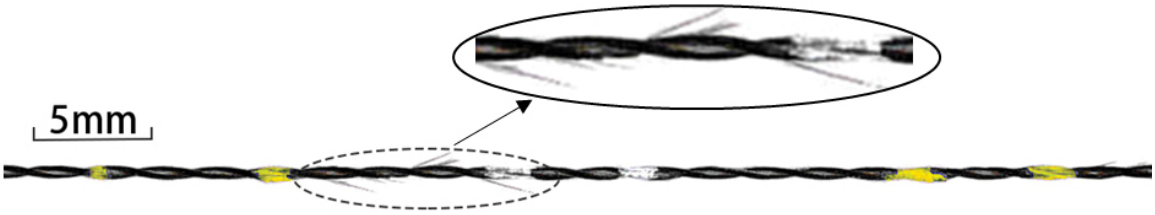

(c) Tufting spacing of 6 mm

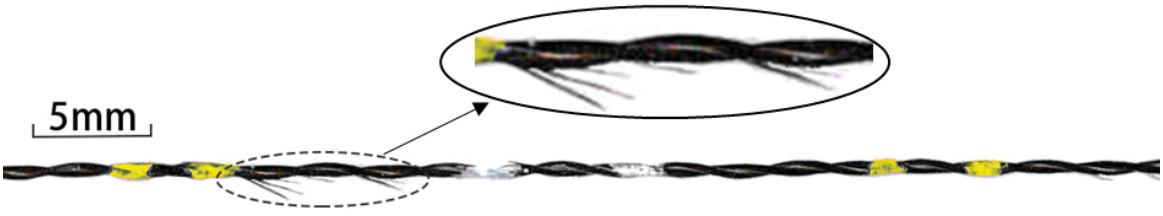

(d) Tufting spacing of 3 mm

Fig. 2-6. Image-observation of the non-inserted tufting thread and the inserted tufting threads with different tufting spacing.

2.3.3 Tensile tests of the tufting threads

Further analysis of the degradation of the inserted tufting threads is conducted by the tensile characterisation tests. Fig. 2-7 shows the tensile test of a single inserted tufting thread. The tensile test of each type of sample is repeated five times to obtain an average value. During the tensile test, the length of the tested thread is 250 mm and the crosshead speed is 5 mm/min.

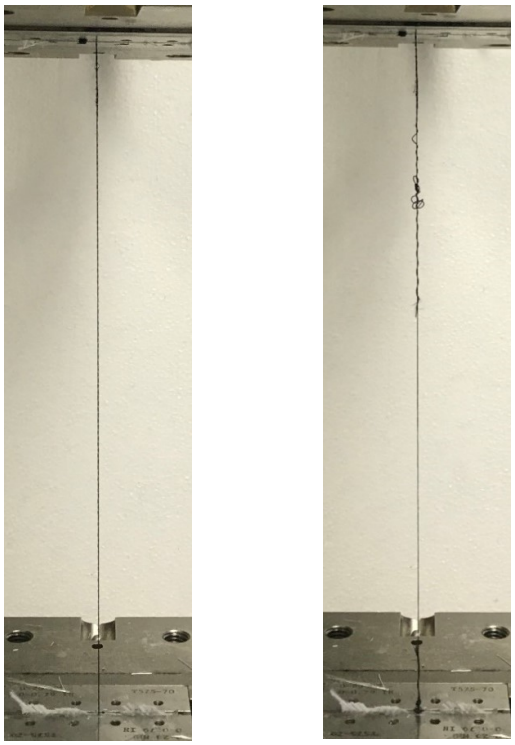

Fig. 2-7. Tensile test of the single tufting thread.

The tensile load/strain curves of the non-inserted and inserted tufting threads are shown in Fig. 2-8. It can be observed that the four curves have a similar profile. It is obviously found that the maximum tensile loads before the break of tufting thread are 121 $\pm$ 2, 112 $\pm$ 3.9 and 109 $\pm$ 0.9 N for the samples with the tufting spacing of 9, 6, and 3 mm, respectively. Compared to the maximum tensile load of non-inserted thread (141 $\pm$ 4.3 N), it can be noted the degradation of the maximum tensile load of 14 %, 21 %, and 23 % for the used tufting spacing of 9, 6, and 3 mm, respectively. Regarding to the strain at break, the degradation of 4 %, 10 % and 15

% can be observed for the tufting spacing of 9, 6, and 3 mm, respectively. The significant degradation to the tensile performance of the inserted tufting threads can be remarked in the classical tufting process. Moreover, the smaller the tufting spacing settled, the higher tufting density, the more friction and degradation produced on the inserted tufting threads, which will bring out the negative influence on the mechanical proprieties of the tufted preforms and composites.

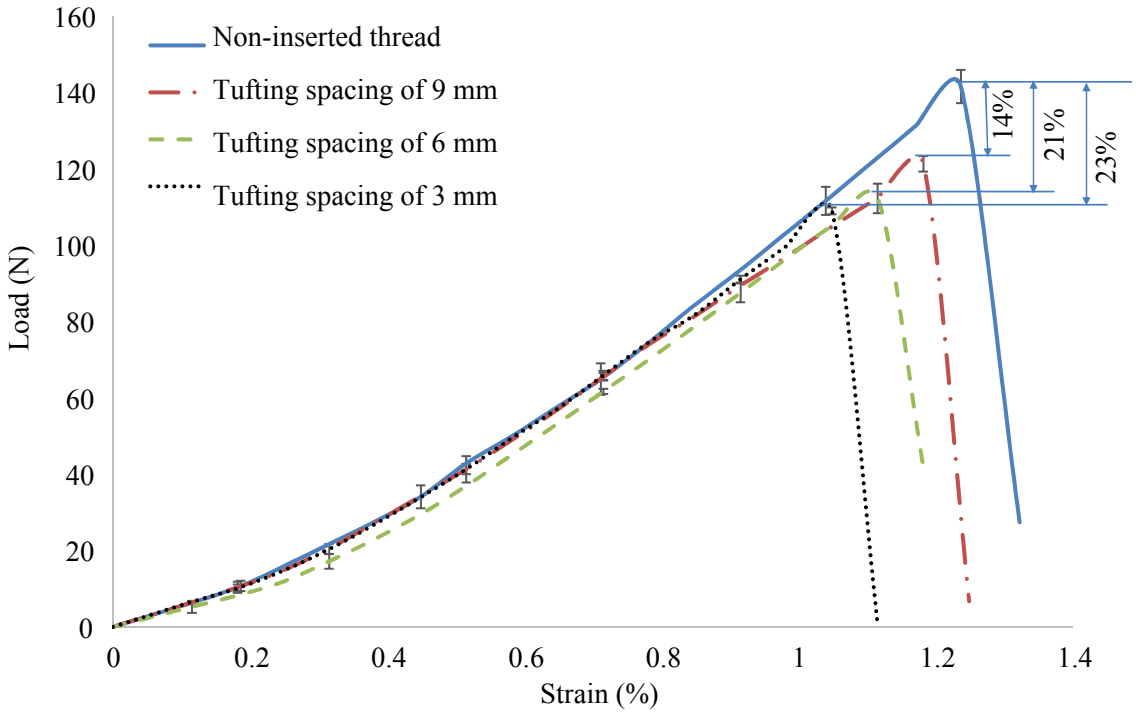

Fig. 2-8. Tensile load *vs.* strain curves of the non-inserted and inserted tufting threads.

As shown in Fig. 2-8, the significant degradation of the inserted tufting threads can occur during the tufting process. The degradation will weaken the mechanical proprieties of the through-the-thickness tufting threads and the final composites. Consequently, the question is if it is possible to reduce the degradation of the inserted threads by means of improving the tufting process. Based on this assumption, an improvement solution is proposed in the following section and the verification tests will be conducted.

2.4 New tufting process

2.4.1 Description of the two-step tufting process

As presented previously, it can be noted that degradation is observed mainly in the L2-in part. It provides that the degradation is produced only by the insertion of the threads due to the first friction between the threads and the preform through the tufting path. Therefore, a 2^{nd} needle quasi-identical, the tufting needle without thread, is proposed as the guide needle to reduce the degradation. The principle of the improvement tufting with two needles (a guide needle without threads + a tufting needle with threads) is shown in Fig. 2-9. It needs two steps in the improved tufting process. The guide needle without threads inserts at first into the preform (Figs. 2.9(a) and 2.9(b)), then the tufting needle with tufting threads inserts into the preform through the same path of the guide needle (Fig. 2.9(c)). Thanks to the insertion of the guide needle at the first step, a space-room is created into the preform (Fig. 2.9(c)). Consequently, the effect of the friction between the threads in L2-in part and the preform decreases due to the decreasing of the lateral contact and transverse compaction of the inserted threads (Fig. 2.9(d)). The diameter of the guide needle is slightly smaller than the tufting needle. The inserted threads need friction and lateral contact to remain their position and to avoid removing from the preform. As this improved tufting process has one more step than the classical one, it is called the two-step tufting process in the following sections.

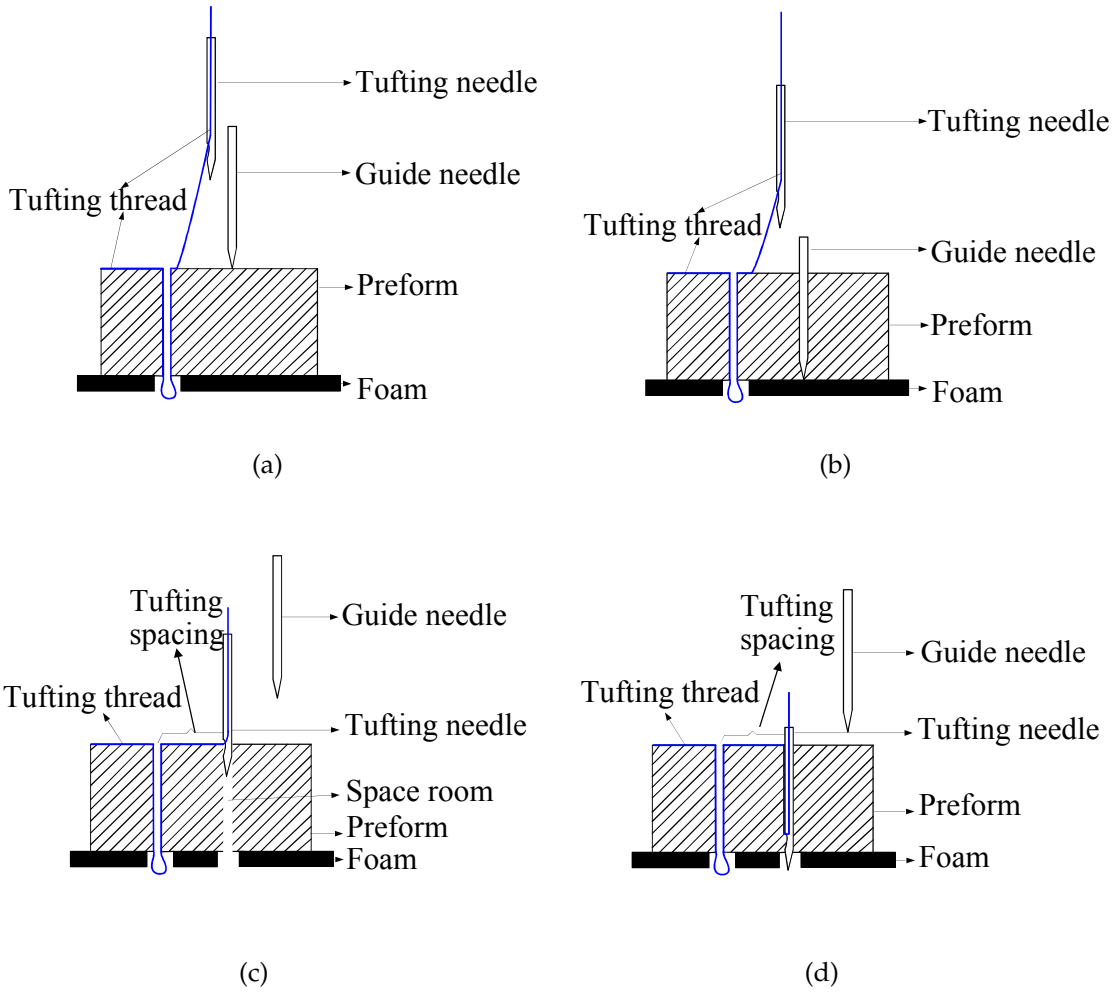

Fig. 2-9. Schematics of two-step tufting process.

2.4.2 Image-observation of inserted tufting threads

Fig. 2-10 shows the image-observation of three inserted thread samples after two-step tufting with tufting spacing of 9, 6, and 3 mm. The degradation can be always observed even if two-step tufting is used. By contrast, the degradation in two-step tufting is much reduced compared to the classical tufting. The measurement of degradation in the pixel is shown in Table 2-3, around 370 pixels.

Table 2-3
Influence of tufting spacing on the degradation of inserted tufting threads.

Ref.of samples	Tufting spacing 9 mm	Tufting spacing 6 mm	Tufting spacing 3 mm
Degradation (pixels)	371 ± 46	375 ± 26	397 ± 43

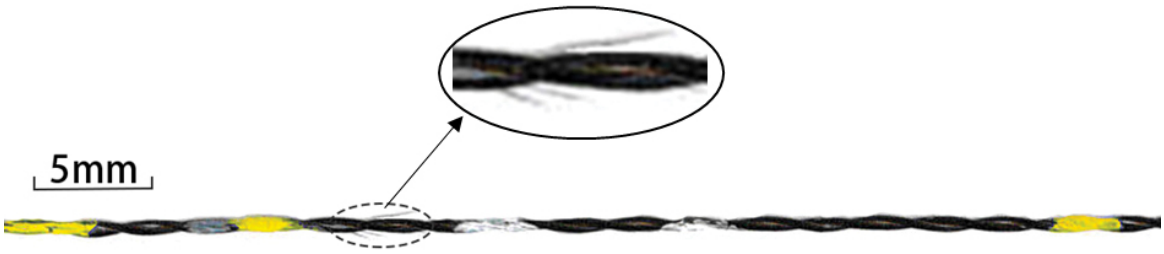

(a) Tufting spacing of 9 mm

(b) Tufting spacing of 6 mm

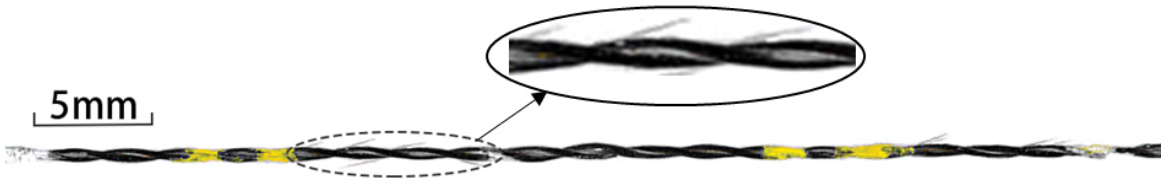

(c) Tufting spacing of 3 mm

Fig. 2-10. Two-step tufted carbon thread with tufting spacing of (a) 9 mm, (b) 6 mm, (c) 3 mm.

The comparison of the degradation in pixel between the classical and two-step tufting is shown in Fig. 2-11. It can remark that a significant improvement of the inserted thread degradation can be achieved in the two-step tufting. Compared to the classical tufting, the degradation decreases by 30 % in the two-step tufting.

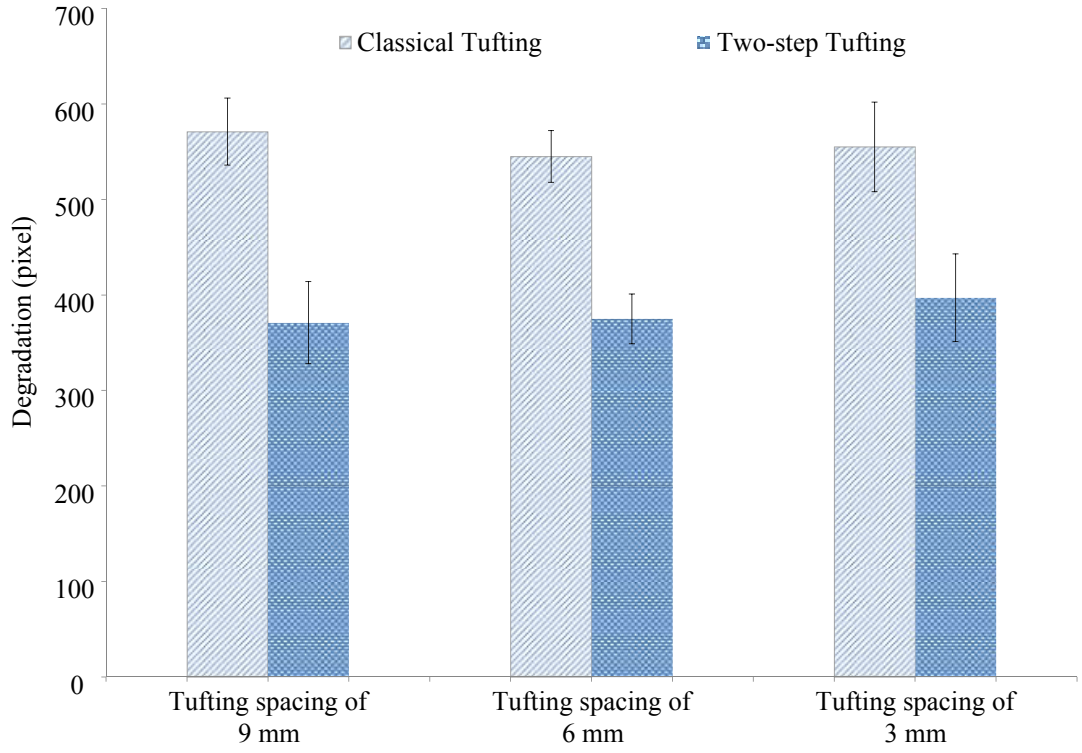

Fig. 2-11. Comparison of the degradation in pixel between the classical and two-step tufting.

2.4.3 Tensile tests of the tufting threads

The tensile load $vs.$ strain curves of the single inserted thread in two-step tufting are shown in Fig. 2-12. The degradation on the tensile performance of the inserted threads and the influence of the tufting spacing can be noted. Both the maximum tensile load and the breaking strain reduce with the decrease of the tufting spacing, the breaking loads are 128 $\pm$ 1.9, 124 $\pm$ 2.9, and 115 $\pm$ 2.9 N and the breaking strains are 1.24 %, 1.18 % and 1.12 % for the tufting spacing of 9, 6, and 3 mm, respectively. Compared to the non-inserted thread (breaking load of 141 $\pm$ 4.3 N and breaking

strain of 1.24 %), there are 9 %, 12 %, and 18 % decreases of the tensile load and 0%, 4 %, and 10 % of the tensile strain in the tufting with the spacing of 9, 6, and 3 mm, respectively.

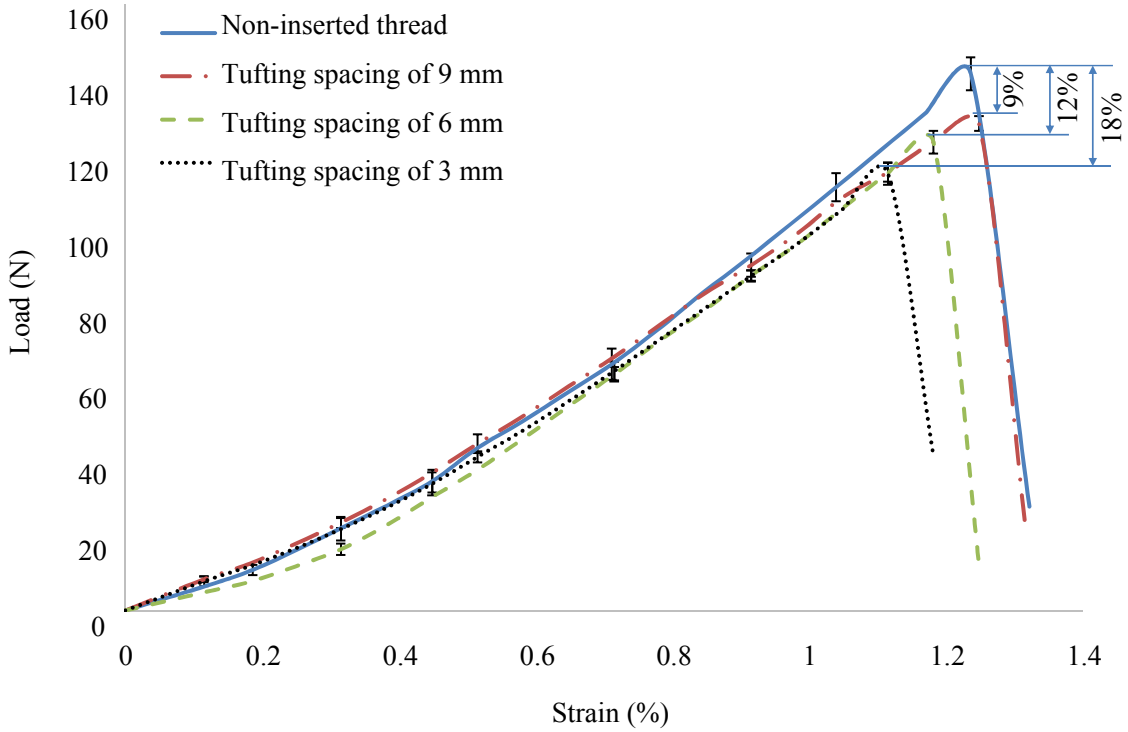

Fig. 2-12. Tensile load *vs.* strain curves of the inserted tufting threads in two-step tufting.

2.5 Discussion

The results of image-observation have demonstrated a big improvement of the degradation of the inserted tufting threads in two-step tufting compared to the classical one (see Fig. 2-11). Fig. 2-13 presents the comparison on the degradation of the tensile proprieties of the inserted threads between the classical and two-step tufting. As for the same tufting spacing, it can be noted the improvement of the breaking load in two-step tufting compared to the classical tufting, nevertheless, it exists also the degradation. It has 5.8 %, 10.7 %, and 5.5 % augmentation for 9, 6,

and 3 mm tufting spacing, respectively when a guide needle was used during two-step tufting process. Compared to the classical tufting, it has 5.7 %, 6.0 %, and 6.3 % improvement of breaking strain by using two-step tufting with 9, 6, and 3 mm tufting spacing, respectively. As regarding the non-inserted threads, more significant improvement is done in breaking strain in two-step tufting. The threads have almost no degradation in breaking strain in two-step tufting with 9 mm spacing. Moreover, the degradation increases with the decreasing of the tufting spacing, which can be noted in the tensile breaking load and in tensile breaking strain in both classical and two-step tufting. It is logical that the decreasing of the tufting spacing leads to the increasing of the number of tufting cycle in the 250 mm tested length. The friction and degradation on the inserted thread reduce consequently.

The image-observation results provide that the degradation is only observed in L2-in part (see Figs. 2-6 and 2-10). Figs 2.9(a) and 2.9(b) obviously indicate that the thread issues from the needle and bends upon the top portion of needle eye as the tufting needle penetrates down into the preform. Followed the thread retained in the preform is in the L2-in part. By analysing this procedure, a relative movement between the thread and needle eye is produced in the bending moment, whilst the varied transverse compactions from the preform bring different friction and degradation on the thread in this position. Meanwhile, the brittle property of the carbon filaments tends the carbon thread easily to degrade under high curvature in the needle eye particularly when the preform is tight used in close preforms [13]. The guide needle can loosen the preform structure. Whilst in the present chapter, the polyethylene foam with a low coefficient of friction reduces friction and degradation on the thread in L3 part. Additionally, the introduce of the hollow needle can make sense to avoid the tufting thread directly contacting with preform or form. From this, it follows that there is no effective friction and degradation on the thread in L1, L3, and L2-out parts.

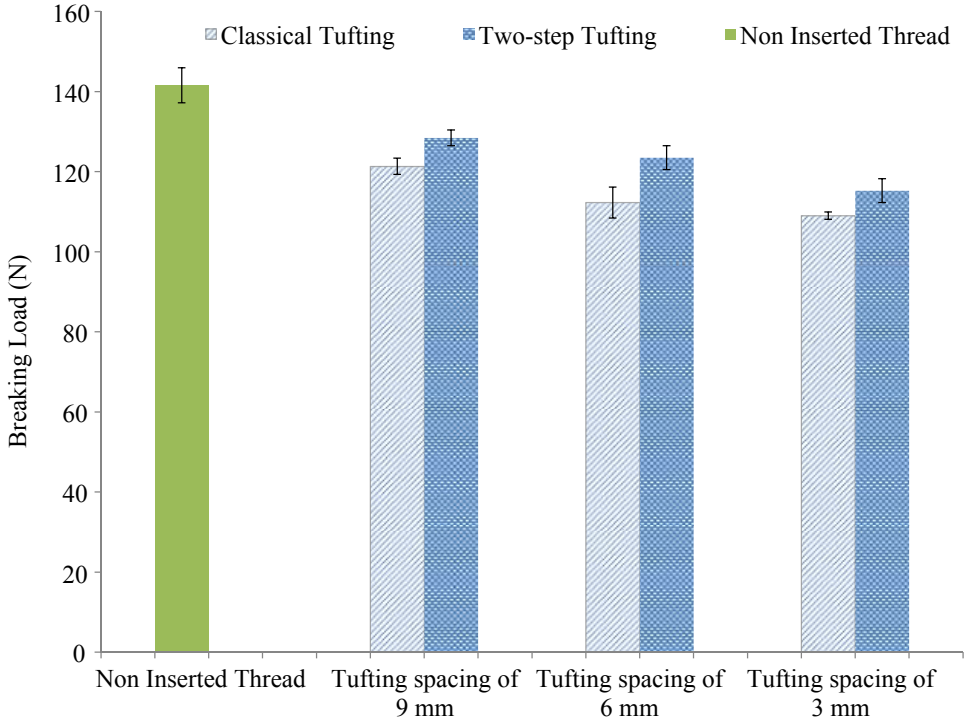

(a) For breaking load

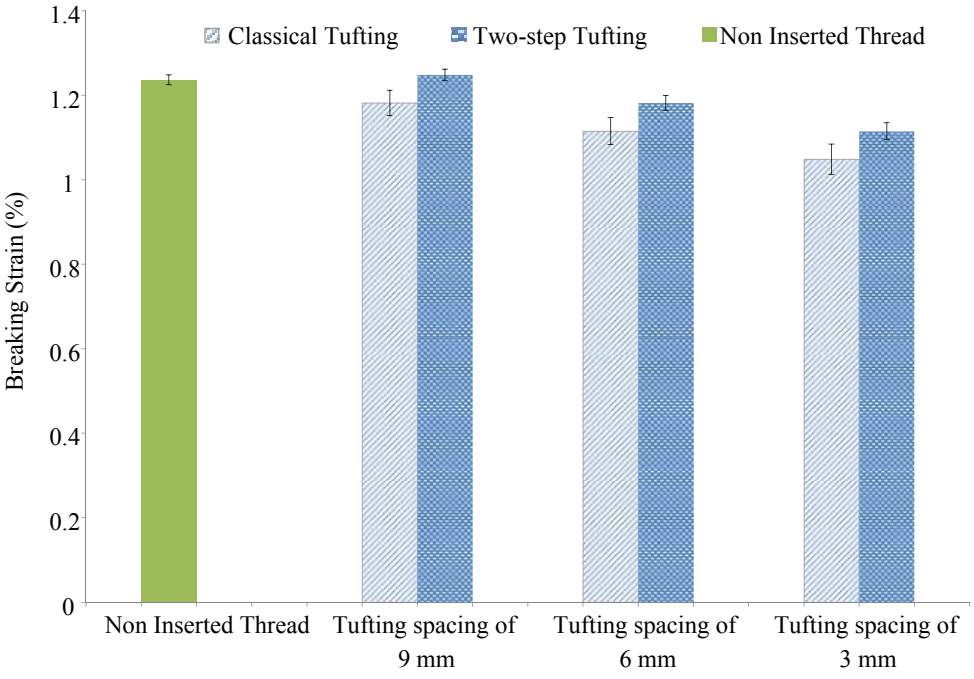

(b) For breaking strain

Fig. 2-13. Comparison of the tensile properties between the classical and two-step tufting.

2.6 Conclusion of chapter two

In the present chapter, the preparation of inserted tufting threads and degradation of these samples are outlined. The definition of tufting degradation is given at first. Due to the presence of tufting thread through the thickness, several mechanical performances of the tufted composites are improved, such as the reduction of delamination effect and the increase of impact resistance. Important degradation of the inserted tufting threads was observed in the classical tufting process, which brings out the significant negative influence on the tensile properties of the inserted tufting threads, the most important deformation mode of the through-the-thickness reinforced threads.

The present chapter carries out the image-observation analysis and demonstrates that the degradation appears only in the path where the tufting needle inserts into the preform (L2-in part in Fig. 2-5) due to the friction among the tufting thread, the tufting needle and the preform. In order to minimize the friction, a guide needle without tufting thread and the two-step tufting were proposed as an improvement method. On account of establishing a space-room before tufting thread passing, the friction effect on the thread of L2-in part is reduced, followed up, reducing the inserted tufting thread degradation, and thereby improving the tensile properties of the inserted tufting thread finally.

The present chapter indicates that the tufting spacing acts as an essential factor during the tufting process, it leads to a trade-off relation to the tensile properties of the inserted tufting thread. Whereas the tufting thread degradation does not vary with the tufting spacing in one tufting cycle. The effect of tufting spacing on degradation and on tensile properties of inserted tufting threads taken from the two-step tufting is a consistent manner than taken from the classical one. A 30 % reduction in degradation by the two-step tufting process is identified as a significant improvement of 3D tufted composite manufacturing.

This two-step tufting method will be employed in the next chapters. It is used to prepare laminated products by tufting, followed by interlaminar shear test. Meanwhile, it is also applied to develop a novel plat assembly composite by tufting.

Bibliography

[1] SD Green, AC Long, BSF El-Said, and SR Hallett. Numerical modelling of 3D woven preform deformations. *Composite Structures*, 108(1):747–756, 2014. ISSN 02638223.

[2] DB Bortoluzzi, GF Gomes, D Hirayama, and AC Ancelotti. Development of a 3D reinforcement by tufting in carbon fiber/epoxy composites. *The International Journal of Advanced Manufacturing Technology*, 100(5-8):1593–1605, 2019. ISSN 14333015.

[3] C Scarponi, AM Perillo, L Cutillo, and C Foglio. Advanced TTT composite materials for aeronautical purposes: Compression after impact (CAI) behaviour. *Composites Part B: Engineering*, 38(2):258–264, 2007. ISSN 13598368.

[4] Y Mahadik, KAR Brown, and SR Hallett. Characterisation of 3D woven composite internal architecture and effect of compaction. *Composites Part A: Applied Science and Manufacturing*, 41(7):872–880, 2010. ISSN 1359835X.

[5] AP Mouritz. Review of z-pinned composite laminates. *Composites Part A: Applied Science and Manufacturing*, 38(12):2383–2397, 2007. ISSN 1359835X.

[6] Kimberley Dransfield, Caroline Baillie, and Yiu Wing Mai. Improving the delamination resistance of CFRP by stitching-a review. *Composites Science and Technology*, 50(3):305–317, 1994. ISSN 02663538. doi: 10.1016/0266-3538(94)90019-1.

[7] G Dell'Anno, JWG Treiber, and IK Partridge. Manufacturing of composite parts reinforced through-thickness by tufting. *Robotics and Computer-Integrated Manufacturing*, 37:262–272, 2016. ISSN 07365845.

[8] V Carvelli, J Pazmino, SV Lomov, and I Verpoest. Deformability of a non-crimp 3D orthogonal weave E-glass composite reinforcement. *Composites Science and Technology*, 73(1):9–18, 2012. ISSN 02663538.

[9] AP Mouritz and BN Cox. A mechanistic interpretation of the comparative in-plane mechanical properties of 3D woven, stitched and pinned composites. *Composites Part A: Applied Science and Manufacturing*, 41(6):709–728, 2010. ISSN 1359835X.

[10] LS Liu, T Zhang, P Wang, X Legrand, and D Soulat. Influence of the tufting yarns on formability of tufted 3-Dimensional composite reinforcement. *Composites Part A: Applied Science and Manufacturing*, 78:403–411, 2015. ISSN 1359835X.

[11] AP Mouritz, MK Bannister, PJ Falzon, and KH Leong. Review of applications for advanced three-dimensional fibre textile composites. *Composites Part A: Applied Science and Manufacturing*, 30(12):1445–1461, 1999. ISSN 1359835X.

[12] LS Liu. *Development and optimization of the tufting process for textile composite reinforcement*. PhD thesis, Université de Lille 1, 2017.

[13] Larissa Born and Markus Milwich. Textile Connection Technology for Interfaces of Fibre-Reinforced Plastic-Concrete- Hybrid Composites. 2018.

[14] JWG Treiber. *Performance of tufted carbon fibre/epoxy composites*. PhD thesis, Cranfield University, 2011.

[15] G Dell'Anno. *Effect of tufting on the mechanical behaviour of carbon fabric/epoxy composites*. PhD thesis, 2007.

[16] G Pappas, S Joncas, V Michaud, and J Botsis. The influence of through-thickness reinforcement geometry and pattern on delamination of fiber-reinforced composites: Part I –Experimental results. *Composite Structures*, 184: 924–934, 2018. ISSN 02638223.

[17] G Pappas, S Joncas, V Michaud, and J Botsis. The influence of through-thickness reinforcement geometry and pattern on delamination of fiber-reinforced composites: Part II –Modeling. *Composite Structures*, 184:379–390, 2017. ISSN 02638223.

[18] A Henao, M Carrera, A Miravete, and L Castejón. Mechanical performance of through-thickness tufted sandwich structures. *Composite Structures*, 92(9): 2052–2059, 2010. ISSN 02638223.

[19] JW Hartley, J Kratz, C Ward, and IK Partridge. Effect of tufting density and loop length on the crushing behaviour of tufted sandwich specimens. *Composites Part B: Engineering*, 112:49–56, 2017. ISSN 13598368.

[20] AP Mouritz, KH Leong, and I. Herszberg. A review of the effect of stitching on the in-plane mechanical properties of fibre-reinforced polymer composites. *Composites Part A: Applied Science and Manufacturing*, 28(12):979–991, 1997. ISSN 1359835X.

[21] AT Martins, Z Aboura, W Harizi, A Laksimi, and K Khellil. Analysis of the impact and compression after impact behavior of tufted laminated composites. *Composite Structures*, 184:352–361, 2018. ISSN 02638223.

[22] M Colin de Verdiere, AA Skordos, M May, and AC Walton. Influence of loading rate on the delamination response of untufted and tufted carbon epoxy non crimp fabric composites: Mode I. *Engineering Fracture Mechanics*, 96:11–25, 2012. ISSN 00137944.

[23] G Dell'Anno, DD Cartié, IK Partridge, and A Rezai. Exploring mechanical property balance in tufted carbon fabric/epoxy composites. *Composites Part A: Applied Science and Manufacturing*, 38(11):2366–2373, 2007. ISSN 1359835X.

[24] M Colin de Verdiere, AK Pickett, AA Skordos, and V Witzel. Evaluation of the mechanical and damage behaviour of tufted non crimped fabric composites using full field measurements. *Composites Science and Technology*, 69(2):131–138, 2009. ISSN 02663538.

[25] M Scott, G Dell' Anno, and H Clegg. Effect of Process Parameters on the Geometry of Composite Parts Reinforced by Through-the-Thickness Tufting. *Applied Composite Materials*, 25(4):785–796, 2018. ISSN 15734897.

[26] LG Blok, J Kratz, D Lukaszewicz, S Hesse, C Ward, and C Kassapoglou. Improvement of the in-plane crushing response of CFRP sandwich panels by through-thickness reinforcements. *Composite Structures*, 161:15–22, 2017. ISSN 02638223.

[27] S Rudov-Clark, AP Mouritz, L Lee, and MK Bannister. Fibre damage in the manufacture of advanced three-dimensional woven composites. *Composites Part A: Applied Science and Manufacturing*, 34(10):963–970, 2003. ISSN 1359835X.

[28] A Leca. *Contribution à l' étude de la santé-matière de préformes carbone*. PhD thesis, Le Havre, 2015.

[29] C Osmiani, G Mohamed, JWG Treiber, G Allegri, and IK Partridge. Exploring the influence of micro-structure on the mechanical properties and crack bridging mechanisms of fibrous tufts. *Composites Part A: Applied Science and Manufacturing*, 91:409–419, 2016. ISSN 1359835X.

[30] PH Tan, WP Han, WJ Zhao, ZH Wu, K Chang, H Wang, YF Wang, N Bonini, N Marzari, N Pugno, G Savini, A Lombardo, and A. C Ferrari. The shear mode of multilayer graphene. *Nature Materials*, 11(4):294–300, 2012. ISSN 14764660.

[31] J Hartley and C Ward. Improving the understanding of tufted energy absorbing sandwich structures. In *32nd Technical Conference of the American Society for Composites*, volume 3, pages 2260–2273, 2017. ISBN 9781510853065.

CHAPTER 3

MULTI-SCALES TUFTED LAMINATES TO THE RESPONSE OF INTERLAMINAR SHEAR PROPERTIES

3.1 Introduction of chapter three

Advanced laminated textile reinforced composites have extensively used in many industrial fields on account of their lightweight properties and better mechanical performance such as in-plane strength and stiffness and resistance to fatigue than metallic materials. However, the lack of the linkage fibre positioned across the thickness direction resulting in the two-dimensional (2D) laminated textile structure shows unsatisfied interlamination shear under mode I opening loading or mode II sliding loading [1–3]. A large number of studies conducted over the last two decades, demonstrate that through-the-thickness reinforcement (TTR) can improve meaningfully the resistance to delamination utilizing inserting threads in the thickness direction [4–8]. TTR three-dimensional (3D) structure can be achieved through various approaches, including integrated 3D technologies such as 3D weaving, braiding, knitting, and other local 3D technologies like z-pinning, stitching, and tufting [7, 9–15]. Out-of-plane performance enhancement exists at the expense of in-plane performance degradation. However, it also depends on the parameters of the TTR 3D reinforcement. Tufting is one of the significant local TTR technologies to assemble dry textile reinforcements or strengthen composites [16, 17],

which first used in carpet fabrication and developed from the stitching technology. In particular, tufting has gradually applied in the fabrication of thicker and complex composites on account of its simple and efficient process [18, 19]. Whilst, Fig. 1-17 (recall 1.3) shows that only one threaded needle penetrates the preform under low tension, the thread is retained within the preform by simple friction when the needle retracts, while forming a tufting loop. Compared to the stitching process, one thread access to only one side of the preform is required [13, 20, 21], thus the stitching effect on the in-plane properties can be effectively reduced during the tufting process [22, 23].

The present chapter will focus on the topic of the improvement of mechanical performance of laminated materials by tufting, which is being widely researched. Majority of researchers have demonstrated the advantages of tufting materials on mechanical performance, especially the delamination resistance properties. For instance, Bortoluzzi et al. [8] have dedicated about 27 % increased resistances to delamination of tufted composites compared to non-tufted one. Besides, Martins et al. [23] have studied the impact as well as the compression after impact (CAI) behaviours of tufted composites. They have mentioned that the delamination area of the tufted composites is decreased with the tufting density increasing compared to the non-tufted composites. Both of them have conducted under the specific delamination mechanism in mode II condition, which is reflected by sliding loading.

As per the literature, varying set-ups can realise mode II delamination experimentation to present different mechanical performance. However, none of them has been standardised. In addition to the end-notch flexure (ENF) [24] and short-beam bending which are used in the abovementioned delamination studies, respectively, the end-loaded split (ELS) [25] is also generally used. Nevertheless, no studies and set-ups to date are taken into account in the interlaminar shearing of tufted materials. Therefore, a modified T-steel shearing test is proposed in the present study, which can explore the interlaminar shearing behaviour of both tufted preforms and composites driven by the mode II sliding loading condition.

The aim of this chapter is to assess under the Mode II loading, i) the effect of tufting density on the interlaminar shear behaviour of tufted preforms and tufted composites, respectively; ii) the effect of the presence of tufting threads on the mechanical

properties of tufted composites; ii) the role of the infusion resin in interlaminar shear performance will be also investigated by means of comparing tufted preforms and tufted composites with the identical tufting density. To ensure the feasibility of the present study, samples with various tufting densities of dry tufted preform (namely, DTP), cured tufted composites with thread (namely, CTC) and without threads (namely, CT'C) will be first prepared in sequence in the present chapter. Meanwhile, the present modified T-steel interlaminar shear set-up will be introduced in detail.

In the present chapter, the tufted preform is carried out by a home-designed tufting device which is introduced in chapter one. Moreover, my colleague, Chen CHEN, whose dedication to the T-steel interlaminar shear experimentation of dry tufted preform ensures the integrity of the present chapter, as shown in Fig. 3-1.

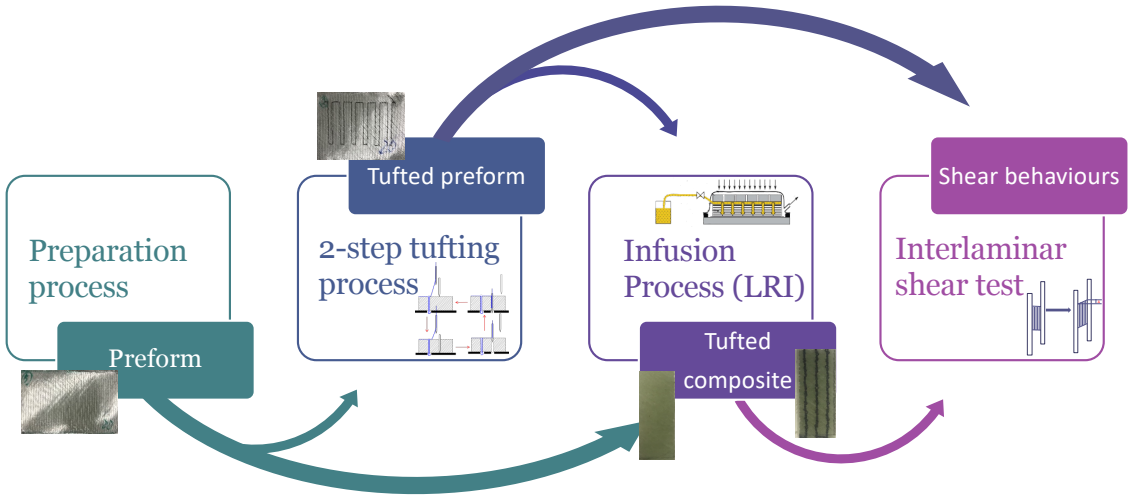

Fig. 3-1. The layout of the chapter

3.2 Materials and methods

3.2.1 Raw materials

Tufted preform or composite materials with and without Z-reinforcement are fabricated using E-glass NCF (Fig. 3.2(a)) with an areal density of 454.5 $\pm$ 5 g/m^2.

Twenty layers of this NCF are then laid up in a stacking sequence with cross-plies [0°/90°]. An example of NCF and its stacking sequence are shown in Fig. 3.2(b). Then to be assembled together by a Tenax® J HTA-40 twisted carbon thread as tufting thread to enhance the interlamination. This tufting thread is shown in Fig. 2-1 and its parameters are given in Table 2-1 (recall to chapter 2). The sample preparation and suitable processes will be introduced in the following paragraphs.

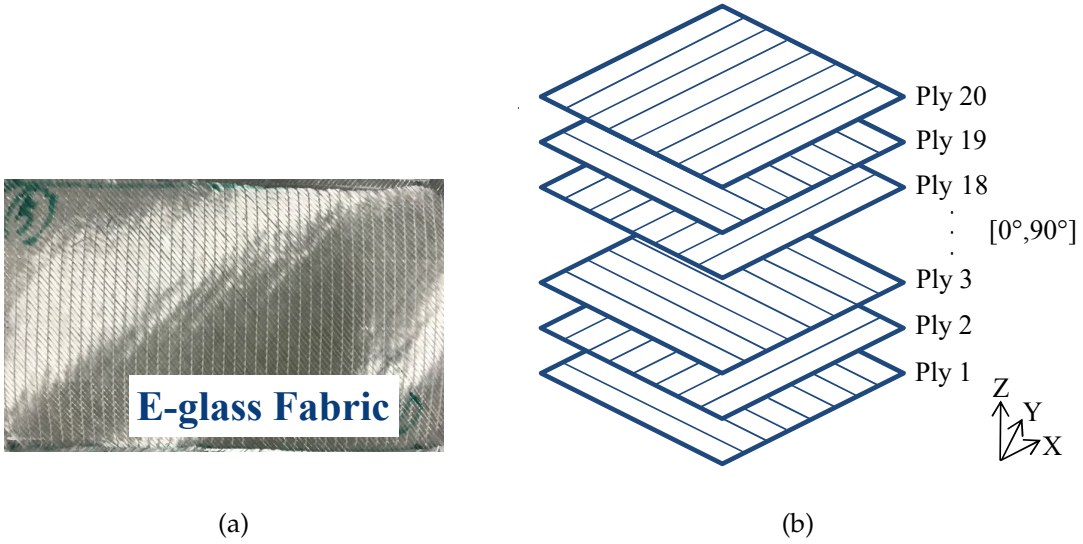

(a) (b)

Fig. 3-2. (a) E-glass fabric and (b) schematic of the laminated preform.

3.2.2 The preparation of test samples

The dry tufted preforms (DTP) are carried out through a 2-step tufting process according to the preset tufting parameters and configurations, which is described in detail in the previous chapter (detailed in section 2.4.1). Meanwhile, a 1-step tufting (classical tufting) process is required to produce dry tufted preforms without threads (DT'P), repeating the same tufting configuration as the DTP. In this process, a hollow needle without thread is applied to accomplish the tufting penetration. These DTP and DT'P samples are performed using a home-design tufting device [18] at GEMTEX laboratory. Fig. 3-3 shows the top and bottom sides of one of the DTP samples. Some of the samples obtained at this stage will be used to manufacture the next composite material. In addition, the others will be directly used for follow-up shearing testing after machining to size.

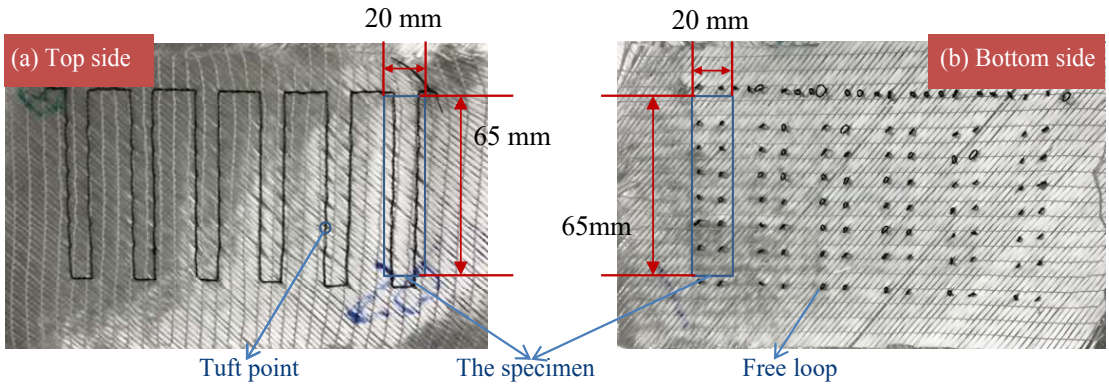

Fig. 3-3. Dry tufted preform (a) top view and (b) bottom view.

Once the tufting process is completed, the 3D DTP samples are afterwards vacuum infused with SICOMIN® SR8200 epoxy resin system (the mass ratio of the resin to hardener is 100 : 37), using LRI (Liquid Resin Infusion) process as shown in Fig. 3-4, which is introduced in detail in section 1.3.2. LRI process is a widely respected infusion process thanks to its cost-effective, which can respond to the production of high-quality, large, thick, or complex composites with simpler equipment [26]. During the LRI process, the resin flows through the thickness of the preform, due to a low pressure between the inlet and the outlet (vacuum pressure: -1 bar). The infused tufted composite is cured at room temperature for forty-eight hours after optimisation. Fig. 3-5 demonstrates the top and bottom sides of an example of CTC samples.

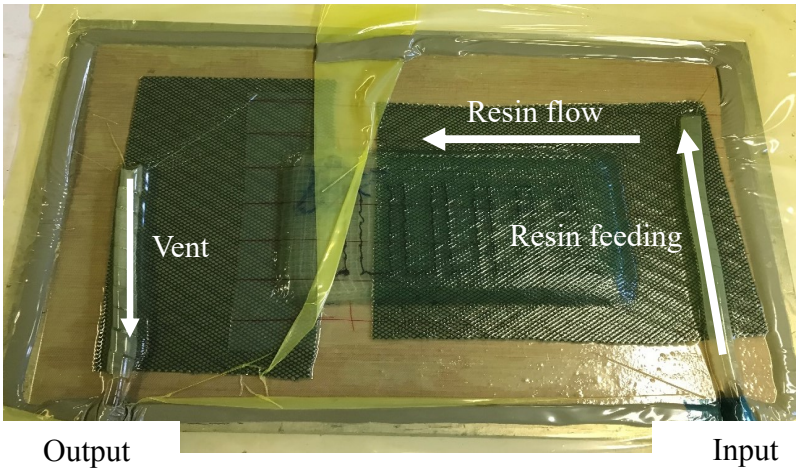

Fig. 3-4. The tufted preform sample under the LRI process.

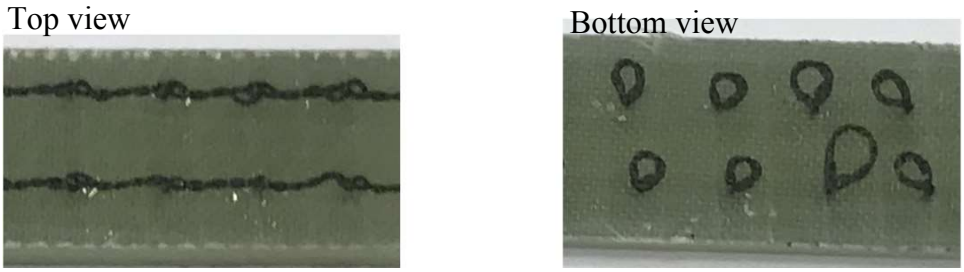

(a) (b)

Fig. 3-5. Cured tufted composite (a) top view and (b) bottom view.

3.2.3 Preparing and setting tufting configurations

To achieve the interlaminar shear test in the next section, it is required to machine the samples to the desired size of 65 mm $\times$ 20 mm in length and width, respectively. The dry preform samples are cut and trimmed into size by electronic scissors. The cured composite samples are machined into size by a water-jet cutter. The variation in the thickness of the final test samples is not large and can be ignored, and the value of their thickness is around 8 ± 0.5 mm. In order to understand the respective contribution of tufting thread, tufting action (typically only tufting needle effect but not the thread) and cured tufting thread on the interlaminar shearing performance under mode II (shear) loading (sliding displacement). Three different series of tufted samples are prepared in terms of the manufacturing process: 1) Dry tufted preform with thread (DTP) sample is concentrated on the role of the tufting thread; 2) Cured tufted composite without thread (CT'C) sample then focuses on the effect of pure tufting action; 3) Cured tufted composite (CTC) sample is for understanding the contribution of cured tufting thread. Moreover, to identify the influence of tufting density on the interlaminar shear properties under mode II loading. Tufting density can be expressed by other tufting parameters (as mentioned in section 1.3.2). In the present case, it is expressed by the tufting spacing (seen in Fig. 2-2). Initially, the non-tufted is investigated as a reference, and meanwhile three various tufting spacings are evaluated: tufting spacing of 9, 6, and 3 mm corresponding to the 9 x 9, 6 x 6 and 3 x 3 mm^2 square patterns, respectively. They are noted as T9, T6, and T3, respectively. Obviously, the smaller the tufting spacing, the larger the tufting density, T3 is the densest one. However, non-tufted preform, as a reference in the DTP series, the lack of reinforcement in the Z-direction (through the

thickness), leads to delamination automatically prior to the shear load applied. No test results from these two preform samples are introduced in the present chapter. Therefore, Table 3-1 summarizes the parameters and manufacture methods of all test samples, except non-tufted preform, and their naming.

Table 3-1
Description of test tufted samples.

Ref. of samples	Tufting spacing (mm)	Methods of manufacture	Infused resin system
DTP-T9	9	2-step tufting	—
DTP-T6	6	2-step tufting	—
DTP-T3	3	2-step tufting	—
Non-tufted	—	LRI	SICOMIN® SR8200
CT'C-T9	9 (tufted without thread)	1-step tufting, LRI	SICOMIN® SR8200
CT'C-T6	6 (tufted without thread)	1-step tufting, LRI	SICOMIN® SR8200
CT'C-T3	3 (tufted without thread)	1-step tufting, LRI	SICOMIN® SR8200
CTC-T9	9	2-step tufting, LRI	SICOMIN® SR8200
CTC-T6	6	2-step tufting, LRI	SICOMIN® SR8200
CTC-T3	3	2-step tufting, LRI	SICOMIN® SR8200

3.2.4 Interlaminar shear characterisation

The present study is to investigate the interlaminar shear behaviours of tufted samples by means of understanding the individual behaviour of tufting thread, tufting action, and cured tufting thread, respectively. Moreover, as shown in Figs. 3-3 and 3-4, each sample is repeated six times in the present shearing test. Therefore, the mean results of each sample can be obtained in the end. This section will present the suitable shear testing procedure for the present study.

"T-steel" shear test fixture
An interlaminar shear test fixture is required in the present chapter, and then the

mode II in-plane shearing (shown in Fig. 3.6(a)) is chosen to achieve the interlaminar shear sliding behaviour of the tufted samples. A "T-steel" shear test fixture is designed as Fig. 3.6(c) and is optimised to be employed on the test samples with an aspect ratio of about 8 (length divided by thickness) in our laboratory (GEMTEX). A total of ten series of samples are tested applying this fixture to undergo the interlaminar shear investigation, and the corresponding test results will be described in a later section.

Bonding the samples to the test fixture

With respect to the interlaminar shear fixture in the present chapter, it is required to bond the sample onto two steel plates. Moreover, the bonding strength has to be strong enough between the sample and two plates to ensure that the effective shear failure occurs on the sample before the adhesive failed. Firstly, the steel plates need to be cleaned up with acetone just before the application of the adhesive. EC-9323B/A from 3M™ Scotch-Weld™, an epoxy-based structural adhesive, is followed to use for bonding the tufting samples to the steel plates. The adhesive is cured in an oven at 65 °C for two hours and post-cured at room temperature for three hours.

Test equipment and test evaluation

The present interlaminar shear testing is performed in a INSTRON universal testing machine (type of 5985) with 250 KN (seen in Fig. 3.6(b)). The present interlaminar shear fixture is to be called the "T-steel" shear fixture is attributed to the using of T-type steel as the steel plates in the present study. Consequently, the special grip is required to design for aiding to mount the fixture system onto the test equipment. The test samples are performed under loading at a constant crosshead speed of 5 mm/min until failure. The representative data of load and displacement are traced during the whole testing process and the representative means shear load-shear angle curve is plotted finally.

In accordance with the present T-steel shear fixture and the theoretical formula of shear behaviour, the average shear properties of all test samples are conducted. All calculations are based on the load-displacement data from the data processing unit of INSTRON. In this way, the shear strength, τ, and the shear strain (Here, expressed by shear angle), ϵ, are calculated using the following formulas as Eqs.

(3.1) and (3.2):

$$\tau = \frac{P}{L \times W} \tag{3.1}$$

$$\epsilon = arctan(tan\frac{\Delta}{T}) \tag{3.2}$$

Where, L, W, and T are the sample length, width, and thickness in mm, respectively; Δ is the relative displacement of the steel plates (to express the specimens deformation which occurs during the shear testing) in mm; ϵ is the shear strain expressed by shear angle, the angle is measured in radians (rad), which is a non-unit (shear strain is dimensionless); P is the shear load in N, When P reaches the peak shear load, then τ expresses the ultimate shear strength (in MPa), noted as τ_{max}.

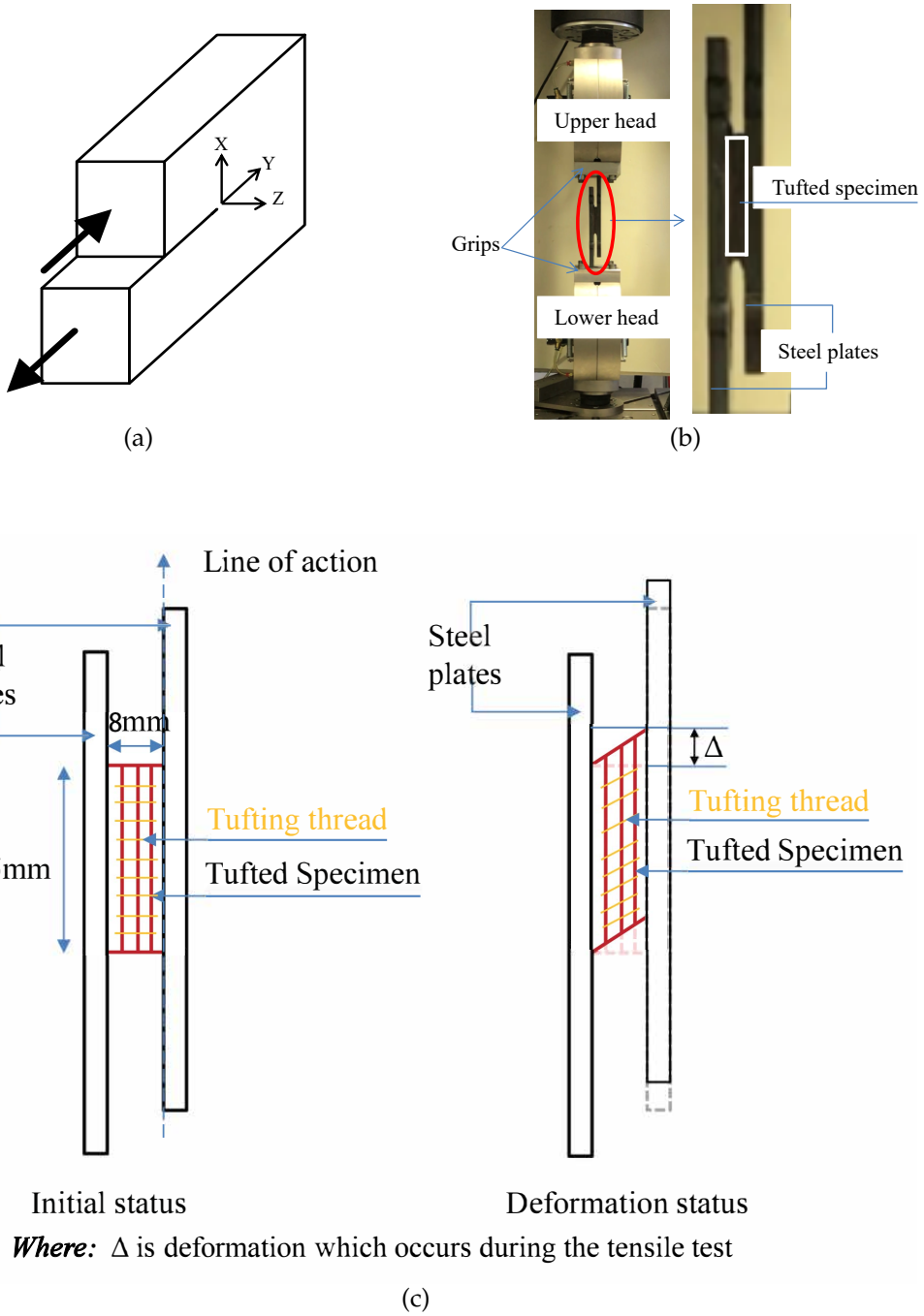

Fig. 3-6. Interlaminar shear (a) mode II shear delamination, (b) test set-up and (c) schematic view.

3.3 Results

Following testing at least six repeated tests for each sample, as introduced in section 3.2.4, and all failures are caused by shearing delamination under mode II loading, the corresponding representative shear load-shear angle curves are then calculated in average. The results will be given by three series samples as DTP, CT'C, and CTC, in accordance with the role of the respective tufting thread, tufting action, and cured tufting thread in the interlaminar shear test, in the following sections, respectively.

3.3.1 Interlaminar shear test of dry tufted preform samples

Fig. 3-7 and shows the representative shear load vs shear angle curves for the DTP samples with three tufting spacings of 9, 6, and 3 mm. It can be observed that the slopes of the three curves are slightly different. In particular, this difference becomes gradually increased after the shear angle of 0.4 rad until the failure. It is considered that the stiffness of the DTP samples can be influenced by the tufting density. And reveals the inversely proportional relationship between them. The smaller the tufting spacing, the denser the tufting density, the stiffer the DTP samples. Regarding the maximum shear load, it can be observed that the average maximum shear loads are 65 $\pm$ 14.1 N, 129 $\pm$ 25.7 N and 192 $\pm$ 30.1 N for DTP-T9, DTP-T6 and DTP-T3, respectively. Furthermore, Fig. 3-8 recaps the ultimate shear strength and the corresponding shear angle of DTP-T9, DTP-T6, and DTP-T3, respectively. Regarding the ultimate interlaminar shear strength, the values are 0.05, 0.1, and 0.15 MPa for the DTP-T9, DTP- T6, and DTP-T3, respectively. It increases with a tolerance of 0.05 MPa when the tufting spacing decreases with a tolerance of 3 mm. Regarding the shear angle at failure, it can be found that they are similar as 1.04 $\pm$ 0.01, 1.13 $\pm$ 0.02 and 1.17 $\pm$ 0.02 rad for DTP-T9, DTP-T6 and DTP-T3, respectively. However, the smaller the tufting spacing, the denser the tufting density, the increased resistance to interlaminar shearing leads to the stronger interlaminar shear strength. It can be noted that tufting spacing has a remarkable effect on the interlaminar shear properties of DTP specimens. The results can be attributed to the presence of tufting threads, which enhance the through-the-thickness stiffness.

With the tufting spacing decrease, the more intertwining between layers, the harder to shearing, thus the stronger shear load is required to apply. Therefore, with the lack of through-the-thickness threads, there is no interlaminar shear behaviour of the non-tufted preform.

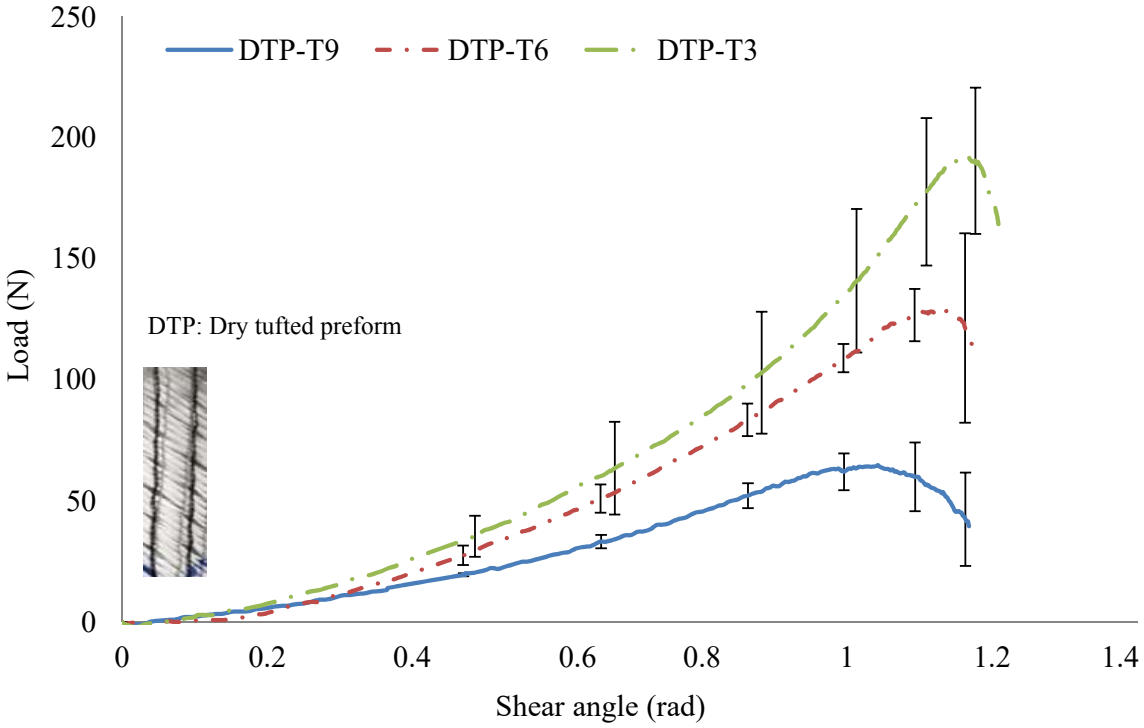

Fig. 3-7. Representative shear load-shear angle curves of DTP specimens

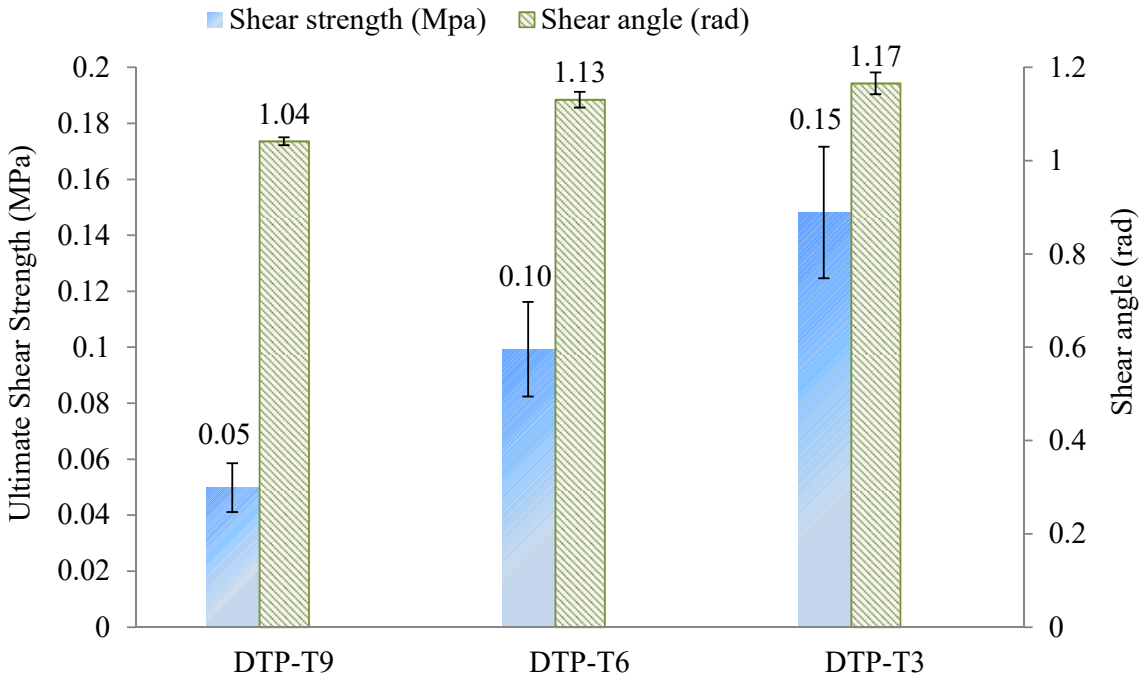

Fig. 3-8. Representative shear properties of DTP specimens.

3.3.2 Interlaminar shear test of cured tufted composite samples

Two series of cured tufted composites samples, CT'C and CTC, are respectively investigated in the present section. Initially, six non-tufted composites are prepared as a reference to be tested. Its average shear failure load is 23 669 $\pm$ 231.8 N, the corresponding shear failure angle is 0.28 $\pm$ 0.01 rad, and 18.2 MPa of its ultimate shear strength. Then the interlaminar shear results of CT'C and CTC are presented in the following.

3.3.2.1 Cured tufted composite without thread (CT'C)

Fig. 3-9 represents the shear angle vs load curves of the CT'C samples with three different tufting spacings and the reference non-tufted sample. It is well observed that the effect of tufting spacing on the shear load is too small to be negligible. For the samples of T9, T6 and T3 are 24 044 $\pm$ 998.2, 24 170 $\pm$ 251.1 and 24 315 $\pm$ 305.2 N, respectively. Compared to the non-tufted composite, the average maximum load

increases 1.6%, 2.1%, and 2.7%, respectively. The shear failure angle of all CT'C samples is similar to that of the non-tufted composite ones, which are detected at about 0.28 ± 0.01 rad. Further results will be discussed later.

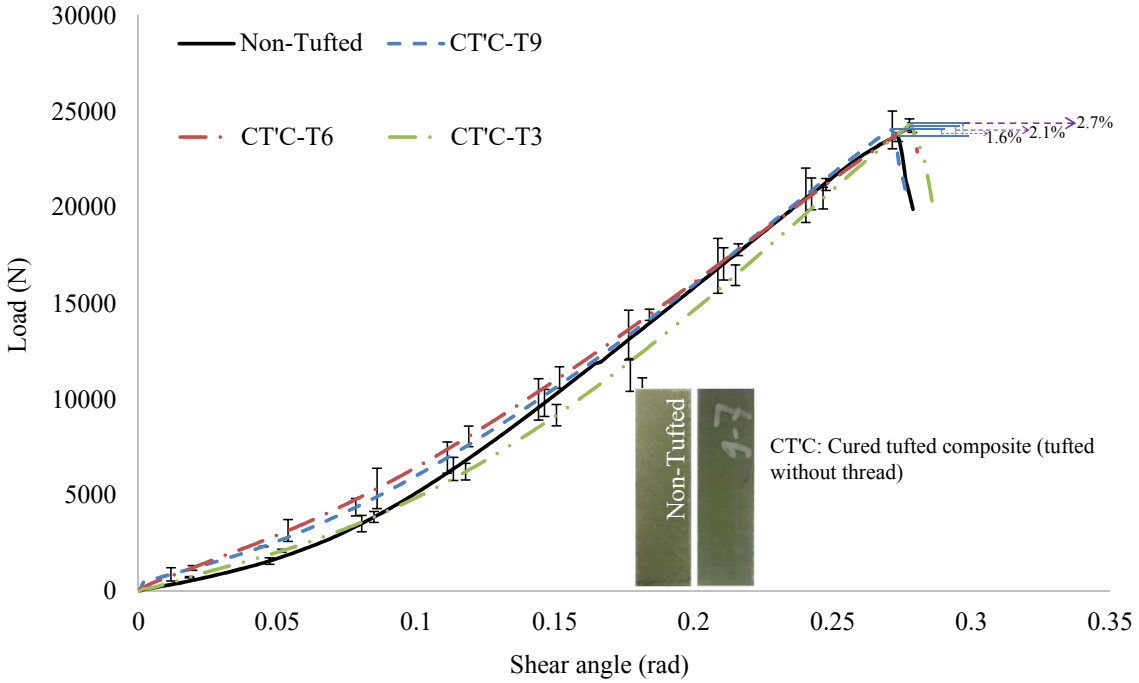

Fig. 3-9. Representative shear load-shear angle curves of CT'C samples.

3.3.2.2 Cured tufted composite with thread (CTC)

As illustrated in Fig. 3-10, the representative shear load vs shear angle curves of the CTC sample with three different tufting spacings and the non-tufted sample are figured out. It reveals that a higher interlaminar shear load is needed to delaminate the denser CTC samples. Since the average maximum shear loads are 22 723 ± 94.1, 24 256 ± 204.5 and 26 568 ± 151.5 N for T9, T6 and T3, respectively. Compared to that of the non-tufted composite, the maximum shear load increase 2.5% and 12.3% for CTC-T6 and CTC-T3, respectively. Unfortunately, the CTC-T9 decreases 4.0%. Regarding the corresponding shear failure angle, it is also clearly found that the smaller the tufting spacing, the denser has a tendency for higher shear strength, the greater shear angle is needed to be reached at failure. As the values are 0.26 ± 0.01, 0.27 ± 0.01 and 0.3 ± 0.01 rad for T9, T6 and T3, respec-

tively. It changes -7.0%, -3.5%, and 7.0% when compared to the non-tufted composite sample, respectively. There is no doubt that compared with the reference non-tufted composite, the increase and decrease of shear failure load and of shear failure angle coexist. Wherein, T6 is a critical tufting spacing to optimise the tufting parameters of the final tufted composites.

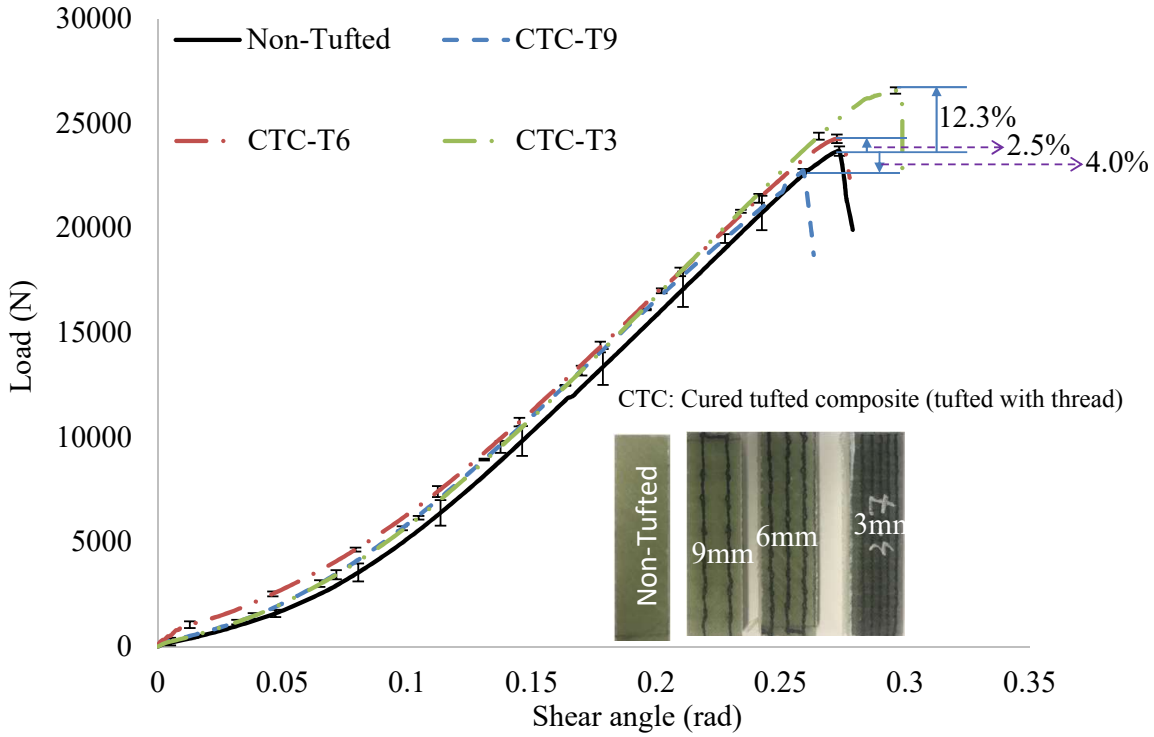

Fig. 3-10. Representative shear load-shear angle curves of CTC samples.

3.3.2.3 Comparison interlaminar shear strength

The comparison results of interlaminar shear properties between CT'C and CTC samples are plotted in Fig. 3-11. It summarizes the average ultimate interlaminar shear strength and the corresponding average shear failure angle shown in 3.11(a) and 3.11(b), respectively. For the same tufting spacing, it can be noted that the improvement of the ultimate shear strength of CTC compared to the CT'C, as 0.4% and 9.3% improvement for the tufting spacing of 6 and 3 mm, however, 2.2% decreases for the tufting spacing of 9 mm. Regarding the corresponding shear failure angle, as depicted in its comparison chart of Fig 3.11(b), increase and decrease by

7% respectively for the tufting spacing of 3 and 9 mm, 3.5% decrease for the tufting spacing of 6 mm. The further discussion will be given in a later section.

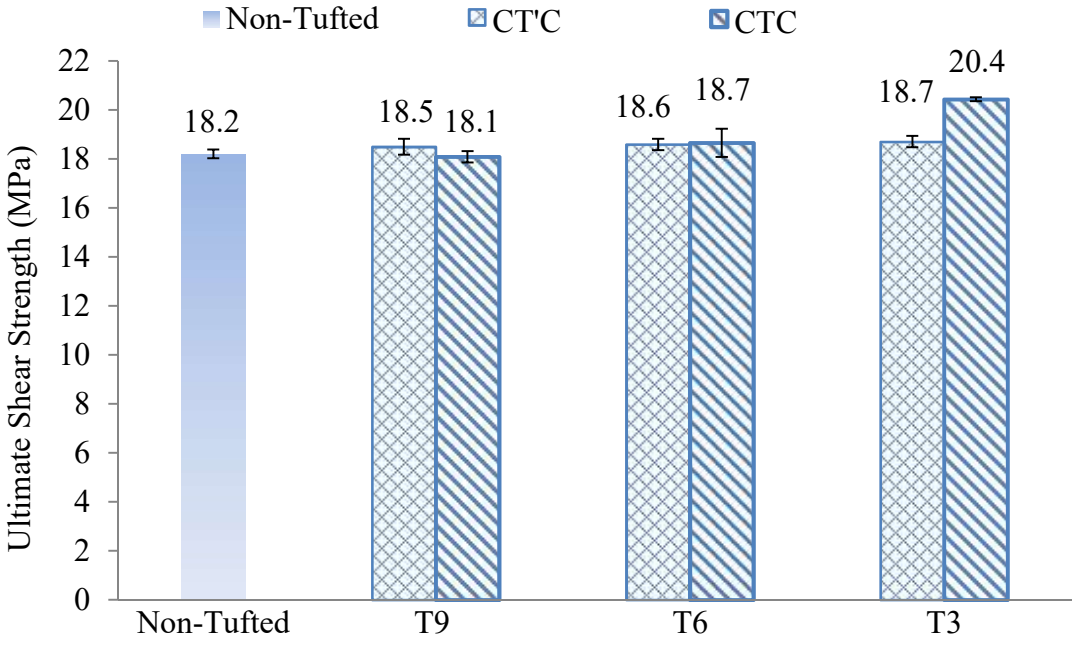

(a) For maximum shear strength

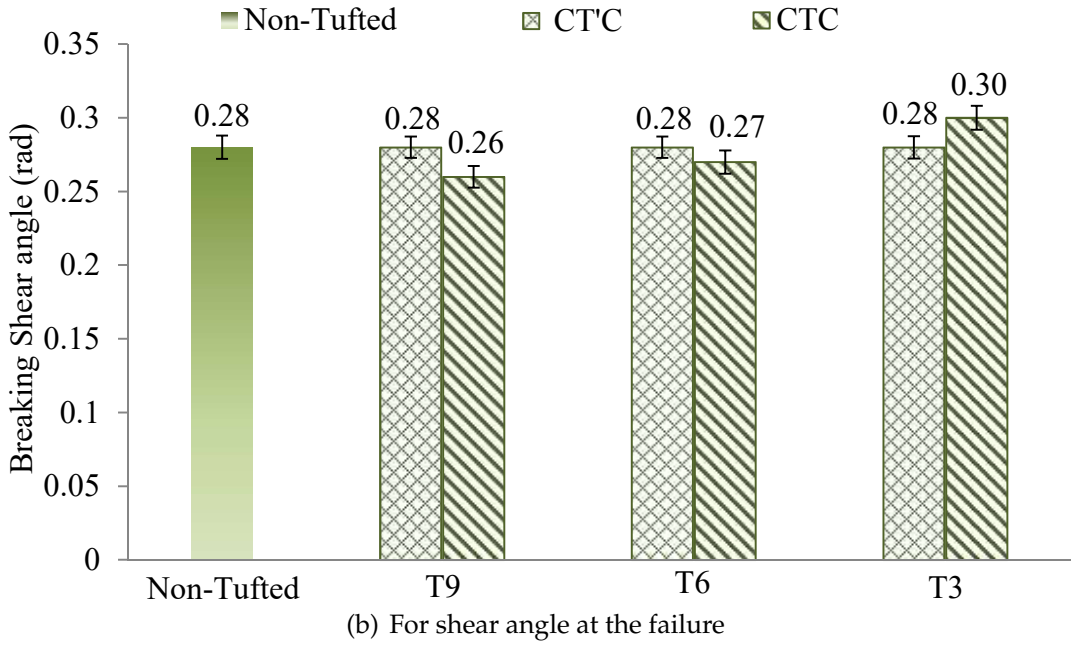

(b) For shear angle at the failure

Fig. 3-11. Comparison of the shear properties between CT'C and CTC samples.

3.4 Discussions

Table 3-2 summarizes the averaged interlaminar shear properties at failure, including the ultimate shear strength and the corresponding shear angle, for all three series samples. It is globally proved that the presence of tufting thread can effectively improve the interlaminar shear performance of the laminated composite under mode II sliding loading condition. The smaller differences in the interlaminar shear strength between the three difference tufting densities of CT'C and the non-tufted composites are negligible. Moreover, the CT'C samples with three different tufting densities yield the same average shear failure angle, actually equal to that of the non-tufted composites, about 0.28 rad. It is believed that the pure tufting action does not significantly affect the interlaminar shear strength. This is due to the lack of in-plane threads in the thickness direction to offer the interlaminar reinforcement in this direction. Therefore, the rationality and feasibility of the two-step tufting method used in the present work are once again confirmed, i.e., a suitable guide needle without thread is placed before the tufting needle. However, it is considered that different tufting needles without threads (pure tufting action) may cause varying degrees of destruction to the preform structure when passing inter layers. It may bring a negative but also a positive effect, even no effect at all. It can nevertheless be controlled by combining the diameter of the tufting needle with the structure of the preform. This topic can be concerned in the future work.

It is to notice that the only tufting configuration which showed lower ultimate shear strength than non-tufted is CTC-T9. In general, the presence of tufting thread effectively binds the laminated preform together to reduce the delamination and then to increase the interlaminar shear strength of the tufted composites. However, i) as the penetration of the tufting thread, the laminate fibres are pushed apart, brings a void which will be filled with resin during the curing process to generate a resin-rich [17, 19, 27], which may weaken the shear loading bearing capacity of CTC-T9 to occur earlier failure under mode ii sliding loading. ii) from the results of DTP seen in Fig. 3-8, it is found that the interlaminar strength of T9 is one-third of T3, much weaker than the others, the destruction to the layer-to-layer or/and inter-layers of the laminate preform may occur with the tufting thread passing through the layers. T9 may not be sufficient to avoid the delamiantion. Therefore, CTC-

T9 may fail due to the weakening of mode II sliding loading bearing, before the tufting thread play its interlaminar enhancement. Tufting density is a remarkable factor to optimise the tufting parameters of the final composites. Wherein, T6 is a critical tufting density to distinguish the positive and negative effect on the present interlaminar shear properties.

By comparing the shear strength curves between DTP specimens and CTC specimens. It is found that the shear strength of the CTC is largely stronger than the DTP's. It thanks to the addition of epoxy resin matrix, it increases the shear mode ii sliding loading bearing to improve the strength performance of the final composites. The same ply stacking sequence and the injection of resin may have contributed to the similar stiffness of all CT'C, CTC samples and non-tufted composites. A large difference in the interlaminar stiffness property between the DTP and the CT'C/CTC is observed with the rigid. This can also be attributed to the presence of epoxy resin matrix

Table 3-2
Conclusive interlaminar shearing resistance results of all samples.

Ref. of sample	Tufting spacing (mm)	Shear strength (MPa)	Shear angle (rad)
DTP-T9	9	0.05 ± 0.01	1.04 ± 0.01
DTP-T6	6	0.10 ± 0.02	1.13 ± 0.02
DTP-T3	3	0.15 ± 0.03	1.17 ± 0.02
Non-tufted	—	18.2 ± 0.18	0.28 ± 0.01
CT'C-T9	9 (tufted without thread)	18.5 ± 0.32	0.28 ± 0.01
CT'C-T6	6 (tufted without thread)	18.6 ± 0.23	0.28 ± 0.01
CT'C-T3	3 (tufted without thread)	18.7 ± 0.23	0.28 ± 0.01
CTC-T9	9	18.1 ± 0.23	0.26 ± 0.01
CTC-T6	6	18.7 ± 0.58	0.27 ± 0.01
CTC-T3	3	20.4 ± 0.81	0.30 ± 0.01

Various delamination positions could be found during the test. Under the continuous loading on the sample, three significant states could occur before it breaks, an

example of the rupture process is shown in Fig. 3-12.

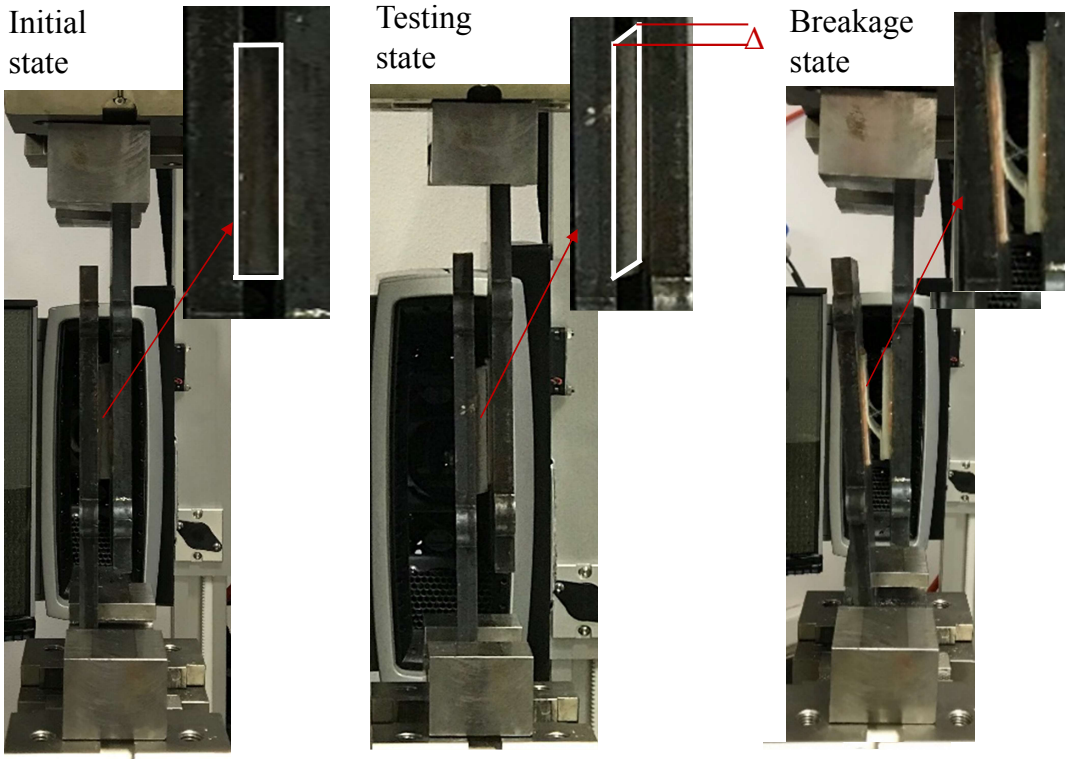

Fig. 3-12. Three principal states of specimens under the Mode II loading test

As shown in Fig. 3-13, it is found that the delamination position among different types of composites is different. The non-tufted one is broken in the middle layer of the composite. However, the delamination position of CTC is totally different than the non-tufted one, they are separated by the applied load on the first top layers (next to the top side) or the last ones (next to the bottom side) of the composite. Nevertheless, tufted with or without thread. It is considered that although the unthreaded tufting process does not bring the enhance of the shear strength, because of the lack of the interlayer bonding strength of the composite material which analysed above. However, due to the movement of the tufting needle between every layer, the yarn of the laminated preform itself has been destroyed to a certain extent, it makes the binding force of the middle layer is higher than the two edges that can be further study in the future.

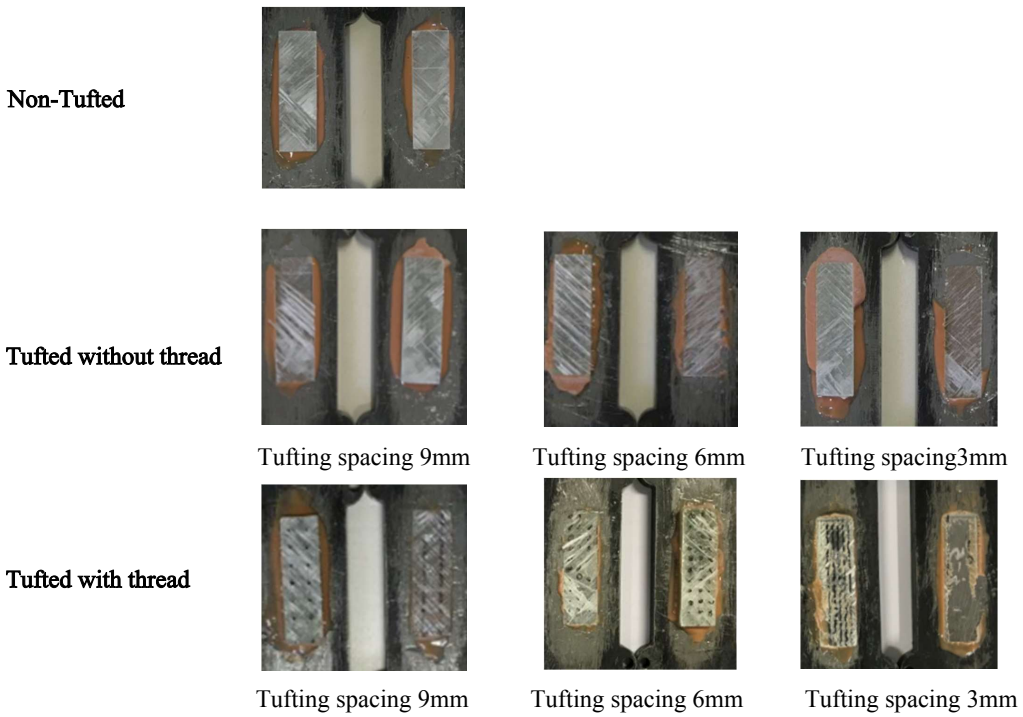

Fig. 3-13. Comparison of rupture position for CTC specimens

3.5 Conclusion of chapter three

In the present chapter, the interlaminar shear performances of multi-scales were studied. Due to the presence of the through-the-thickness tufting thread, reducing the shearing sliding of the laminated sample. Thereby, the mechanical performance of interlaminar shearing under mode ii sliding loading condition is corresponding improved. Several significant conclusions are listed as follows:

- A modified T-steel shearing test is designed that can be effective to study the pure interlaminar shear performance of tufted laminates under three tufting scales (DTP, CT'C and CTC) under mode II sliding loading condition.
- At DTP scale, there is a positive proportional relationship of tufting density and interlaminar shear properties in terms of shear stiffness and strength.
- At CT'C scale, there is an identical result for CT'C series and the non-tufted composites of interlaminar shear properties, regardless the various tufting

densities. The shear stiffness is improved with the resin infused, so does the shear strength and shear angle.

- At CTC scale, with the tufting density increasing, only the shear strength increases. Meanwhile, tufting density brings out positive and negative effects on the interlaminar shear strength compared to the non-tufted. The introduce of Z-direction thread could degrade the interlaminar shear properties under mode II sliding loading condition if the tufting density does not meet the need. Wherein, T6 is the critical tufting density in the present study.

The present focused on the interlaminar shear strength under Mode II sliding loading condition. Therefore, fracture toughness can be subjected to future work. Meanwhile, due to the low-cost, high stiffness, and strength to weight ratio of the tufting process and the tufted composite, developing a new structure to expand its application field is also a worthy work, which will be presented in the following chapter.

Bibliography

[1] A Faggiani and BG Falzon. Predicting low-velocity impact damage on a stiffened composite panel. *Composites Part A: Applied Science and Manufacturing*, 41(6):737–749, 6 2010. ISSN 1359835X.

[2] BG Falzon, SC Hawkins, CP Huynh, R Radjef, and C Brown. An investigation of Mode I and Mode II fracture toughness enhancement using aligned carbon nanotubes forests at the crack interface. *Composite Structures*, 106:65–73, 12 2013. ISSN 02638223.

[3] S Ali, Xm Liu, S Fawzia, J Wu, and YT Gu. A Review on Exploring the Behavior of Multi-Layer Composite Structures Under Dynamic Loading. *International Journal of Structural and Civil Engineering Research*, 5(1):44–51, 2016. ISSN 23196009.

[4] SD Green, AC Long, BSF El-Said, and SR Hallett. Numerical modelling of 3D woven preform deformations. *Composite Structures*, 108(1):747–756, 2014. ISSN 02638223.

[5] Y Mahadik, KAR Brown, and SR Hallett. Characterisation of 3D woven composite internal architecture and effect of compaction. *Composites Part A: Applied Science and Manufacturing*, 41(7):872–880, 2010. ISSN 1359835X.

[6] C Scarponi, AM Perillo, L Cutillo, and C Foglio. Advanced TTT composite materials for aeronautical purposes: Compression after impact (CAI) behaviour. *Composites Part B: Engineering*, 38(2):258–264, 2007. ISSN 13598368.

[7] AP Mouritz. Review of z-pinned composite laminates. *Composites Part A: Applied Science and Manufacturing*, 38(12):2383–2397, 2007. ISSN 1359835X.

[8] DB Bortoluzzi, GF Gomes, D Hirayama, and AC Ancelotti. Development of a 3D reinforcement by tufting in carbon fiber/epoxy composites. *The International Journal of Advanced Manufacturing Technology*, 100(5-8):1593–1605, 2019. ISSN 14333015.

[9] Kimberley Dransfield, Caroline Baillie, and Yiu Wing Mai. Improving the delamination resistance of CFRP by stitching-a review. *Composites Science and Technology*, 50(3):305–317, 1994. ISSN 02663538. doi: 10.1016/0266-3538(94)90019-1.

[10] G Dell'Anno, JWG Treiber, and IK Partridge. Manufacturing of composite parts reinforced through-thickness by tufting. *Robotics and Computer-Integrated Manufacturing*, 37:262–272, 2016. ISSN 07365845.

[11] AP Mouritz and BN Cox. A mechanistic interpretation of the comparative in-plane mechanical properties of 3D woven, stitched and pinned composites. *Composites Part A: Applied Science and Manufacturing*, 41(6):709–728, 2010. ISSN 1359835X.

[12] AP Mouritz and BN Cox. Mechanistic approach to the properties of stitched laminates. *Composites Part A: Applied Science and Manufacturing*, 31(1):1–27, 2000. ISSN 1359835X.

[13] AP Mouritz, MK Bannister, PJ Falzon, and KH Leong. Review of applications for advanced three-dimensional fibre textile composites. *Composites Part A: Applied Science and Manufacturing*, 30(12):1445–1461, 1999. ISSN 1359835X.

[14] AP Mouritz, KH Leong, and I. Herszberg. A review of the effect of stitching on the in-plane mechanical properties of fibre-reinforced polymer composites. *Composites Part A: Applied Science and Manufacturing*, 28(12):979–991, 1997. ISSN 1359835X.

[15] Xiaogang Chen, Lindsay Waterton Taylor, and Li ju Tsai. An overview on fabrication of three-dimensional woven textile preforms for composites. *Textile Research Journal*, 81(9):932–944, 2011. ISSN 00405175. doi: 10.1177/0040517510392471.

[16] LS Liu, T Zhang, P Wang, X Legrand, and D Soulat. Influence of the tufting yarns on formability of tufted 3-Dimensional composite reinforcement. *Composites Part A: Applied Science and Manufacturing*, 78:403–411, 2015. ISSN 1359835X.

[17] G Dell'Anno, DD Cartié, IK Partridge, and A Rezai. Exploring mechanical property balance in tufted carbon fabric/epoxy composites. *Composites Part A: Applied Science and Manufacturing*, 38(11):2366–2373, 2007. ISSN 1359835X.

[18] LS Liu. *Development and optimization of the tufting process for textile composite reinforcement*. PhD thesis, Université de Lille 1, 2017.

[19] JWG Treiber. *Performance of tufted carbon fibre/epoxy composites*. PhD thesis, Cranfield University, 2011.

[20] LS Liu, P Wang, X Legrand, and D Soulat. Investigation of mechanical properties of tufted composites: Influence of tuft length through the thickness reinforcement. *Composite Structures*, 172:221–228, 2017. ISSN 02638223.

[21] J Bertrand and B Desmars. Aerotiss® O3S stitching for heavy loaded structures. *JEC Magazine #18*, pages 34–36, 2005.

[22] DDR Cartié, G Dell'Anno, E Poulin, and IK Partridge. 3D reinforcement of stiffener-to-skin T-joints by Z-pinning and tufting. *Engineering Fracture Mechanics*, 73(16):2532–2540, 2006. ISSN 00137944.

[23] AT Martins, Z Aboura, W Harizi, A Laksimi, and K Khellil. Analysis of the impact and compression after impact behavior of tufted laminated composites. *Composite Structures*, 184:352–361, 2018. ISSN 02638223.

[24] AJ Smiley and RB Pipes. Rate sensitivity of mode II interlaminar fracture toughness in graphite/epoxy and graphite/PEEK composite materials. *Composites Science and Technology*, 29(1):1–15, 1 1987. ISSN 02663538.

[25] AJ Brunner, BRK Blackman, and P Davies. A status report on delamination resistance testing of polymer-matrix composites. *Engineering Fracture Mechanics*, 75(9):2779–2794, 6 2008. ISSN 00137944.

[26] P Wang, S Drapier, J Molimard, A Vautrin, and JC Minni. Characterization of Liquid Resin Infusion (LRI) filling by fringe pattern projection and in situ thermocouples. *Composites Part A: Applied Science and Manufacturing*, 41(1): 36–44, 1 2010. ISSN 1359835X.

[27] C Osmiani, G Mohamed, JWG Treiber, G Allegri, and IK Partridge. Exploring the influence of micro-structure on the mechanical properties and crack bridging mechanisms of fibrous tufts. *Composites Part A: Applied Science and Manufacturing*, 91:409–419, 2016. ISSN 1359835X.

CHAPTER 4

A NOVEL PLATE ASSEMBLY BY TUFTING AND THE OPTIMISATION OF MANUFACTURING PARAMETERS

4.1 Introduction of chapter four

Improved understanding of the pros and cons of tufting technology in the composites field has inspired increasing interest in the development of its potential structures. The structure of tufting is characterised by the insertion of threads in the thickness direction [1, 2] to improve the mechanical properties, for instance, the resistance to delamination, impact resistance, damage tolerance, and joint strength [3–7]. Consequently, its main contribution is to produce lighter and stronger composites parts, which will improve fuel economy and safety in the aerospace, transport, energy, or civil engineering industries [8, 9].

Tufting is an Aerotiss®03S technology [10–12] to assembly dry textile reinforcements by inserting only one thread on one side of the preform, instead of two, along the through-the-thickness (TTR) direction [13, 14]. The thread (Z-reinforcement) is introduced into the preform under relatively low tension, and the needle is retreated while leaving a free tufting loop (FTL) external to the laminate and sometimes remaining internal to it. Currently, tufting is a promising attempt to manufacture thicker and more complex structures [9, 15], given that it is a more flexible local

three-dimensional (3D) technology, differing from other integrate 3D technologies, such as interlocking. Meanwhile, tufting can link together various structures: NCF, braided and woven fabrics, etc.

The application of tufting technology originates from the traditional carpet manufacturing field. However, an infusion technique of resin as the matrix has led the tufting technology to be applied in the high-tech composites manufacturing field for the first time, and the date can be back to 1973 [16, 17] in the open published literature. Follow-up, the researchers are dedicated to expanding its application by the development of new tufting structures. In the early 1990s, several prototypes of tufting structures [18–21] which would be applied in aerospace, have been proposed by Airbus Group SAS. For instance, it is employed in the manufacture of 3D frame, beam and stringer structures on the back of an integrated aircraft door [22]. Furthermore, the excellent performance of tufting in the manufacture of complex 3D structures has resulted in its successful application in an undercarriage demonstrator. It well makes up for the limitation of spatial restrictions of other textile technologies eg. ITA one-sided stitching (OSS) technology [6, 23]. Meanwhile, tufting is also successfully used in the production of automotive frame rails to join I-stiffeners to a braided oval crash tube to enhance its energy absorption during impact [24]. The application of tufting in such stiffener reinforcement has been fully investigated. For instance, a T-stiffener is explored in terms of bending performance and damage tolerance [7, 11, 25], while some focus on the the effect of tufting density and thread materials [26]. Furthermore, Stickler et al.[27–31] used the unique feature of partial tuft insertion to join a novel T-shaped composite butt joint. Another tufted J-stiffener structure that triples the maximum load bearing capacity before failure has been mentioned in [6]. Additionally, Préau et al. [32] demonstrate their research on the manufacture of Ω-stiffener by tufting technology.

Based on literature research, it is also found that tubular assembly is a common component in industrial areas where tufting technology has been applied, such as nozzle assembly in the aerospace field. Unfortunately, there are no applications, or even prototypes, that have been proposed concerning it in the past researches. Therefore, it motivated the idea of manufacturing tubular assemblies by means of tufting technology. Fig. 4-1(a) shows a new conception prototype of the tubular as-

sembly structure by tufting is proposed. However, due to the limitations of the tufting device and in order to better investigate its mechanical properties, the present work initially will focus on the establish of a tufted plate assembly structure (see in Fig. 4-1(b)) and performing fundamental investigations on its performance.

The aim of the present study is to develop the abovementioned tufted plate assembly composites and evaluate its mechanical properties, typically those of the tufting threads. To meet this aim, it firstly to manufacture a typical tufted plate assembly composite suitable for tensile loading testing based on preliminary results. Furthermore, the effect of tufting density, free tufting loop (FTL), and tufting pattern on the failure behaviours and mechanical properties under tensile load need to be taken into account. Meanwhile, the definition of tufting density is given in the present chapter to better characterise the influence factors. Finally, the results will be discussed in terms of the damage repair, mechanical properties, and lightweighting of composites respectively. Wherein, lightweighting will be determined by a relative physical quantity called "Specific Breaking Force" in the present chapter.

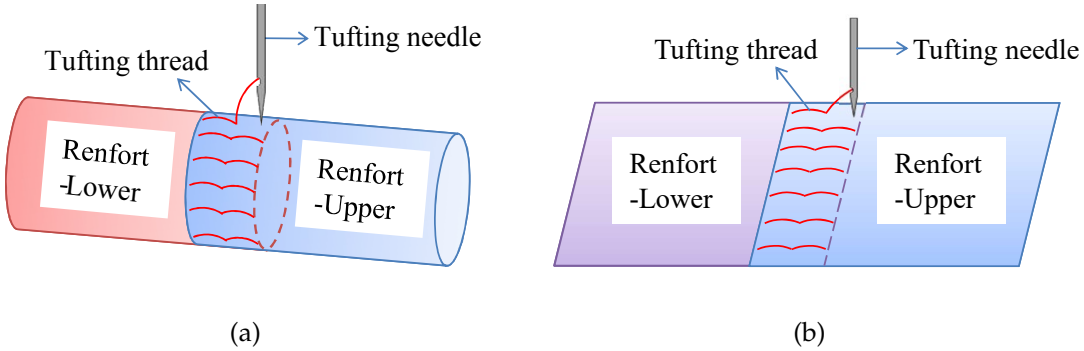

Fig. 4-1. Schematic view of (a) tufted tubular assembly, (b) tufted plate assembly.

4.2 Materials and methods

4.2.1 Materials and samples

The material under investigation is manufactured using 2-step tufting and liquid resin infusion (LRI) techniques, which are introduced in sections 2.4.1 and 1.3.2,

respectively. Besides, tufted preforms are performed by a home-designed tufting device[1] (shown in Fig. 2.3(c)) under the pressure of 2.5 bar (seen in section 1.3.1) and with two hollow needles, seen in Fig.2.4(a), which are a guide needle and a tufting one, respectively. Taking into account the need to extend the research to a subsequent tufted tubular assembly study in the future, a braided fabric with this specific shape advantage is selected as the preform, and its parameters are as follows: Braided E-glass fabric with a braiding angle of 45° and an areal density of 747.4 ± 32 g/m^2. In order to the feasibility of the present study, the braid is firstly cut into a plate shape (namely cut-braided fabric) with a thickness of 1.5 mm and a width of 170 mm (after pretrimmed). Fig. 4-2 shows a schematic representation of the sample stack configuration and an example of a dry tufted plate assembly preform: Two layers of cut-braided E-glass fabrics are superposed in the same orientation with a preset overlap length (noted as Lassy), 35 mm in the present study. Meanwhile, a thin release film is required to be added between the two layers before tufting, which makes the assembly effect focus and only focus on the tufting thread, avoiding the adhesive of infusion resin. This release film is a kind of E2760 red micro-perforated Teflon film manufactured by Cytex. Moreover, the trace dry powder (epoxy as raw material, white colour) is evenly spread on both sides of the braided fabric, to ensure the consolidation of the structure of the preform during the whole preform preparation, even the latter tufting process. However, its potential or possible effect on mechanical properties, in particular the tensile properties, is not taken into account in the present chapter. The overlap is assembled by a twisted 2 x 1k TEX Tenax® JHTA- 40 carbon thread, as shown in Fig. 2-1 and Table 2-1 offers its parameters (in section 2.2). The tufted plate assembly mainly consists of two zones: the "Tuft-assembly" and "Tuft-free" zones, respectively. The existence of the release film, combing the path of the tufting thread, divides the tuft-free zone into the upper one and the lower. These tufted plate assembly preforms are then vacuum infusion on a flat plate, using SICOMIN® SR8200 resin system (with a weight ratio of 100: 37) by LRI (Liquid Resin Infusion) process to produce the tufted plate assembly composites (recall Fig.1-27 in section 1.3.2). The infused composites are cured at room temperature for forty-eight hours. Later, they are machined into the desired dimensions addressed in the following test procedure section using a water-jet cutting technique.

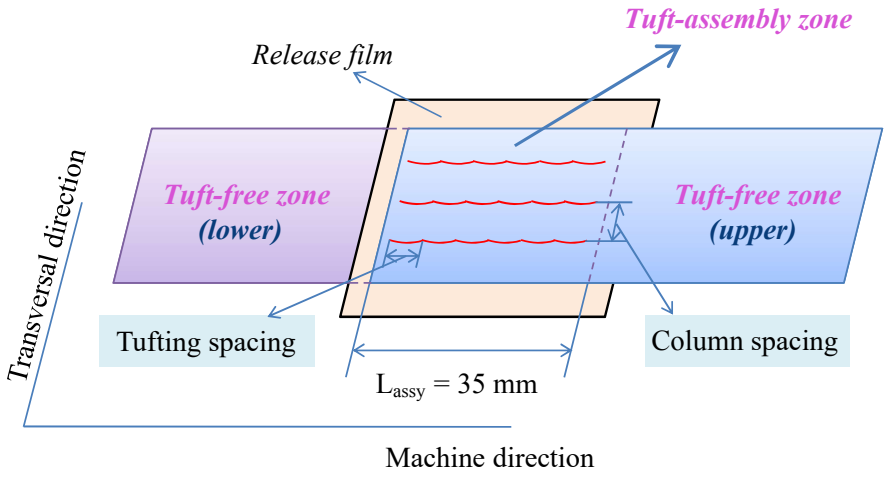

(a) Schematic view of tufted plate assembly.

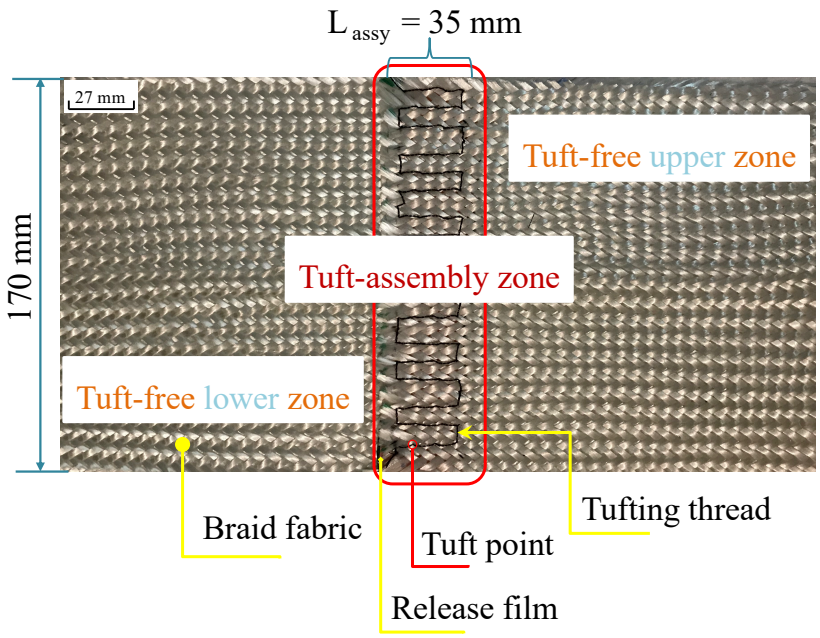

(b) Dry tufted plate assembly preform samples with a tufting spacing of 9 mm.

Fig. 4-2. Tufted plate assembly (a) schematic view, (b) dry preform samples with a tufting spacing of 9 mm.

In order to optimise the tufting parameters on the tensile properties of tufted plate assembly composites. Three group samples are prepared in response with three varying tufting parameters: i) Group A samples are tufted with various tufting densities; ii) Group B samples are prepared without free tuft loop (FTL); iii) Group C samples are tufted at $\pm$ 45° path direction to determine the effect of the tufting pattern. They are introduced in the following paragraphs. Taken into account the potential influence parameters and to uniform the tufting density for the following various tufting configurations, the definition of tufting density needs to be redefined initially as total tuft points (tufts for short) per unit square (pts/mm^2), which has been given in chapter 1/section 1.3.2. Furthermore, the column spacing for all samples are constant as 6 mm in the present study. Meanwhile, the ***tufting spacing*** is used to be characterised as the tufting density in the sample preparation stage. Moreover, it is used as the basis for naming samples. Table 4-1 summarizes the description of each group sample as reported in detail in the following paragraphs.

Group A: This group studies mainly on the influence of tufting density on the mechanical properties of tufted plate assembly composites. Firstly, the minimum tufting spacing that can be prepared is 3 mm (noted as A3), because of the limitation of the 2 mm diameter of the tufting needle. Meanwhile, in order to ensure that the sample does not delamination before testing to meet the research feasibility, two tufts at least in each column, that is, at least a total of 6 pts of tufts. In addition, leaving a suitable distance to the edge, 27 mm of tufting spacing is finally selected to prepare an A27 sample with 6 tufts in total of the sample (called ***total tufts in sample*** with the unit of pts). And on this basis, A9 is prepared to correspond to the 27 mm tufting length of each column in the above. Finally, returning to the original intention of the samples in this group, six samples with respective tufting spacing from 8 mm to 4 mm (diminished at intervals of 1 mm) are also prepared to meet the requirements of sufficient tufting density. Furthermore, all samples in this group are tufted into rectangular patterns, it means that the tufting path direction is consistent with the machine direction (tufting path angle of 0°). The top and bottom sides of the typical samples in the group A are included in the inserts of Fig. 4-4.

Group B: This group focus on the influence of FTL on the mechanical properties of tufted plate assembly composites. An important challenge for response samples

in this group is to remove the FTL, but how? The first thing to determine is to better remove FTL under the principle of avoiding the destruction of the original mechanisms of tufted plate composites to the maximum extent. A special foam, which does not absorb the resin and retains the FTL inside, is placed under the preform during the whole tufting process and resin infusion stages. After the resin infusion, these FTLs are then trimmed off manually by scissors followed by peeling off the foam with preform, but with a little loss of surface finish of the composites anyway. And then to accomplish the research about the influence of FTL on the tufted plate assembly composites. According to the dense, medium, and loose of tufting density level, the samples with FTL with tufting spacing of 27, 9, and 3 mm are selected from group A as three comparative samples. Consequently, in the B group, samples in rectangular patterns without FTL of B27, B9, and B3 are prepared finally. Same as group A, the top and bottom sides of the typical samples in group B are included in the inserts of Fig. 4-5.

Group C: This group concentrates on the influence of tufting pattern on the mechanical properties of tufted plate assembly composites. The difference from the samples of group A and group B is that the tufting path angle is in $\pm$ 45° for samples in group C, which makes the tufting patterns are totally different with the rectangular one. However, these two varying tufting patterns are with an identical column spacing of 6 mm: i) C1 with a - 45° direction of the initial step, namely "cross". It is because that there is a cross point between the two tufting columns, but without any effective influence on the final tufted product, for its penetrate-free into the preform, which makes the real column spacing is 12 mm. The row spacing is also predetermined as 12 mm, resulting a tufting spacing of 8.49 mm. ii) C2 with a 45° direction of the initial step, namely "reciprocation" as well, all because of the tufting pattern showing a reciprocating path on the top surface of the preform. Since the presetting of column spacing and row spacing are both 6 mm, and the tufting spacing is calculated as 16.97 mm. The top side of these two typical samples C1 and C2 are included in the inserts of Fig. 4-6.

The preliminary non-tufted plate assembly composite sample with release film can be separated without applied load. No test results are conducted in a later section. Therefore, except for the non-tufted plate assembly composites, Table 4-1 summarizes the description of the tufting configuration for all samples in the three groups

as reported in detail above. Moreover, As recapped in Table 4-1, it is found that the same total tufts in sample may with different tufting density, A7 and A8, for example. The tufting density and total tufts in sample of C1 (0.69 pts/cm^2 and 8 pts respectively) are similar to the A27 (0.62 pts/cm^2 and 6 pts respectively); On the contrary, the same tufting density may with different total tufts in sample, A6 and C2 with the same tufting density of 2.78 pts/cm^2, for example, have different total tufts in sample of 18 pts and 16 pts, compare to A7 and A8, respectively. Therefore, in the following discussion, as long as the tufting density is involved, the total tufts in sample should be taken into account as a factor.

Table 4-1
Samples that meet various influencing factors and their designated nomination.

Ref. of sample	Free tuft loop (FTL) (with/without)	Column spacing (mm)	Tufting path direction (°)	Row/Tufting spacing (mm)	Tufting density (pts/cm^2)	Total tufts in sample (pts)
A27	with	6	0	27	0.62	6
A9				9	1.86	12
A8				8	2.09	15
A7				7	2.39	15
A6				6	2.78	18
A5				5	3.34	21
A4				4	4.17	27
A3				3	5.56	36
B27	without	6	0	27	0.62	6
B6				6	2.78	18
B3				3	5.56	36
C1	with	6	$\pm$ 45	12 / 16.97	0.69	8
C2				6 / 8.49	2.78	16

4.2.2 Testing procedure

The tensile test is used to require test dimensions of 130 $\times$ 25 mm^2 (after optimisation) in the present chapter. Meanwhile, the alignment tabs of dimensions 20 mm $\times$ 25 mm $\times$ 1.5 mm (in length $\times$ width $\times$ thickness, respectively) are placed at the two ends of the tufted assembly sample, prior to the resin infusion stage as shown in Figure 4.3(a), to ensure the centring of the sample between the tensile testing grips, so as to avoid alliteration during the tensile testing. Therefore, thirteen prepared tufted plate assembly composites with different tufting configurations can be cut into a total of seventy-eight samples, six for each tufting configuration, with an overall dimensions of 170$\times$ 25 mm^2. The default overlap dimensions are 35 $\times$ 25 $\times$ 2.7 ($\pm$ 0.3) mm^3. The test sample is mounted onto the Instron® Universal Testing Machine (Model: 5985) as shown in Fig. 4.3(b) to undergo a tensile test on the tufted plate assembly composite. Tensile loading is directly applied at the centre of the tested samples until failure. During the tensile test, one end of the tested sample is always required to be fixed on the central position of the lower head in the longitudinal direction, whereas another one is carried by the upper head moved upwards at a constant crosshead speed of 2 mm/min. Meanwhile, the initial tensile load vs displacement diagram for each test is traced and plotted in the whole testing. Six-time tests are repeated to be conducted for each configuration of the tufted plate composite samples under identical conditions to calculate the average results.

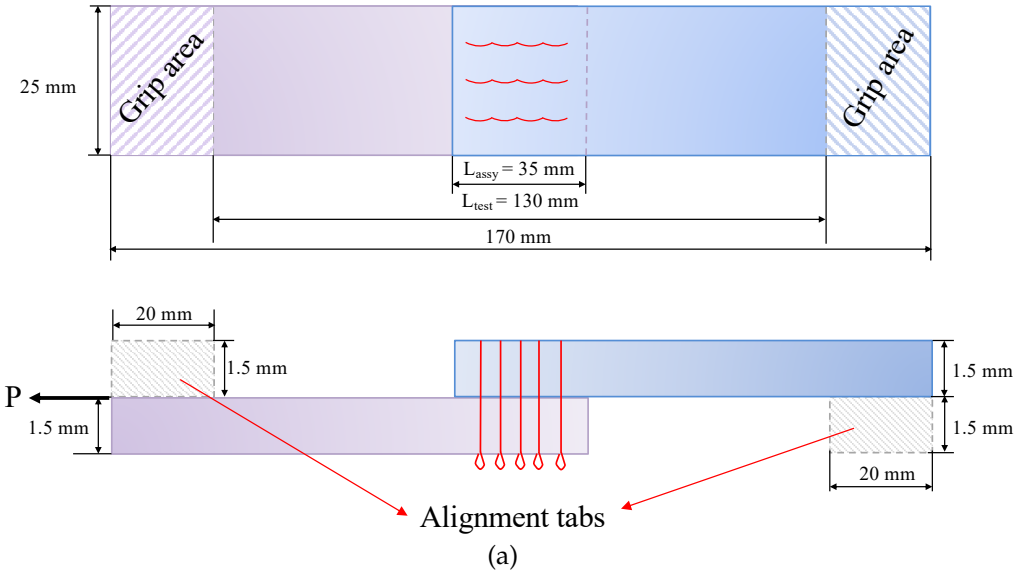

(a)

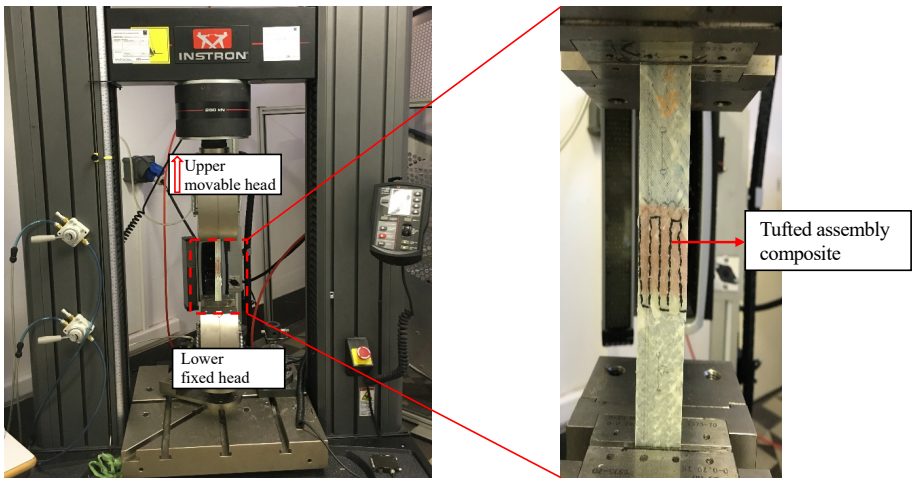

(b)

Fig. 4-3. (a) Dimensional schematic of tensile test for tufted plate assembly sample (*Top:* Top view; *Bottom:* Front view). (b) *Left:* INSTRON® Universal Testing Machine; *Right:* Tensile test set-up.

4.3 Results

4.3.1 Failure position observations

Initially, images of the two typical failure positions, at the "Tuft-assembly" zone and the "Tuft-free", of all tufted plate assembly composite samples are included in the inserts of Table 4-2. The tufting density/total tufts in sample has a remarkable influence on the failure behaviour, whereas it has nothing to do with the tufting pattern or the FTL in the present study. Furthermore, it is can be found that the samples with total tufts in sample of 6 pts (A27 and B27), 8 pts (C1), and 12 pts (A9 and B9) are totally delamination to failure at the "Tuft-assembly" zone shown in the three columns to the left of Table 4-2. On the contrary, the other samples have the occurrence of fracture before delamination (respectively, including A8 and A7 with total tufts in sample of 15 pts and C2 with a total tufts in sample of 16 pts), or even never delamination (samples of A6, A5, A4 and A3 as well B3 with total tufts in sample of 18 pts, 21 pts, 27 pts and 36 pts, respectively) as shown in the three columns to the right of Table 4-2. Whilst, it is revealed that the effective total tufts in sample to avoid delamiantion needs to be equal or superior to 15 pts. Further findings will be reported in a later discussion section.

Table 4-2
Failure position of tufted assembly.

At "Tuft-assembly" zone		At "Tuft-free" zone	
Reference	Total tufts in sample (pts)	Reference	Total tufts in sample (pts)
A27	6	A8	15
B27	6	A7	15
C1	8	C2	16
A9	12	A6	18
B9	12	A5	21
		A4	27
		A3	36
		B3	36

4.3.2 Tensile testing results

The load-strain curves of each group sample will be illustrated in the following sections. To optimize the tufting parameter by means of the intragroup and intergroup comparisons of the results. Wherein, the intragroup comparison results mainly focus on the influence of tufting density; the intergroup comparisons are concentrated on investigating the effect of FTL (groups A and B) and the influence of tufting path direction/tufting pattern (groups A and C).

4.3.2.1 Influence of tufting density

Group A

The tensile load-strain curves of samples in the group A with eight different tufting spacings are illustrated in Fig. 4-4. Overall, all slopes of the curves are similar. It is found that A27 reaches its maximum load at a breaking strain of 1.6 $\pm$ 0.08 %, which is only 1889 $\pm$ 76 N. However, the maximum load of A3 has been already up to 3238 $\pm$ 78.2 N (about 71% stronger than the A27), and its corresponding breaking

strain reaches 4.4 ± 0.15 %. In addition, draw support from Table 4-3 in order to more clearly investigate the relationship between tufting density (the total tufts in sample in particular) and tensile properties. For instance, A8 and A7 own the same total tufts in sample of 15 pts, with the similar maximum tensile load (2505 ± 113.8 N and 2545 ± 87 N, respectively) and the similar corresponding breaking strain (2.5 ± 0.09 % and 2.4 ± 0.21 %, respectively). Moreover, Table 4-3 also recaps that with the density increases, the total tufts in sample also increase, but the growth rate of the maximum tensile load gradually decreases. Such as A6 and A5 (3 pts difference of total tufts in sample) are with similar maximum tensile loads of 2833 ± 116.7 N and 2913 ± 128.8 N and the similar corresponding breaking strain of 3.2 ± 0.11 %, 3.0 ± 0.17 %, respectively. However, the total tufts in sample of A4 is 9 pts less than that of A3, with the similar maximum tensile loads of 3310 ± 92 N and 3238 ± 78.2 N, meanwhile, the similar corresponding breaking strain of 4.3 ± 0.2 %, 4.4 ± 0.15 %, respectively.It can be observed that as the density increases, the maximum tensile required roughly increases.

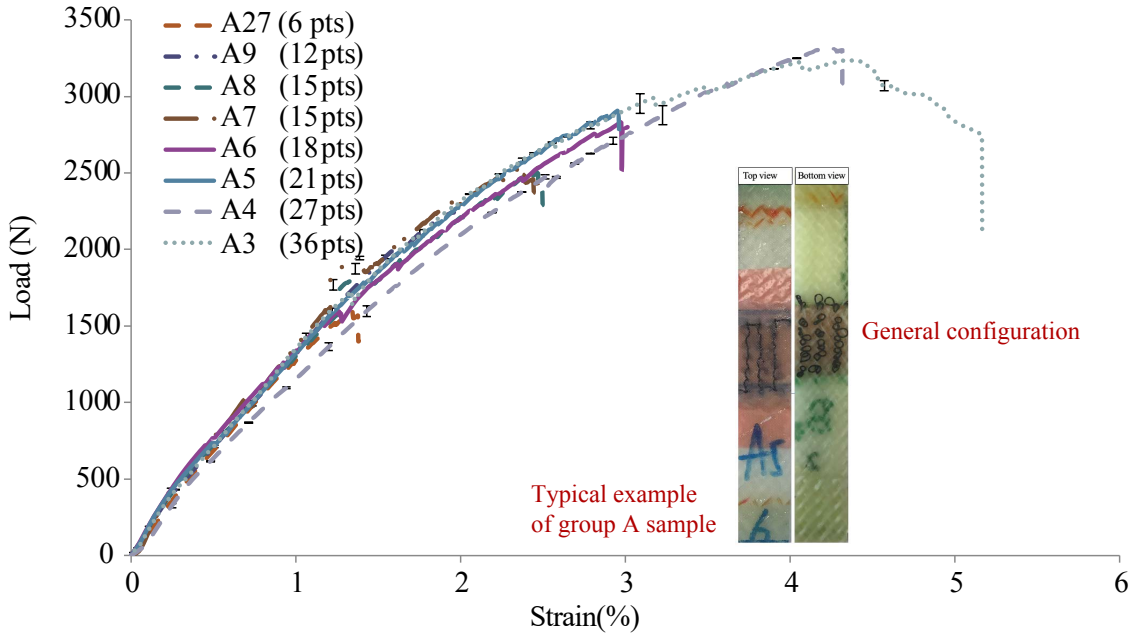

Fig. 4-4. Tensile load *vs.* strain curves of group A samples.

Table 4-3
Tensile properties of group A samples.

Ref. of sample	Total tufts in sample (pts)	Tufting density (pts/cm^2)	Breaking strain (%)	Maximum tensile load (N)
A27	6	0.62	1.6 ± 0.08	1889 ± 76.0
A9	12	1.86	2.0 ± 0.14	2242 ± 44.4
A8	15	2.09	2.5 ± 0.09	2505 ± 113.8
A7	15	2.39	2.4 ± 0.21	2545 ± 87.0
A6	18	2.78	3.2 ± 0.11	2833 ± 116.7
A5	21	3.34	3.0 ± 0.17	2913 ± 128.8
A4	27	4.17	4.3 ± 0.20	3310 ± 92.0
A3	36	5.56	4.4 ± 0.15	3238 ± 78.2

Group B

The load-strain curves of samples without FTL in group B are plotted in Fig. 4-5 and the values are listed in Table 4-4. These samples are trimmed off the FTL at the bottom side prior to the resin infusion. The maximum tensile of 1941 ± 59.7 N, 2232 ± 27.8 N, and 3238 ± 76.4 N for B27, B9, and B3, respectively. Regarding to the corresponding breaking strain, 1.5 ± 0.13 %, 2.1 ± 0.08 %, and 4.3 ± 0.08 % for B27, B9, and B3, respectively. It directly confirms that as the tufting density increases and the total tufts in sample increases, the tensile properties will also increase, which gives very consistent results compared to those with FTL in group A.

Table 4-4
Tensile properties of group B samples (Without FTL).

Ref. of sample	Total tufts in sample (pts)	Tufting density (pts/cm^2)	Breaking strain (%)	Maximum tensile load (N)
B27	6	0.62	1.5 ± 0.13	1941 ± 59.7
B9	12	1.86	2.1 ± 0.08	2232 ± 27.8
B3	36	5.56	4.3 ± 0.08	3238 ± 76.4

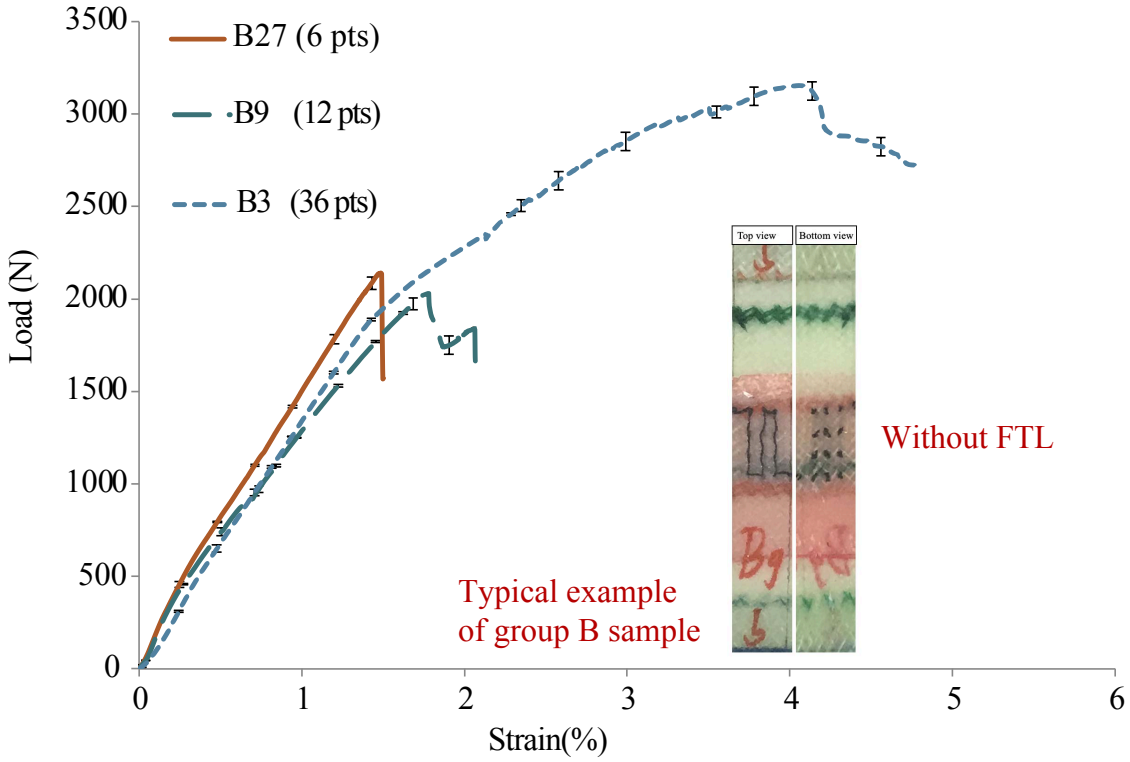

Fig. 4-5. Tensile load *vs.* strain curves of group B samples (without FTL).

Group C

The tensile load *vs* strain curves of C1 and C2 are illustrated in Fig 4-6 and the value results are listed in Table 4-5. These samples are tufted at ± 45°. The maximum tensile of 1795 ± 29.2 N and 2508 ± 127.5 N for C1 and C2, respectively. Regarding to the corresponding breaking strain, 1.3 ± 0.08 % and 2.3 ± 0.14 % for C1 and C2, respectively. It is also found that the denser the tufting density and the more the total tufts in sample, the stronger the strength of the sample, which still gives fairly consistent results regardless of the comparison with group A or B.

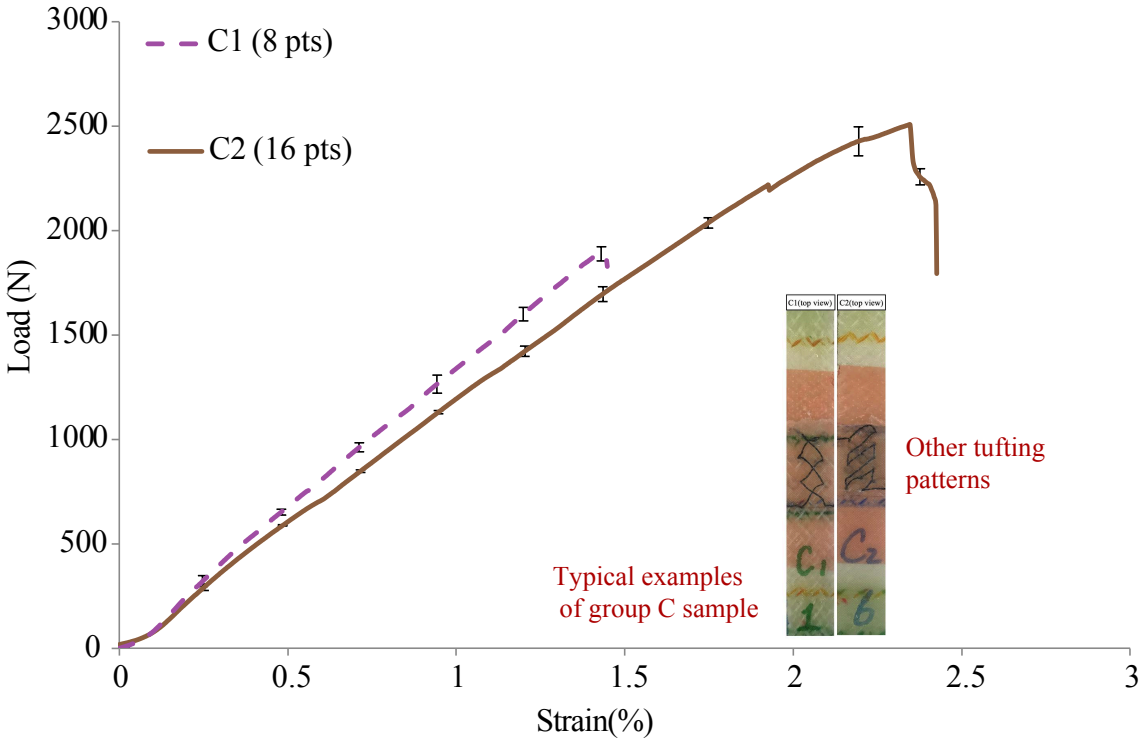

Fig. 4-6. Tensile load *vs.* strain curves of group C samples (± 45° tufting patterns).

Table 4-5
Tensile properties of group C samples (± 45° tufting patterns).

Ref. of sample	Total tufts in sample (pts)	Tufting density (pts/cm^2)	Breaking strain (%)	Maximum tensile load (N)
C1	8	0.69	1.3 ± 0.08	1795 ± 29.2
C2	16	2.78	2.3 ± 0.14	2508 ± 127.5

4.3.2.2 Influence of free tuft loop (FTL)

Fig. 4-7 summarizes the comparison of the mean maximum tensile load and the corresponding failure strain between group A and group B, with and without FTL respectively. There is no missing force for B27, B9, and B3 with the FTL trimmed off under identical conditions of A27, A9, and A3, respectively. Although there are only three tufting densities, the comparison results are still sufficiently representative, as they represent loose, medium, and dense tuft levels, respectively. It is obviously noted that the same proportion improvement of mechanical properties under tensile loading between group A and group B with the tufting density increased, corresponding to the results in the previous subsection. However, as for the same tufting density, there are no important differences as to be negligible in group B samples without FTL compared to group A. The similar maximum failure load is required when the failure strains reach the similar value. Therefore, without doubt that it is not a perfect agreement between group A and group B, but the trend is definitely the same. It can be considered that there is no influence of FTL on the mechanical properties under tensile loading of the tufted plate assembly composite, regarding either in terms of the maximum tensile load or the corresponding breaking strain.

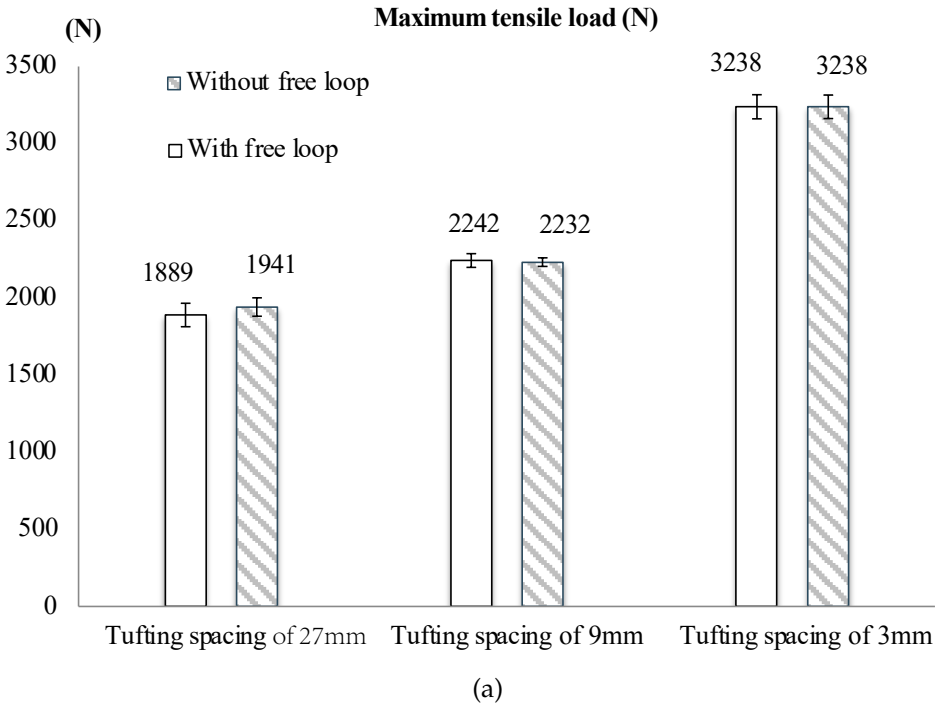

(a)

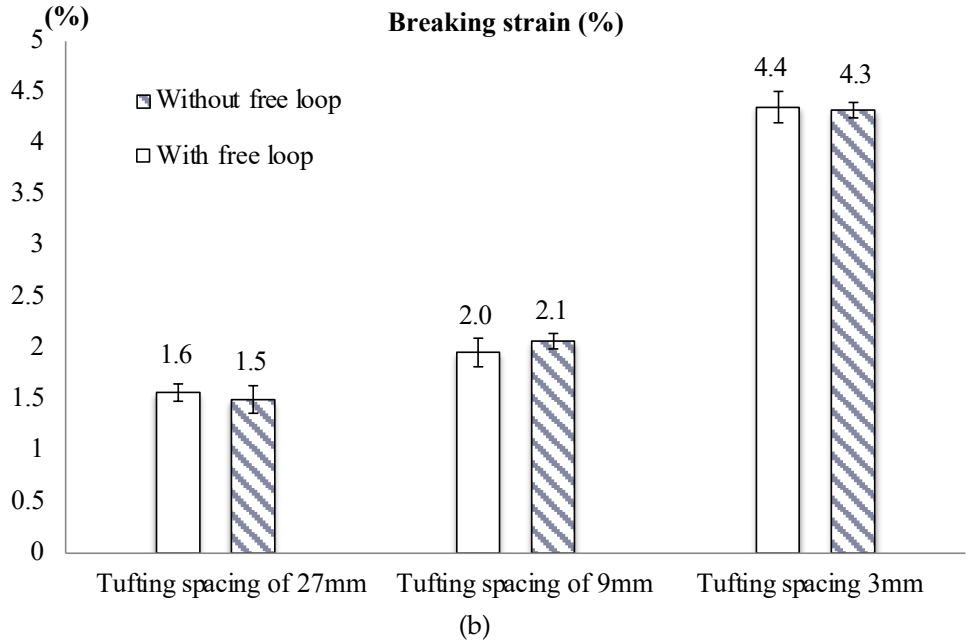

(b)

Fig. 4-7. Comparison of the tensile properties (a) maximum tensile load and (b) breaking strain of tufted plate assembly composite between with and without FTL.

4.3.2.3 Influence of tufting pattern

Fig. 4-8 revels the comparison of the mean maximum tensile load and the corresponding failure strain between group A and group C, under varying tufting patterns. In the present work, that is, the comparison of tufting path angles of 0° and ± 45°, respectively. This intergroup comparison is based on tufting density per area and on total tufts in sample, respectively. Wherein, the tufting density of C1 (0.69 pts/cm^2 and 8 pts in total) is similar to the A27 (0.62 pts/cm^2 and 6 pts in total). However, with regard to tufting density per area, C2 (2.78 pts/cm^2) is identical to the A6 (2.78 pts/cm^2), while in terms of total tufts in sample, C2 (16 pts) is similar to A7 and A8 (15 pts).

Firstly, comparing C1 and A27, the respective maximum tensile load and failure strain of C1 are 94 N and 0.3 % smaller than those of A27, although both are within the margin of error, C1 is slightly denser than A27, a little contrary to the previous intragroup results. Next, the comparison of C2 with group A: i) C2 and A6 with the same tufting density per area of 2.78 pts/cm^2, but the total total tufts in sample of C2 (16 pts) are 2 pts less than for A6 (18 pts) , it is relatively logical that there are 325 N and 0.9 % decrease of C2 than A6 for the maximum tensile load and failure strain, respectively. ii) C2 and A7 as well A8 with a similar total total tufts in sample of about 16 or 15 pts, although the tufting density of C2, A7, and A8 are slightly differences as 2.78 pts/cm^2, 2.39 pts/cm^2 and 2.09 pts/cm^2, respectively, the maximum tensile load and failure strain are similar. It is logical that when describing the tufting density, the total number of total tufts in sample is more accurate.

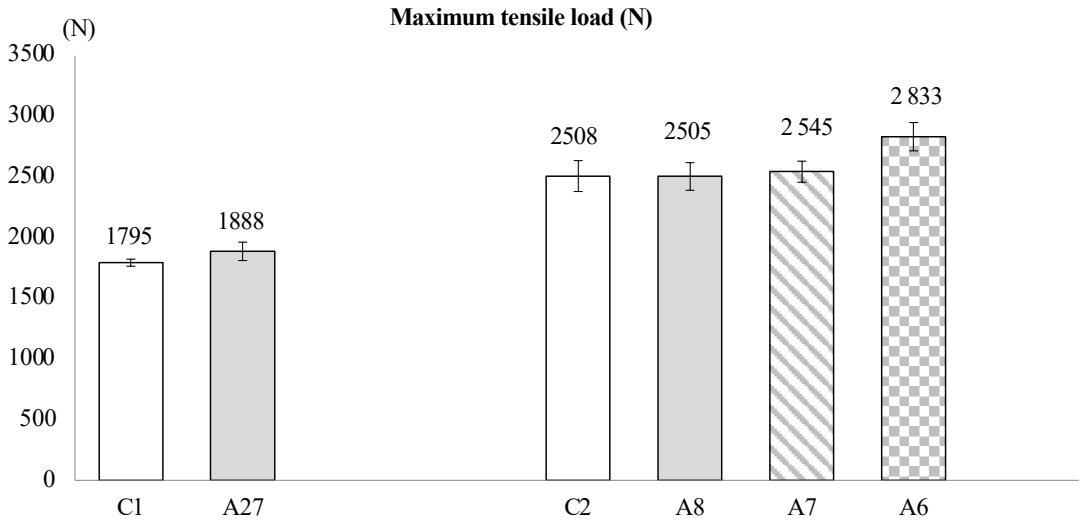

(a) For maximum tensile load.

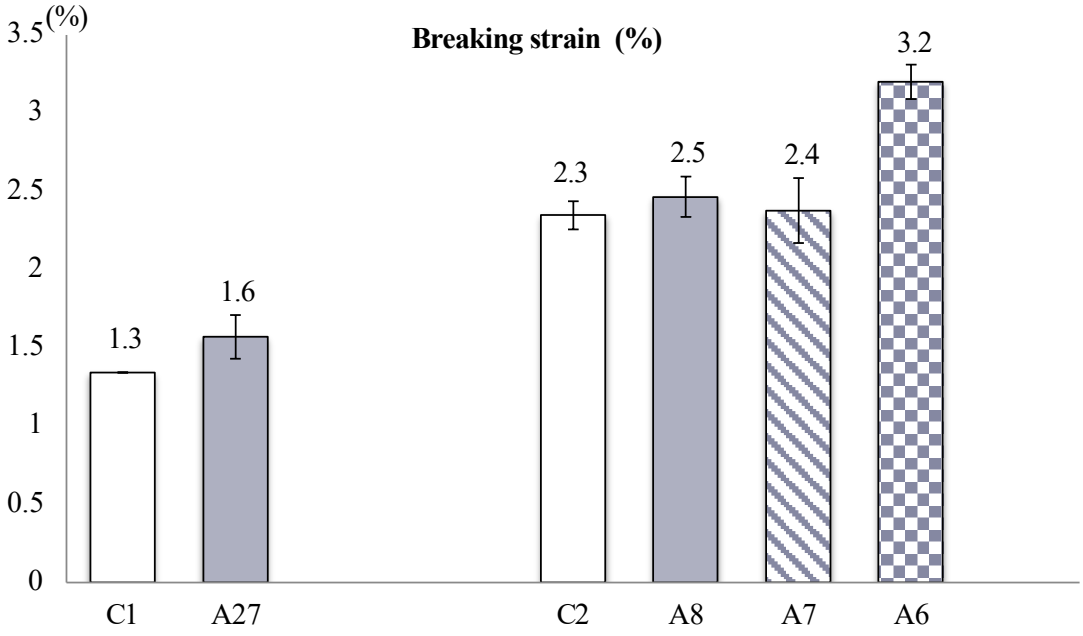

(b) For breaking strain corresponding to the maximum load.

Fig. 4-8. Comparison of the tensile properties of tufted plate assembly composite with different pattern.

4.4 Discussion

The results of the tensile test in group C have demonstrated that the total total tufts in sample with its higher accuracy has a certain essential to replace the total tufts per unit area in mm^2 to express the influence of tufting density parameter on the tensile performance of the tufted plate assembly composite (see Fig. 4-8). There is no typical influence of the presence of FTL of tufting thread on the tensile properties in terms of experimentation (call Fig. 4-7). However, the absence of FTL can reduce the weight of the composite part. To better understand this point of view, it is deemed that the tensile behaviour can be reasonably well characterized using a "specific breaking force" for the tufted plate assembly composite, especially in the industrial applications field. It is calculated by the following equation (4.1)

$$Specific\,breaking\ force\ (N/g) = \frac{Breaking\ force\ (N)}{Weight\ (g)} \tag{4.1}$$

Fig. 4-9 presents the specific breaking force curves of tufted assembly composites with and without FTL. As for the same total tufts in sample, it can be fairly noticed a big improvement of the specific breaking force in the tested samples without FTL, compared to the tested samples with FTL. And it is logical that as the number of total tufts in sample increases, the advantage of tufted plate assembly composites without FTL is more outstanding. As shown in Table 4-6, there are 0.9 %, 5.7 %, and 20 % improvement for the total tufts in sample of 6 pts, 12 pts, and 36 pts, respectively, when the FTLs are trimmed off. its in the composite design and responds to the demand for lightweight in the industrial field. It makes perfect sense in the design of composite materials and can satisfy the demand for lightweight industrial applications. Dell'Anno et al. [2] have discussed that it is doable to remove FTLs in tufted samples prior to or after resin infusion. However, regardless of the methods mentioned in their article or what used in the present chapter are manual removal with scissors, which is unfeasible in industrial mass production and market applications. Nevertheless, they also proposed that the industrial shearing machines used in mass carpet production may be a viable commercial solution to this FTL removal issue. It is considered as a cutting-edge front in the future investigation on the application of tufting technology in the composites industry field.

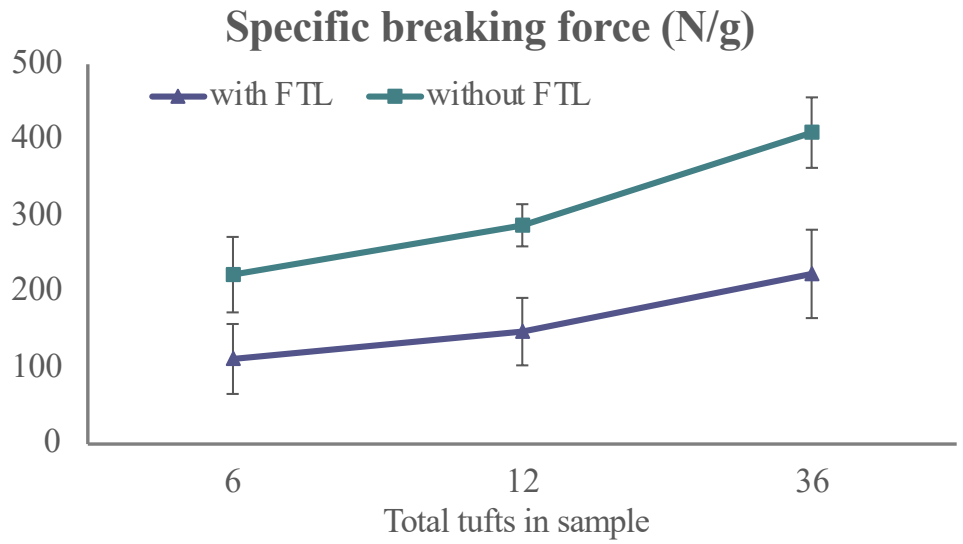

Fig. 4-9. Comparison of specific breaking force between tufted assembly composite part with FTL and without FTL.

Table 4-6
The comparison results of specific breaking force between tufted plate assembly composites with and without FTL.

	Group	Total tufts in sample (pts)		
		6	12	36
specific breaking force (N/g)	A	111	140	186
	B	112	148	224
Increase ratio (%)		0.9	5.7	20

The failure position observation results of all tested tufted plate assembly composite samples have demonstrated three types of failure modes (see Table 4-2): i) only delamination, ii) post-fracture delamination, and iii) only fracture. Firstly, delamination failure obviously occurs at the "Tuft-assembly" zone. However, the fracture failure usually occurs at the "Tuft-free" zone and infinitely close to the "Tuft-assembly" zone but away from the edge, as noted by the yellow ellipse in the rightmost illustration in Table 4-2, where is the stress concentration location, at which failure typically occurs first. Additionally, the fracture failure caused by stress concentration precedes the delamination failure for the tufted plate assembly composite when the number of total tufts in sample reaches a critical value, 15 pts in the present study. Secondly, comparing these two failure positions, the failure at the "Tuft-free" zone, particularly under the failure mode iii (fracture), due to time and economic savings, is a more expected result from the perspective of composites damage repair in the industrial field. Meanwhile, all of these observed tensile failure behaviours are the contribution of the tufting threads, which are isolated in all samples, using the release film between two assembled layers as described in the material description section in the present chapter. Consequently, it is required that at least 18 pts of total tufts in sample, based on the tufted plate assembly composites samples in the present chapter, can effectively avoid delamination under the present tensile conditions, regardless of with or without FTL. It is believed that these failure modes can be dominated by the total tufts in sample of the tufted plate assembly composite sample. However, with the lack of other tufting patterns in mode iii failure, it is not sufficient to reveal whether the tufting patterns will not affect the failure mode. Meanwhile, it is not entirely possible to determine that the tufting pattern has no effect on the mechanical properties under tensile loading due to the insufficient of samples in group C. Both of them are worthy to be investigated and discussed in future work.

4.5 Conclusion of chapter four

In order to expand the application of tufting technology in composites industry field, a novel tufting tubular assembly structure was proposed in the present chapter. Due to the limitation of tufting device and the lack of basic research data, a new

plate assembly composites by tufting and infused by LRI is firstly manufactured to study in the present work. Basic tensile tests were conducted for various tufting parameters of tufted plate assembly composites in groups. And their mechanical performances under this loading condition were analysed. Each intragroup analyses demonstrated that the tufting density is a significant influence factor, and has a positive relevant relationship with mechanical properties. The removal of FTL is of major interest in lightweight design in the composites industry a 20 % improvement of specific breaking force could be reached with a total tufts in sample of 36 pts in the assembly zone. Even the least with 6 total tufts in sample had a 0.9 % increase. Meanwhile, a method to trim off has been presented, whereas it is not available for mass production due to the time cost. Three modes of failure position under the identical tensile loading condition were identified as delamination occurring in the "Tuft-assembly" zone; post-fracture delamination and fracture occurring first in the "Tuft-free" zone. They are depending on the tufting density. By contrast, studies on the effects of tufting patterns on plate assembly composites by tufting have been carried out but are not yet sufficient and could be subjected to future research. Meanwhile, the method or device of manufacturing tubular assembly by tufting and the related mechanical performance studies can be taken into account for future research work.

Tufting thread is a significant factor. A geometry method of tufting thread, which will be briefly presented in the latter section. Meanwhile, plate/tubular assembly composites by tufting are as a novel conception for manufacturing the integrated composite product, there are several problems that need to be studied. Further investigation on this front will be required in the future.

4.6 Perspective of chapter four

4.6.1 Modelling of the tufting thread

Abovementioned results reveal that the tufting threads play a significant role on the tensile properties of tufted plate assembly composites. Therefore, in this mod-

elling, the geometry of the tufting thread is well considered. In this section, a geometrical model of tufted plate assembly is proposed, meanwhile, the study is focused on that of the tufting thread. The present modelling is for the Tenax®-J HTA-40 carbon thread, which is used in this thesis, and its properties are shown in Table 2-2 in chapter 2 / section 2.2.

4.6.1.1 Preliminary study of tufting thread

Thanks to Mme. MAKHSIYAN Nouné, a graduated master IMS student of ENSAIT, she gives various hypotheses of the tufting thread shown in Fig. 4-10. Taken account of the negligible influence of FTL on the mechanical properties, it is therefore only chosen one type of modelling. To confirm these hypotheses, it is necessary to be prepared the tufted composite plate thick enough to visualize the morphology of the tufts loop.

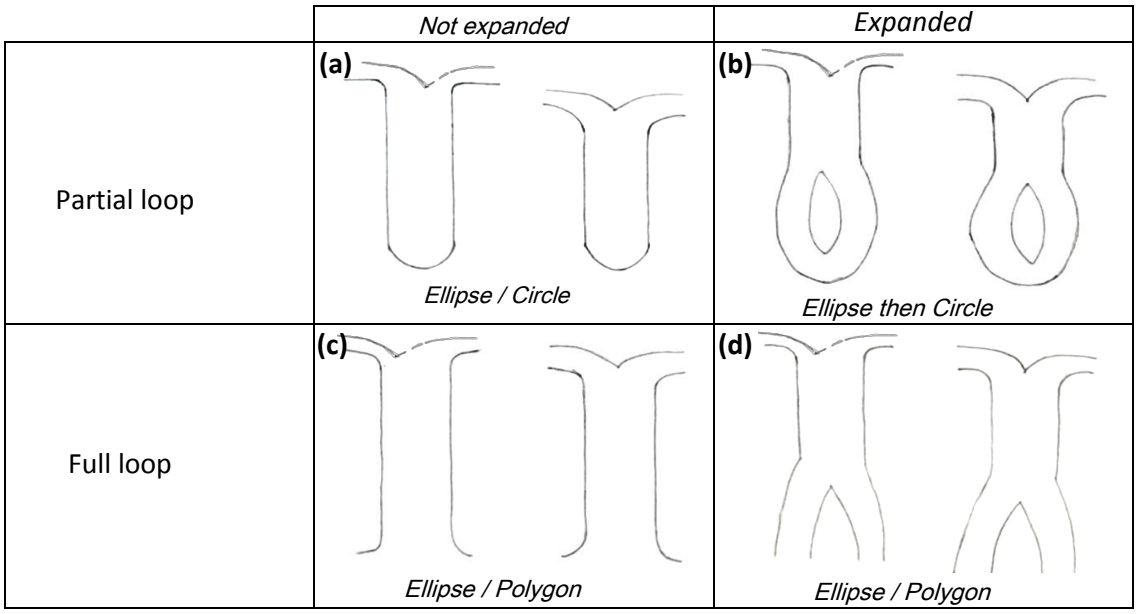

Fig. 4-10. Basic morphology assumption of tufting thread

- **Shape and path of tuft loop**

The cut tufted composite plate needs to be polished until the tufting thread cross-

section can be clearly observed. Then a sectional view of the tufting thread through the thickness is shown in Fig. 4-11. The micro-observation sample is that some points are confirmed concerning the adaption of the thread according to the space offered, although it is not visible on this plan for the shape of the section. Therefore, the images clearly show that the expansion of the loop does not prove to be applied each time on the tufting thread with a free loop. Moreover, according to the sample loops, the expansion does not form an ellipse but rather a parallelogram (according to the vertical path of the needle), this is why it is necessary to verify that the model behaves as closely as possible to the observed reality. And this, even if the modelled shape is elliptical.

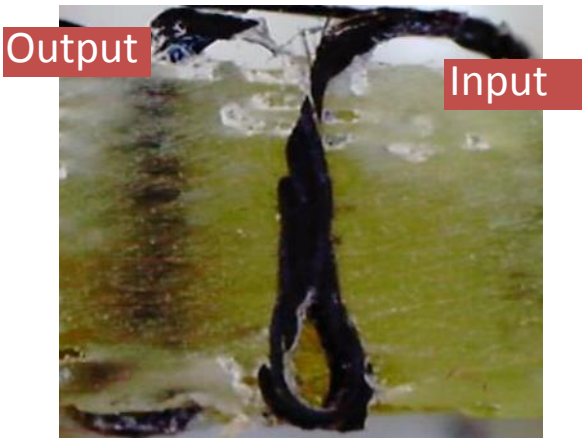

Fig. 4-11. The sectional view of tufting thread through the thickness by ***QMicro-Capture***.

According to the tufting process, the input and output of the tufting thread can be easily indicated on the image above (Fig. 4-11) The initial step of the free loop is positioned lower than another side, because the thread is retracted, a slight displacement could be produced.

- **Cross-section of tufting thread**

An ideal type of tuft loop is sketched and implemented on ***Solidwork***-aided, which can minimise the design steps. It is important for our model to point out the polygonal cross-section of the tufting threads. The image is imported into the software, then the cross-section can be extracted by color recognition or by sketching the

boundary using the sketch basics tool. It is therefore possible to vary the tolerance of the color and shape, as close as possible to the shape by segments, or distant via curves called "splines". Finally, some polygonal cross-sections can be observed in Fig. 4-12.

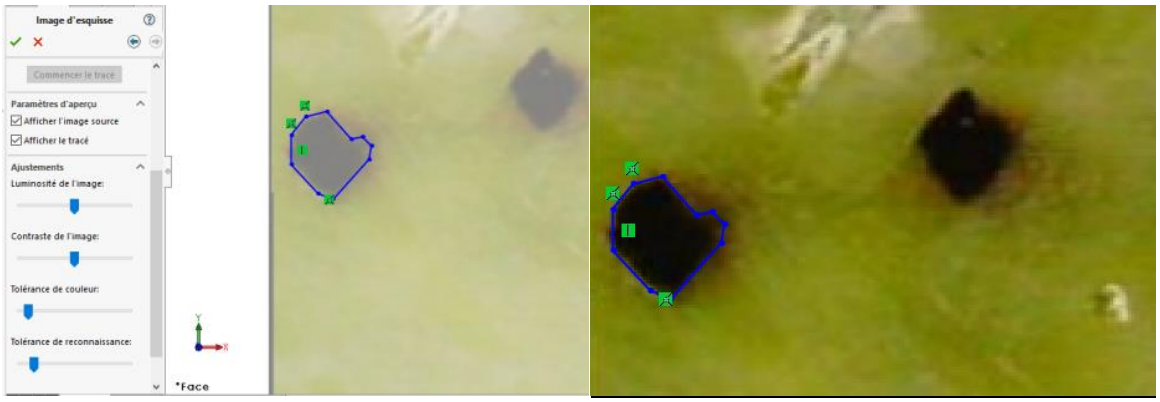

Fig. 4-12. Polygonal section-cross by ***Solidwork***.

4.6.1.2 Geometrical model of tufting thread

The geometrical and mechanical model of textile implemented in ***TexGen***. It offers two ways to implement the internal geometry of almost all types of textile structures. One is to input the necessary data into the software interface directly, another needs the aide of ***Python algorithm***. In the present study, by writing the python script to realise the geometry model of tufting thread and unit cell of the tufted preform. As the general geometry method for the thread shape, it is known that the cross-section is cylindrical or elliptical. However, either is the most realistic for the sample observed. To get closer to the shape of the real tufting thread, the tufting thread model is improved to the polygonal shape in the present study. And three kinds of polygonal cross-section shapes are assumed, illustrated in Fig. 4-13. Because, it is found that the model with less than 6-sides polygon is too rigid, whereas the model with more than 8-sides polygon is too close to a circle (less significance to assign the cross-section as a polygon). The length of the tufting thread loop is depended on the whole plate tufted assembly composite in the present study, the thickness of the tufting thread is defined by its own parameters, and the width of the model is accordance with the tufting density. Meanwhile, it is assumed that the

distribution of fibres over a cross-section is uniform for simplifying the following model calculated. This tuft thread loop model is saved as the STEP file which can transfer to the FE software ***Abaques***.

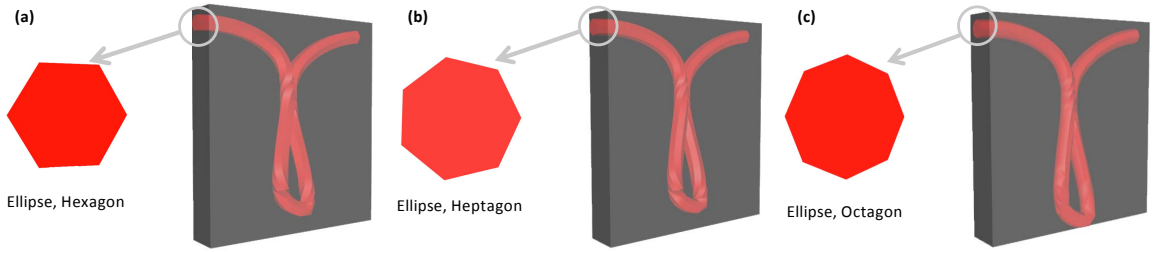

Fig. 4-13. Geometrical model of tufting thread by ***TexGen***.

This model is saved as ".stp" file to be imported into the ***Abaqus*** to further design the model tufted plate assembly and meshing it for validating the model used to finite element (FE) analysis by the macro (M)-level model.

4.6.2 Modelling of the tufted plate assembly composite

- **Modelling approach**

In this chapter, a macro(M)-level model is established in FE software ***Abaqus***. The present study is still based on the cohesive zone model, the difference is that using the established geometrical model of tufting thread instead of the connector element, which used in other models. A model without cohesive zone will be established after this study, which is for the comparison. Therefore, there are four parts used to assemble the final tufted plate composite as shown in Fig. 4-14. They are two glass/epoxy elements, one tufting thread element, and a cohesive element.

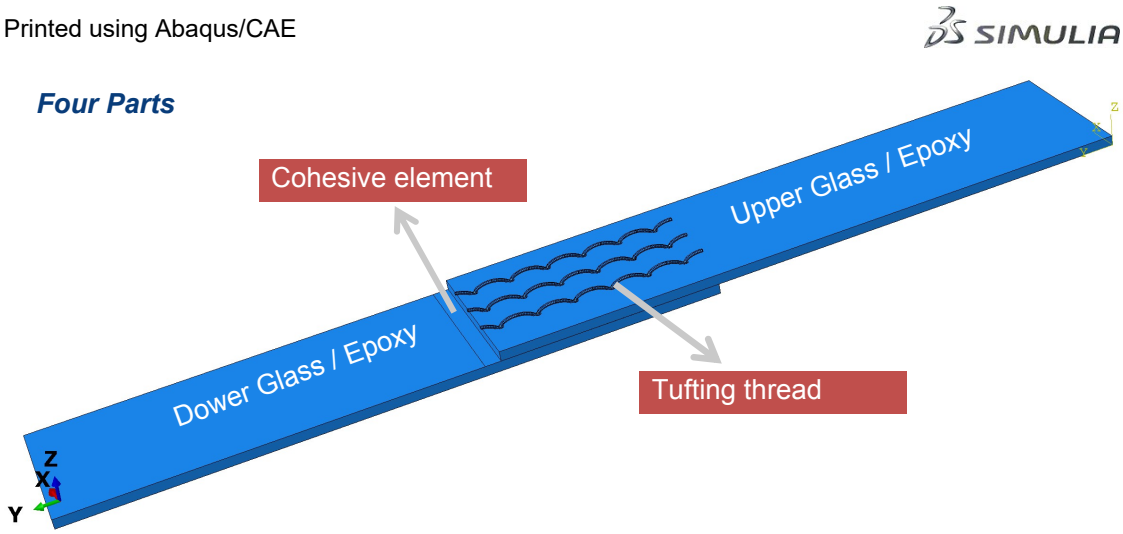

Fig. 4-14. Parts of tufted plate assembly model.

The "cohesive zone model" is typically for the laminated composite. COHESIVE is a new area to divide two layers to characterise the delamination properties. COHESIVE area can be regarded as an area with excess resin, but different from the pure resin area. Its main function is to connect the upper and lower single layers. There are three types of stress on the bonding surface, defined in the following Eq. 4.2:

$$\begin{aligned} \int_0^{\delta_n^{max}} t_n(\delta) d\delta_n &= G_C^n \\ \int_0^{\delta_s^{max}} t_s(\delta) d\delta_s &= G_C^s \\ \int_0^{\delta_t^{max}} t_t(\delta) d\delta_t &= G_C^t \end{aligned} \tag{4.2}$$

The constitutive equation of COHESIVE element is B-K criteria (illustrated in Eq. 4.3), which is with respect to the traction-separation law.

$$G^C = G_n^C + (G_s^C - G_n^C)(\frac{G_S}{G_T})^\eta \tag{4.3}$$

where, $G_S = G_s + G_t, G_T = G_n + G_S$.

Two layers are both glass/epoxy, and everyone is regarded as a whole element, which is defined as isotropic transverse, which is as another constitutive equation of this model. It is assumed that the tufting thread and composite plates are elastic, meanwhile the degradation and damage are not considered.

- ***Model validation (meshing)***

The model can be meshed directly in software Abaqus, then to validation. In this model, four parts under three-type elements use their three mesh types. Fig. 4-15 illustrates the meshing of glass/epoxy and cohesive elements, where the glass-epoxy element is assigned C3D8R element type (An 8-node linear brick, reduced integration, hourglass control), the cohesive element is assigned COH3D8 element type (An 8-node three-dimensional cohesive element). Because of the complex shape of the tufting thread model, C3D4 (A 4-node linear tetrahedron) element is used to assign the tufting thread mode shown in Fig. 4-16 (a). It is not hard to notice that this kind of element type meshing is too rigid. However, the worst thing about this model is that the mesh of tufting thread is unsuccessful, highlighting the default areas in Fig. Fig.4-15(b).

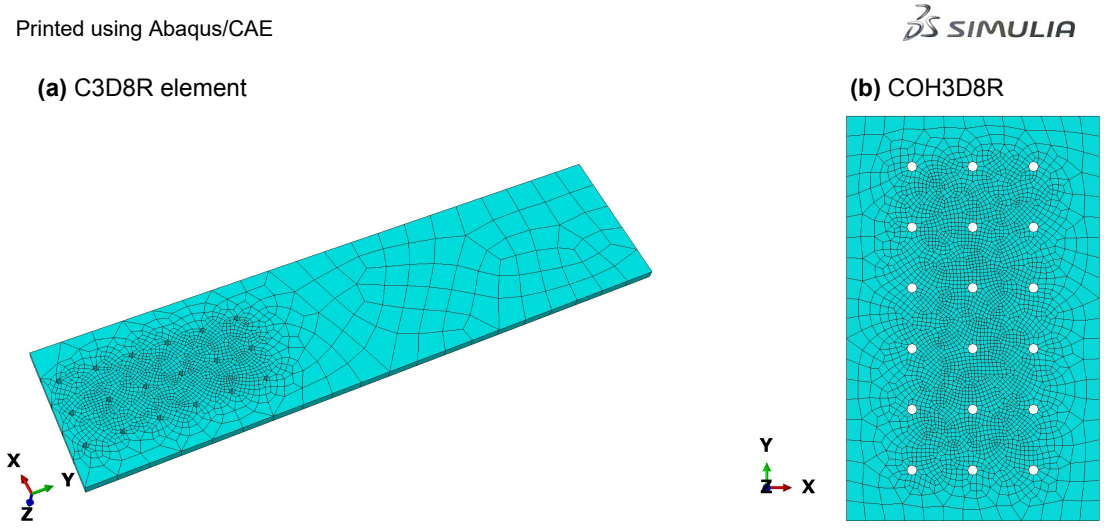

Fig. 4-15. Element meshing (a) glass/epoxy element and (b) cohesive element

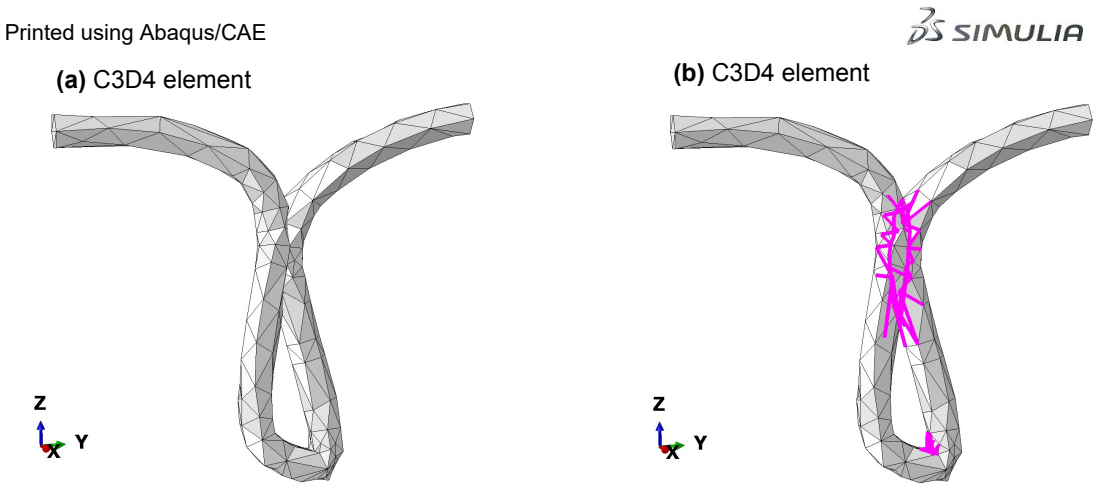

Fig. 4-16. Tufting thread meshing

It is believed that the reason for the failure of mesh creation is its boundary intersection, after several recalculations failures, and the model tufting thread should be optimized, the result is shown in the following:

- **Optimization of tufting thread model**

Fig. 4-16 (b) demonstrates that there are two areas with "boundary intersections". Without changing the basic parameter of tufting thread, the problem is easily become to the thread path. Firstly, for the intersections with "input of tuft free loop" area, the sinking distance at the beginning of the forming the free loop is reduced. Then, for the intersections with "tuft loop" area, to minimize their intersection surface. An important principle is to respect the actual path as much as possible. Therefore, the abovementioned three polygonal cross-sections are optimized. It is found that the mode with 7-gon is much more approximately to the reality. The optimised model and its meshing results are shown in Fig. 4-17.

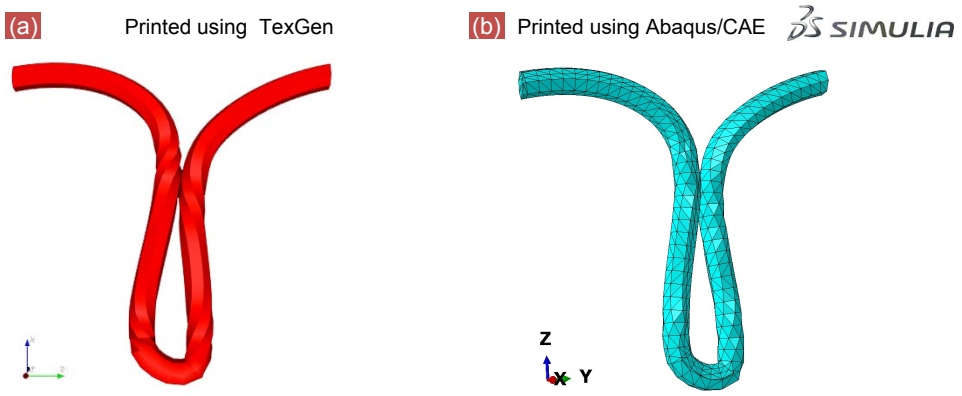

Fig. 4-17. Tufting thread (a) optimized geometrical model and (b) meshing resolution

The meshing of the tufted plate assembly is demonstrated in Fig. 4-18, until now, this model can be used to simulate the mechanical behaviour by the Element Finite (FE) method, which can be the further work.

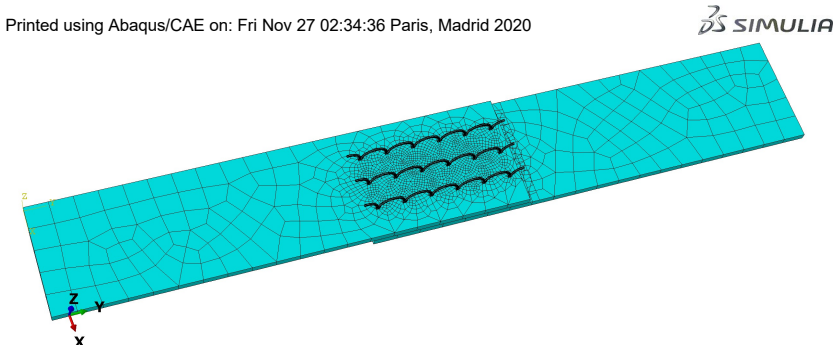

Fig. 4-18. Overall view of tufted plate assembly meshing

Furthermore, this section will focus on the geometrical modelling of tufted plate assembly, which is an interest for the macro(M)-level FE to simulate the mechanical properties. This work is different from other researchers which is focused on modeling the thread, instead of the cylindrical model. Therefore, a model without cohesive element need to be established to fully on the assembly effect only by tufting thread. Regretfully, the lack of some foundations data of materials, this model is on the prototype stage. It will be an interesting and meaningful project worth looking into.

Finally, Fig. 4-19 is the establishment of this unit cell based on the tufting thread

established in this chapter. After optimising the geometrical of the tufting thread, this unit cell can be used to meso(m)-level FE in the further work.

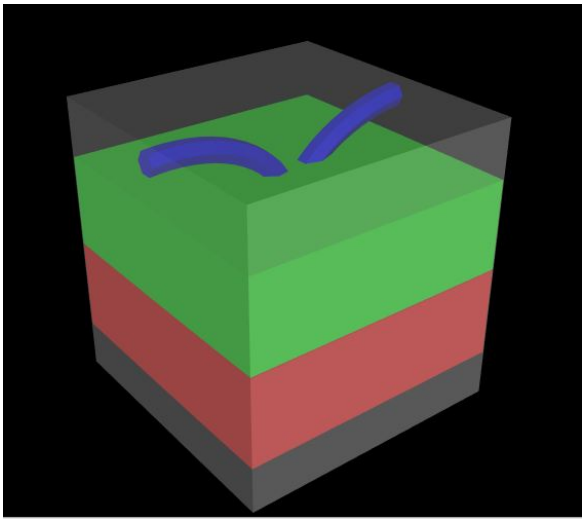

Fig. 4-19. The unit cell of tufted architecture.

Bibliography

[1] LS Liu, P Wang, X Legrand, and D Soulat. Investigation of mechanical properties of tufted composites: Influence of tuft length through the thickness reinforcement. *Composite Structures*, 172:221–228, 2017. ISSN 02638223.

[2] G Dell'Anno, JWG Treiber, and IK Partridge. Manufacturing of composite parts reinforced through-thickness by tufting. *Robotics and Computer-Integrated Manufacturing*, 37:262–272, 2016. ISSN 07365845.

[3] DB Bortoluzzi, GF Gomes, D Hirayama, and AC Ancelotti. Development of a 3D reinforcement by tufting in carbon fiber/epoxy composites. *The International Journal of Advanced Manufacturing Technology*, 100(5-8):1593–1605, 2019. ISSN 14333015.

[4] AT Martins, Z Aboura, W Harizi, A Laksimi, and K Khellil. Analysis of the impact and compression after impact behavior of tufted laminated composites. *Composite Structures*, 184:352–361, 2018. ISSN 02638223.

[5] A Martins. *Analysis of damage mechanisms in composite structures reinforced by tufting*. PhD thesis, Université de technologie compiègne, 2018.

[6] JWG Treiber. *Performance of tufted carbon fibre/epoxy composites*. PhD thesis, Cranfield University, 2011.

[7] J Kratz, H Clegg, G Dell'Anno, and IK Partridge. Improving the damage tolerance of composite joints with tufting. In *Proceeding of the 20th International Conferences on Composite Materials (ICCM20)*, pages 19–24, Copenhagen, 2015.

[8] C Scarponi, AM Perillo, L Cutillo, and C Foglio. Advanced TTT composite materials for aeronautical purposes: Compression after impact (CAI) behaviour. *Composites Part B: Engineering*, 38(2):258–264, 2007. ISSN 13598368.

[9] LS Liu. *Development and optimization of the tufting process for textile composite reinforcement*. PhD thesis, Université de Lille 1, 2017.

[10] J Bertrand and B Desmars. Aerotiss® O3S stitching for heavy loaded structures. *JEC Magazine #18*, pages 34–36, 2005.

[11] P Pérès, B Desmars, and JP Léard. Composite behavior of assemblies with AEROTISS® 03S technology. In *16th International conference on composite materials*, pages 1–5, 2007.

[12] G Cahuzac. A revolutionary way for assembling Aerotiss® O3S technology. In *Composie 2003-matériaux et structure composites*, Paris, 2003.

[13] AP Mouritz, MK Bannister, PJ Falzon, and KH Leong. Review of applications for advanced three-dimensional fibre textile composites. *Composites Part A: Applied Science and Manufacturing*, 30(12):1445–1461, 1999. ISSN 1359835X.

[14] KP Plain and LY Tong. The effect of stitch incline angle on mode I fracture toughness - Experimental and modelling. *Composite Structures*, 92(7):1620–1630, 2010. ISSN 02638223.

[15] LS Liu, T Zhang, P Wang, X Legrand, and D Soulat. Influence of the tufting yarns on formability of tufted 3-Dimensional composite reinforcement. *Composites Part A: Applied Science and Manufacturing*, 78:403–411, 2015. ISSN 1359835X.

[16] DW Bauer and WV Kotlensky. Relationship between structure and strength for CVD carbon infiltrated substrates. Part II- Three dimensional woven, tufted and needled substrates. *SAMPE Quarterly*, 4(2):10–20, 1973.

[17] S.D. Green and G. Dell'Anno. Impact resistance of carbon/epoxy L-sections reinforced through-the-thickness by tufting. In *Proceeding of the 21th International Conferences on Composite Materials(ICCM)*, 2017.

[18] Cahuzac Georges and François Monget. Process and machine for the production of armature for a piece of composite material: France, FR0678609 B1[P], 1994.

[19] Georges Cahuzac. Stitching head and machine for producing a plate-shaped frame for a piece of composite materialm: France, FR2718759[P], 1994.

[20] Jean-Louis Darrieux. Procede pour la realisation d'une armature de fibres pour piece de matiere composite, et piece composite comportant une telle armature: France, FR2687173[P], 1992.

[21] Georges Cahuzac. Process for producing a fiber reinforcement for a composite material part with non-coplanar walls, and a composite part comprising such an armature: France, FR2687174[P], 1992.

[22] J Sloan. Integrated, optimized aircraft door. *High-performance composites*, pages 61–68, 2012.

[23] E Laourine. *Einseitige Nähtechnik für die Herstellung von dreidimensionalen Faserverbundbauteilen*. PhD thesis, Lehrstuhl für Textilmaschinenbau und Institut für Textiltechnik, 2005.

[24] P Schiebel and AS Herrmann. Textile preform technologies in the aviation sector –chances and challenges for the automotive sector. In *Industrial Fabrics Association International-Advanced Textiles Europe Conference*, 2008.

[25] DDR Cartié, G Dell'Anno, E Poulin, and IK Partridge. 3D reinforcement of stiffener-to-skin T-joints by Z-pinning and tufting. *Engineering Fracture Mechanics*, 73(16):2532–2540, 2006. ISSN 00137944.

[26] AR Mills and J Jones. Investigation, manufacture, and testing of damage-resistant airframe structures using low-cost carbon fibre composite materials

and manufacturing technology. In *Proceedings of the Institution of Mechanical Engineers, Part G: Journal of Aerospace Engineering*, volume 224, pages 489–497. SAGE Publications Sage UK: London, England, 2010.

[27] PB Stickler, M Ramulu, and PS Johnson. Experimental and numerical analysis of transverse stitched T-joints in bending. *Composite Structures*, 50(1):17–27, 2000. ISSN 0263-8223.

[28] PB Stickler and M Ramulu. Investigation of mechanical behavior of transverse stitched T-joints with PR520 resin in flexure and tension. *Composite Structures*, 52(3):307–314, 2001. ISSN 0263-8223.

[29] PB Stickler and M Ramulu. Parametric analyses of stitched composite T-joints by the finite element method. *Materials & Design*, 23(8):751–758, 2002. ISSN 0261-3069.

[30] PB Stickler and M Ramulu. Damage progression analyses of transverse stitched T-joints under flexure and tensile loading. *Advanced Composite Materials*, 15(2):243–261, 1 2006. ISSN 0924-3046.

[31] PB Stickler and M Ramulu. Experimental study of composite T-joints under tensile and shear loading. *Advanced Composite Materials*, 15(2):193–210, 2006. ISSN 09243046.

[32] IK Pattridge, JWG Treiber, and M Préau. Deformation and failure in a tufted carbon fabric / epoxy Ω –stiffener. In *Proceeding of the 11th international conference on deformation and fracture of composites.*, pages 1–5, 2011.

General Conclusions

This chapter summarizes what we have done in this thesis and points out what will be done in the future...

Conclusions

The present thesis conducts orderly and progressive investigation research on the following three tufting scales: **tufting thread** in chapter 2, **tufted laminate composite** in chapter 3 and**tufted plate assembly composite** in chapter 4.

- **Definition of tufting density**

In section 1.3.2 has given a definition of tufting density suitable to express the varying tufting patterns. Besides, there is a trade-off between tufting density and tufting spacing.

- **Optimization of tufting thread degradation**

Tufting thread degradation is observed during the tufting process, by means of image-observation and quasi-static tensile properties. Besides, it is proved that the tufting density can effect the generation of tufting thread degradation, the denser the tufting density, the worse the degradation. Furthermore, a novel tufting process (namely, two-step tufting process) is proposed, and it is proved to effectively reduce the degradation of the tufting thread.

- **Investigation of interlaminar shear properties under mode II loading condition for DTP, CT'C and CTC, respectively**

The effect of tufting density on the interlaminar shear behaviours under mode II sliding loading of tufted preforms and composites. The results show that the introduction of tufting thread can bring both positive and negative effects according to the tufting density. T6 is a critical tufting density in the present research. The negative effect acts on the composite, which with the tufting density looser than that of T6, while the opposite is the positive effect. Besides, it is proved that the tufting thread is at work, not the tufting action.

- **Development of tufted plat assembly composite**

A tensile experiment is carried out on the tufted plate assembly under various tufting parameters, and the results reveal that the FTL has no influence on this property, but it has a significant contribution to the composites industry of lightweight. Furthermore, the tufting density plays an essential role on the present mechanical properties. Finally, an macro(M)-level model of tufted plate assembly composite is proposed in the present thesis based on the model of tufting thread introduced as follows:

- **Design of geometrical model of tufting thread**

Studies in the present thesis demonstrate that tufting thread plays an essential role in the tufted products. Thus, it is interesting to simulate a tufting thread in the state of tufted composite. A geometrical model of the tufting thread is established with the assistance of TexGen and validation by meshing in Abaqus software.

Perspectives

For future work, the following suggestions can be used as research entry points:

- **Exploration on the tufted laminate preforms/composites**

In chapter 3 of this thesis, the results of the load-displacement curve of tufted preform/composite under mode II loading condition are discussed. Whereas the rupture position of the tufted composite is shown in Fig. 3-13 in section 3.4, the R-Curve of delamination properties can be explored in the future.

- **Exploration of the effect of tufting pattern on the tufted plate assembly composite and its other mechanical properties**

The configuration of tufting thread on the laminate preform leads to various tufting patterns for the tufted composite, it would be interesting to study the influence of tufting pattern on the mechanical properties. Furthermore, more mechanical performances should be studied, e.g., the pull-off behaviour, the crack initiation, and its propagation under different loading conditions can be calculated by the next researchers. There is an interest to explore the possibilities of assembling advanced and complex structures for broadening the application of tufting technology.

- **Optimization on the tufting thread model of the non-regular polygonal cross-section and exploration on the meso-scale FE of tufting thread**

Our model of tufting thread is to assign a regular polygonal cross-section, however, the reality is not always regular. Therefore, the researcher can be conducted on the optimization of the tufting thread model. Meanwhile, our model of tufted plate assembly is a macro(M)-level model, which distributes the local reinforcement properties, and the overall loading conditions act on the parts. Further work can first be done by refining the base information of material to complete our model finite element (FE) analysis. Then a meso (m)-level of tufted composite, an unit cell of tufted composite is proposed in Fig. 4-19 in perspective 4.6 of chapter 4. Further work can conduct with the homogenisation of mechanical properties, determination of damage initiation conditions and simulation of damage development aided with this unit-cell. Furthermore, to establish a model only assembly by tufting thread without "cohesive element".

- **Optimization on the tufting device and corresponding testing device**

Finally, in order to facilitate and simplify in academic research, it is imperative to optimize and develop the tufting device which can achieve various complex structures, tufted tubular assembly, tufted sandwich composite for example, and which can be adapted to more aspects of research, same to the testing device...

Résumé

Renforcement textile basé sur une technologie textile avancée pour la fabrication de composites

Les composites stratifiés tridimensionnels (3D) sont de plus en plus utilisés dans différents secteurs industriels. Leurs caractéristiques mécaniques sont intéressantes, en particulier par leur résistance et leur rigidité supérieures dans le sens de l'épaisseur. Le piquage est une des technologie qui permettent un recherche et dévelppement, qui non seulement s'adapte à divers matériaux, mais qui permet également de réaliser motifs et formes variés. Cette thèse est dédiée du développement de l'assemblage tubulaire par la technologie de piquage, d'analyse de l'influence des paramètres de piquage sur les performances mécanique du composite assemblé à plate est étudié. En plus les propriétés de cisaillement de la préforme piquée et du composite piqué, les comportements de dégradation du fil de piquage sont également étudiés. Alors, un mécanisme de piquage d'amélioration est proposé. Des configurations de produits piqués en 3D ont été conçues et les paramètres importants ont pu ajustés par la machine de piquage du GEMTEX. L'influence de la densité de piquage sur les propriétés de cisaillement mode II dans le plan de la préforme piquée et du composite piqué ont promis d'optimiser notre processus de piquage. L'étude de la dégradation du fil de piquage par l'essai de traction et l'observation d'image a conduit à la définition d'un processus de piquage amélioré. Ainsi, afin de discuter l'assemblage tubulaire, des essais à plat ont été menés . Ces travaux ouvert le developpment de cette technologie d'assemblage avec de nouvelles utilisations.

Motclés: Composite textile, assemblage tubulaire / plaque, piquage, performance mécanique, modélisation géométrique

Abstract

Textile reinforcement based on advanced textile technology for composite manufacturing

Three-dimensional (3D) laminated composites are increasingly used in different industrial areas. Their mechanical characteristics are advantageous, in particular by their better through-the-thickness strength and stiffness. Tufting is an ongoing technology, which not only adapts to various materials but also easy to achieve various patterns and shapes. This thesis is dedicated to the development of tubular assembly composite by tufting technology, the analysis of the influence of tufting parameters on mechanical performance by the plate assembly composite instead of the tubular assembly is to simplify the experimental study. In addition to the shear properties of the tufted preform and the tufted composite are introduced, the degradation behaviours of tufting thread are also studied. Then,an improvement tufting mechanism is proposed. The configurations of 3D tufted products have been designed and the significant parameters can be adjusted on the home-designed tufting device by GEMTEX. The influence of tufting density on Mode II in-plane shear properties of the tufted preform and the composite promised to the optimisation of the tufting process. Tensile test and the image-observation methods of tufting thread are carried out to determine the degradation behaviours, meanwhile to improve a novel tufting mechanism. Moreover, in order to discuss the tubular assembly, the tests on the plat assembly are carried out. These works open up the development of the new applications under this assembly technology.

Keywords: Textile composite, Tubular/plate assembly, Tufting, mechanical performance, geometry modelling